The Iby and Aladar Fleischman Faculty of Engineering
The Zandman-Slaner School of Graduates Studies

Direct Position Determination of Cyclostationary Signals

A thesis submitted toward the degree of
Master of Science in Electrical and Electronic Engineering

by

Alit Mendelson-Reuven

November, 2007

The Iby and Aladar Fleischman Faculty of Engineering
The Zandman-Slaner School of Graduates Studies

Direct Position Determination of Cyclostationary Signals

A thesis submitted toward the degree of
Master of Science in Electrical and Electronic Engineering

by

Alit Mendelson-Reuven

This research was carried out in the Department of Electrical Engineering – Systems
under the supervision of Prof. Anthony J. Weiss

November, 2007

To my mother, Dalia

Acknowledgments

First and foremost, I wish to thank my supervisor, Prof. Anthony J. Weiss for his assistance, fruitful discussions, and availability during this research.

Special thanks are given to my husband for his great patient and support, and to my entire family for their help and understanding.

Finally, I would like to dedicate this work to my mother. Without her endless care and encouragement, this research would not have been completed.

Abstract

Direct Position Determination (DPD) was proposed recently as a new method for passive localization of narrowband radio transmitters. Its superior performance, especially in the low SNR (signal-to-noise ratio) regime, is ascribed to both the joint optimization it performs over all base stations that participate in the estimation process and the direct determination of the emitter position as opposed to conventional methods which typically process the information from the individual base stations separately and determine the location using two estimation steps.

The wide use nowadays of communication signals which possess the special property of *cyclostationarity* calls for extending the conventional DPD to a dedicated algorithm for cyclostationary processes, offering performance enhancement.

In this work, we introduce the *Cyclic Direct Position Determination* (CDPD) algorithm, a novel method which is the cyclostationary counterpart of the DPD. Despite its name, the CDPD is not a simple extension of the DPD but a unique algorithm which deviates substantially from its ancestor. Yet, the CDPD enjoys both the benefits of the DPD algorithm and the great performance robustness in the presence of narrowband interferences thanks to its cyclostationarity exploitation.

The performance of the CDPD is analyzed under small errors assumption and the Cramér-Rao lower bound for the problem at hand is also considered. Thereafter, the CDPD performance is tested empirically using Monte Carlo simulations in terms of several system parameters such as the SNR and observation time for both a white Gaussian noise environment and a mixture of the latter with a narrowband interferer. Likewise, the empirical performance of the CDPD is compared to the performance of other localization methods, as well as to the predicted performance derived from the analysis of this method. Eventually, the robustness of the CDPD method to narrowband interferences is also demonstrated by comparing the cost function contours of the different algorithms in a noise environment consisting of both a narrowband interferer and a white Gaussian noise.

Contents

List of Abbreviations

AOA	Angle of Arrival
AWGN	Additive White Gaussian Noise
CADPD	Cyclic AOA Direct Position Determination
CDPD	Cyclic Direct Position Determination
CMA	Conditional Maximum Assumption
CML	Conditional Maximum Likelihood
CRLB	Cramér-Rao Lower Bound
CTDPD	Cyclic TDOA Direct Position Determination
DFS	Discrete Fourier Series
DPD	Direct Position Determination
FIM	Fisher Information Matrix
ML	Maximum Likelihood
MSE	Mean Square Error
MUSIC	Multiple Signal Classification
PAM	Pulse Amplitude Modulation
PDF	Probability Density Function
PSK	Phase Shift Keying
QAM	Quadrature Amplitude Modulation
RF	Radio Frequency
RMS	Root Mean Square
RV	Random Variable
SEA	Small Error Analysis
SIR	Signal-to-Interference Ratio
SNR	Signal-to-Noise Ratio
SOI	Signal of Interest
SVD	Singular Value Decomposition
TDOA	Time Difference of Arrival
TOA	Time of Arrival

ULA	Uniform Linear Array
UMA	Unconditional Maximum Assumption
UML	Unconditional Maximum Likelihood

List of Figures

1 Introduction and Literature Survey

This work proposes a new passive localization method for narrowband cyclostationary signals which will be henceforth called C*yclic Direct Position Determination* (CDPD). The performance of this algorithm is analyzed, verified using Monte Carlo simulations, and compared to the performance of other localization methods. We shall start the work with a literature survey describing some of these methods.

1.1 Localization Methods

The signal processing problem of passive source localization is of great interest since World War I. It has various applications in both civil and defense-oriented fields. Within the military applications we can mention localization systems for intelligence purposes, and electronic warfare while for civil applications we can count direction finding for navigation, vehicle location and tracking systems, and law enforcement in general such as detecting violators of communication regulations. The extensive use of cellular telephony lately has even increased the popularity of this signal processing field so that localization of cellular phone users is one of the major civil applications nowadays. For example, see the wireless Enhanced 911 (E911) review by Zagami *et al*. [26].

Unlike active localization systems such as radar [13] or sonar [2] which transmit a known signal to the target they wish to detect and then process the returns from it, in passive localization systems, the processor uses the signal transmitted by the emitter as its input data. Clearly, in many cases, this signal waveform is unknown at the processor.

When talking about localization methods, there exist two main processing approaches: centralized and decentralized processing. Among the decentralized approach algorithms we may find the methods: *angle of arrival* (AOA) (sometimes referred to also as direction of arrival – DOA) which was covered by the comprehensive review paper by Krim and Viberg [12], *received signal strength* (RSS), *time of arrival* (TOA) and *time difference of arrival* (TDOA). In the decentralized approach the processing is divided into two stages. In the first stage, each base station performs an estimation of a specific parameter of the received signal such as impinging angle or propagation delay. Subsequently, in the second stage, these estimations are collected from all of the base stations to derive the location estimation. This mechanism was comprehensively discussed for both AOA and TDOA by Torrieri [22]. In the centralized approach, which the method of *direct position determination* (DPD) ([25], [1]) belongs to, the received samples from all of the base stations are conveyed to a common central unit which jointly processes the base stations data and estimates the transmitter location in a single step. Obviously, because of the incomplete data batch used by each base station processor and the over-parameterization, decentralized processing is sub-optimal unlike centralized processing as explained in [1].

Another distinction that can be made between different localization methods is related to their signal selectivity nature, meaning whether they are designed for the general case or for a specific signal type. Traditionally, most of the location finding algorithms which are based on AOA (e.g., MUSIC [19]) or TDOA (e.g., Cross-Correlation [4], [3]) were developed as general algorithms in the sense that they assume an arbitrary signal waveform and thus do not exploit any special property of the signal. However, almost

every digital signal exhibits a unique property called (wide sense) *cyclostationarity*. This property means that both the first and second moments of such a process are periodic in time as opposed to stationary processes. Naturally, due to the digital nature of communications nowadays a new class of localization algorithms which exploit the cyclostationarity property has evolved. This led to the development of many "cyclic" versions of existing conventional localization methods such as the Cyclic MUSIC which was first introduced by Gardner [6] for the case of a single transmitter and afterwards was generalized to handle multiple emitters [17], and Cyclic Cross-Correlation [9]. Obviously, the main advantage of the "cyclic" methods over their "conventional" counterparts is their ability to mitigate both thermal noise and interferences which do not share the same cycle frequency as the signals of interest (SOIs) and which can severely degrade the performance of the conventional methods.

The purpose of this work is to present a new algorithm which combines the two concepts discussed above, namely, centralized processing and cyclostationarity exploitation. The algorithm, called henceforth CDPD, is the cyclic counterpart of the DPD algorithm which was first suggested by Weiss [25] for the case of a single transmitter, and afterwards was generalized to multiple transmitters [1]. However, as will be explained in detail later, the CDPD cannot be viewed as a mere expansion of the conventional DPD but as a unique algorithm with a novel cost function. A detailed overview of centralized processing and cyclostationarity is given in the following two sections.

1.2 Fundamentals of Cyclostationary Processes

Many communication signals such as PAM, PSK, and QAM signals possess the cyclostationary property as being digitally modulated signals. We shall now start with a brief introduction to the basic concepts and definitions associated with cyclostationary processes.

A continuous random process $x(t)$ is said to be cyclostationary in the wide sense, with period T if its expectation, $m_x(t)$, and autocorrelation function, $R_{xx}(t,\tau)$, are periodic functions of the time t, with period T. That is,

$$m_x(t) \equiv E\{x(t)\} = m_x(t+kT), \tag{1}$$

$$R_{xx}(t,\tau) \equiv E\{x(t+\tau/2)x^*(t-\tau/2)\} = R_{xx}(t+kT,\tau), \tag{2}$$

where k is any integer, $[\cdot]^*$ denotes complex conjugate, and $E\{\cdot\}$ denotes statistical expectation.

Since the autocorrelation function, $R_{xx}(t,\tau)$, is periodic in t with period T, we can write its Fourier series coefficients as follows

$$R_{xx}^{\alpha}(\tau) \equiv \mathcal{F}\{R_{xx}(t,\tau)\}_{n=\alpha T} = \langle R_{xx}(t,\tau)e^{-j2\pi\alpha t}\rangle_T, \tag{3}$$

where $\mathcal{F}\{R_{xx}(t,\tau)\}_{n=\alpha T}$ is the nth Fourier series coefficient, that is, the Fourier coefficient at frequency $\alpha = n/T$ for some integer n, and where $\langle\cdot\rangle_T$ denotes time-average over a period of T:

$$\langle \cdot \rangle_T \equiv \frac{1}{T} \int_{-T/2}^{T/2} \cdot \ .$$

The function $R_{xx}^{\alpha}(\tau)$ defined in Eq. (3) is called the *cyclic autocorrelation* of the process $x(t)$, and α is referred to as the *cycle frequency* parameter of this function. It can be seen that for $\alpha = 0$ and a stationary process $x(t)$, $R_{xx}^{\alpha}(\tau)$ reduces to the conventional autocorrelation function, $R_{xx}(\tau)$, and so, $R_{xx}^{\alpha}(\tau)$ can be viewed as a generalization of the ordinary autocorrelation function. Likewise, we observe that while Eq. (3) is identically zero for all $\alpha \neq 0$ when the process is stationary, it is nonzero only for a set of discrete values of α, when the process is cyclostationary. Generally speaking, the cycle frequencies of a cyclostationary process will be usually equal to the doubled carrier frequency, harmonics (integer multiples) of the baud rate, and their sums and differences, as described in [5], [7]. This of course depends directly on the modulation type that is applied to the data and on the nature of this data. For example, consider the case of amplitude modulation in which a cyclostationary signal is obtained when purely stationary amplitude is modulated by a certain carrier (sine wave) and thus, the resulting cycle frequency is equal to the doubled carrier frequency. Alternatively, this purely stationary data can be modulated by a train of pulses of width T, as in the case of PAM, which yields a cyclostationary baseband signal with cycle frequencies equal to the harmonics of the baud rate, $1/T$. In this work, we will concentrate mainly on cyclostationary baseband signals, i.e., in the complex envelope resulting from the demodulation process and therefore, the cycle frequencies are always equal to harmonics of the baud rate, unless otherwise stated.

Additional note should be set forth regarding another parameter of $R_{xx}^{\alpha}(\tau)$ – the lag parameter, τ. While the conventional autocorrelation function peaks at $\tau = 0$, the cyclic autocorrelation function frequently gains its maximum value for $\tau \neq 0$. For example, constant modulus signals such as BPSK modulated signals with rectangular shaping of width T have cyclic autocorrelation function which is zero for $\tau = 0$ and peaks at $\tau = T/2$.

By analogy with Eq. (3), we define the *cyclic cross correlation* between two continuous random processes, $x(t)$ and $y(t)$ as

$$R_{xy}^{\alpha}(\tau) \equiv \mathcal{F}\left\{R_{xy}(t,\tau)\right\}_{n=\alpha T} = \langle R_{xy}(t,\tau)e^{-j2\pi\alpha t}\rangle_T \,, \tag{4}$$

where

$$R_{xy}(t,\tau) \equiv E\left\{x\left(t+\tau/2\right)y^*\left(t-\tau/2\right)\right\}. \tag{5}$$

Hitherto we developed a statistical version of the cyclic autocorrelation function which is based on the ensemble average of the data samples. However, in practice, only sample estimates for the quantities discussed above are available, implying that the probabilistic formulation obtained so far should be replaced with its empirical counterpart. The non probabilistic version of the cyclic autocorrelation function based on a temporal average rather than a statistical one is thus obtained as

$$\overline{R}_{xx}^{\alpha,T'}(\tau) \equiv \left\langle x\left(t+\tau/2\right)x^*\left(t-\tau/2\right)e^{-j2\pi\alpha t}\right\rangle_{T'} \,, \tag{6}$$

$$\overline{R}_{xx}^{\alpha}(\tau) \equiv \lim_{T'\to\infty} \overline{R}_{xx}^{\alpha,T'}(\tau) \,, \tag{7}$$

where T' is the observation time for which the temporal averaging is done.

Similarly, the non-probabilistic version of the cyclic cross correlation function is defined as

$$\overline{R}_{xy}^{\alpha,T'}(\tau) \equiv \left\langle x\left(t+\tau/2\right)y^{*}\left(t-\tau/2\right)e^{-j2\pi\alpha t}\right\rangle_{T'}, \tag{8}$$

$$\overline{R}_{xy}^{\alpha}(\tau) \equiv \lim_{T'\to\infty} \overline{R}_{xy}^{\alpha,T'}(\tau). \tag{9}$$

Since the complex sine wave factor, $e^{-j2\pi\alpha t}$, in Eqs. (6) and (8) can be associated with either data scalar in the lag product shown in these equations, we observe that the cyclic autocorrelation, as well as the cyclic cross correlation, can be viewed also as a conventional cross correlation between frequency-shifted versions of the corresponding signals.

If we further assume that $x(t)$ and $y(t)$ are cycloergodic then $\overline{R}_{xx}^{\alpha}(\tau)$ and $\overline{R}_{xy}^{\alpha}(\tau)$ coincide with $R_{xx}^{\alpha}(\tau)$ and $R_{xy}^{\alpha}(\tau)$, respectively, so we can replace the ensemble average with a temporal one, assuming that the averaging time T' goes to infinity.

Next, we present the equivalent definitions for the discrete-time model. This model is obtained by sampling its continuous counterpart with sampling time of T_s so that the relation between the two models is given by

$$x(l) = x(t)\big|_{t=lT_s}. \tag{10}$$

A discrete-time random process $x(l)$ is said to be cyclostationary in the wide sense, with period N if its expectation, $m_x(l)$, and autocorrelation function, $R_{xx}(l,z)$, are periodic functions of the discrete time l, with period N. That is,

$$m_x(l) \equiv E\{x(l)\} = m_x(l+kN)\,, \tag{11}$$

$$R_{xx}(l,z) \equiv E\{x(l)x^*(l-z)\} = R_{xx}(l+kN,z)\,. \tag{12}$$

Similarly to the continuous case, we define the cyclic autocorrelation with cycle frequency α as the discrete Fourier series (DFS) coefficient [14], at frequency $\alpha = n/T$, of the autocorrelation function, $R_{xx}(l,z)$

$$R_{xx}^{\alpha}(z) \equiv \mathcal{F}\{R_{xx}(l,z)\}_{n=\alpha T} = \frac{1}{N}\sum_{l=0}^{N-1} R_{xx}(l,z)e^{-j2\pi\alpha l T_s}\,. \tag{13}$$

Likewise, the temporal average counterpart of the cyclic autocorrelation function in Eq. (13) is defined as

$$\overline{R}_{xx}^{\alpha,N_s}(z) \equiv \frac{1}{N_s}\sum_{l=0}^{N_s-1} x(l)x^*(l-z)e^{-j2\pi\alpha l T_s}\,, \tag{14}$$

$$\overline{R}_{xx}^{\alpha}(z) \equiv \lim_{N_s\to\infty} \overline{R}_{xx}^{\alpha,N_s}(z)\,, \tag{15}$$

where N_s is the total number of samples (discrete observation time) for which the temporal averaging is done. When the process $x(l)$ is also cycloergodic then $\overline{R}_{xx}^{\alpha}(z)$ coincides with $R_{xx}^{\alpha}(z)$ and the statistical average in Eq. (13) can be replaced with a temporal one assuming that N_s goes to infinity.

Finally, in order to complete the discrete-time formulation, the cyclic cross correlation between two discrete-time random processes, $x(l)$ and $y(l)$ is given by

$$R_{xy}^{\alpha}(z) \equiv \mathcal{F}\left\{R_{xy}(l,z)\right\}_{n=\alpha T} = \frac{1}{N}\sum_{l=0}^{N-1} R_{xy}(l,z)e^{-j2\pi\alpha l T_s} \ , \tag{16}$$

where

$$R_{xy}(l,z) \equiv E\left\{x(l)y^*(l-z)\right\}, \tag{17}$$

and its non-probabilistic version can be written as

$$\overline{R}_{xy}^{\alpha,N_s}(z) \equiv \frac{1}{N_s}\sum_{l=0}^{N_s-1} x(l)y^*(l-z)e^{-j2\pi\alpha l T_s} \ , \tag{18}$$

$$\overline{R}_{xy}^{\alpha}(z) \equiv \lim_{N_s\to\infty} \overline{R}_{xy}^{\alpha,N_s}(z) \, . \tag{19}$$

Last note should be stated regarding the minor inconsistency between the continuous and the discrete-time definitions of the cyclic autocorrelation function. One should note that the symmetric definition of the continuous-time cyclic autocorrelation function as appears in Eq. (3) (together with Eq. (2)), cannot be directly extended to the discrete-time case, since intermediate samples are obviously not available. Therefore, we have chosen for convenience in Eq. (13) (together with Eq. (12)) to follow the asymmetric definition of the discrete-time cyclic autocorrelation function by contrast to the definition of [8].

1.3 DPD Algorithm Concepts

In this section, we introduce the main ideas and concepts related to the DPD algorithm [25]. In addition, we shall describe the advantages and drawbacks of this method with respect to previous approaches.

Most prevalent emitter localization algorithms usually consist of two stages. The first stage is to derive an estimate of one of the SOI location parameters such as AOA or TOA. Thereafter, in the second stage, this parameter estimates are sent to a central processing unit where another algorithm, usually the least squares algorithm, is applied to the various estimates from all of the base stations in order to devise the final estimation which is the emitter location. It is important to note that the estimation of the SOI location parameter carried out in the first stage is done independently in each base station, so that each base station exploits the samples received by its own antenna array. There are, of course, some exceptions to this rule; For example, derivatives of the AOA and TOA methods such as TDOA estimation in which the parameter estimated is a differential one so that the measurements from base station pairs is used in order to accomplish the estimation.

Comparing to the above-mentioned methods, there are two novel concepts in the DPD algorithm. The first one is that the DPD algorithm skips the first stage of parameter estimation described above and performs instead only one-stage estimation. That is, in the DPD algorithm, the emitter location is directly estimated from the samples received by the multiple antenna arrays without making any additional intermediate estimation. Naturally, we cannot estimate an emitter location using measurements of a single base station. For this sake, we need measurements from at least two base stations. Here we introduce the second concept of the DPD algorithm: It is clear that the existing localization algorithms, in which the estimation is done independently in each base station, are indeed suboptimal since they do not apply the constraint that the measurements from all of the base stations correspond to the same emitter. The DPD

algorithm, on the contrary, uses the measurements from all of the base stations together in order to estimate the emitter location. This difference between the two estimation approaches is equivalent to the difference between a single optimization performed on the entire data set and a concatenation of two optimization steps where the first one is carried out, independently, on disjoint subsets of the entire data set, thereby generating intermediate estimates. This step is followed by a second optimization step which processes these intermediate estimates to provide the final position estimation.

To conclude, the DPD algorithm is a one-step algorithm in which the position determination is based on a multi-base station optimization. Thus, its advantage is twofold: better performance over the conventional methods utilizing the same data inputs, and the conceptual simplicity by deriving a one-step processing implemented by a single central processor. This conceptual simplicity means that while in the conventional approaches, all of the L base station processors perform single base station optimization and then a central processor applies a multi-base station optimization to these estimates, in the DPD algorithm, a single central processor performs one multi-base station optimization so no processing is required in any of the base stations. Clearly, in order to develop this algorithm, the conventional problem formulation used so far by the previous algorithms should be rephrased in terms of the emitter location. This formulation is introduced in the following chapter. The drawbacks of the DPD algorithm is that it requires the re-direction of the samples received by all of the base station to the central processing unit and not just the estimations of the SOI parameter as in second stage of the conventional methods. Similarly to the DPD algorithm proposed for stationary processes, in this work we present the CDPD algorithm which targets cyclostationary processes.

1.4 Outline

We shall now present a brief preview of the work. This work is organized as follows:

- Chapter 1 (this chapter) introduces this work, previous works in the area of source localization, and the main concepts behind the CDPD algorithm.
- Chapter 2 presents the model used throughout this work and the assumptions led to it.
- Chapter 3 includes the main part of this work – derivation of the CDPD algorithm.
- Chapter 4 introduces a small error analysis of the CDPD algorithm. We develop a closed-form expression for the mean square error (MSE) of the CDPD which will be corroborated empirically in Chapter 6.
- In Chapter 5 we study the theory of the Cramér-Rao lower bound and examine its application to the problem at hand.
- Chapter 6 presents a numerical study of the CDPD performance using Monte Carlo simulations. This empirical performance is compared both to the MSE of other localization methods and to the analytical results developed in Chapter 4.
- Chapter 7 concludes this work with a summary and some suggestions for future work.

2 Problem Formulation

2.1 Assumptions

Before delving into the mathematical notations of the model assumed in this work we shall briefly discuss the assumptions led to the model and the motivation behind it. We start this part with the assumptions made on the wave propagation nature of the impinging signals. The model used throughout this work treats electro-magnetic waves. Such waves have a spherical wavefront. However, if the radius of propagation which is the distance between the transmitter and the antenna array is much greater than the array aperture (the physical size of the array) then a planar wavefront can be considered instead. This assumption which is called a far field assumption will be adopted for the rest of this work.

Another aspect of the wave propagation is the distinction between line-of-sight (LOS) propagation and a non-line-of-sight (NLOS) propagation. For the LOS propagation case, the signals reception is assumed to be coherent, i.e., the signal received by the base station is a scaled and delayed version of the transmitted signal. In this case, the path loss coefficient representing the channel attenuation is usually modeled as a fixed power of the distance between the transmitter and the base station. For the NLOS propagation case however, the coherency of the signals reception is not necessarily maintained as the traveling signal may experience multipath during its propagation. In the case of multipath, the signal received by the base station is a sum of different delayed and scaled versions of the transmitted signal. Likewise, the various path loss factors, each associated

with a different delayed version of the transmitted signal, are not always fixed but can vary in time. Usually, each one of these path loss coefficients is modeled as a random process drawn from a Rayleigh distribution. Throughout this work we assume for simplicity that there is no multipath at the reception but in order to be more general we do not impose any specific model for the path loss factor and consider it as a random variable (RV) which is fixed during the measurement time. Therefore, the model described in this work can be viewed as based on a mixture of LOS and NLOS assumptions.

The next assumption applied during the model derivation refers to the bandwidth of the signal. Throughout this work we will deal with radio frequency (RF) signals which are classified as narrowband signals. This means that the traverse time of the SOI across the array aperture is much smaller than the inverse of the signal bandwidth so that any relative delay between the array elements hardly changes the complex envelop of the signal and thus will be neglected in the envelop term. It should be mentioned in addition, that for convenience, we will limit our mathematical description to baseband signals only, i.e. to the signals complex envelopes which remain after dropping the carrier term. This is done also from practical reasons as the RF signal is usually down converted to the baseband before sampling.

Another assumption made is on the number of SOIs appearing in the model. The model presented in this chapter assumes a single SOI, meaning that all the other existing signals are classified as thermal noise or as interferers which do not share the same cycle frequency as the SOI. This kind of model can fit either the obvious situation in which

there exists only a single emitter in the system with the cycle frequency of interest or the case that all users in a certain network do share the same cycle frequency but their data is completely unsynchronized so that by invoking the Central Limit Theorem, their aggregate contribution can be viewed as an additive white Gaussian noise (AWGN), provided that there is no dominant interferer. Furthermore, the case for which a dominant interference does exist in the system and is found to be much stronger than the other interferes is modeled in this study as a mixture of both AWGN and interference and will be addressed in Section 6.3. Finally, it should be stated that extending the model to the case of multiple transmitters of interest, all of which sharing the same cycle frequency, is straightforward but is out of the scope of this work.

2.2 Mathematical Description

After covering the assumptions made on the observed data we now describe the data model which will be used in the remainder of this work. Consider a single transmitter and L base stations intercepting the transmitted signal which is assumed to be narrowband, cyclostationary, and cycloergodic RF signal with a baud rate of $1/T$. The carrier frequency of the impinging signal will be denoted by f_c. Each base station is equipped with a sensor array of arbitrary geometry consisting of M antenna elements. The positions of the transmitter and the lth base station will be denoted by the $D \times 1$ vectors of coordinates, $\boldsymbol{p}$ and $\boldsymbol{q}_l$, respectively. Obviously, D will be 2 for the case of planar geometry and 3 for the general case (3D geometry). The complex envelope of the signal observed by the lth base station array is given by

$$\boldsymbol{r}_l(t) = b_l \boldsymbol{a}_l(\boldsymbol{p}) s(t - \tau_l(\boldsymbol{p}) - t_0) + \boldsymbol{n}_l(t), \tag{20}$$

where $\boldsymbol{r}_l(t)$ is a time-dependent $M \times 1$ vector, and b_l is an unknown complex scalar representing the channel effect (attenuation). As was already explained in the model assumptions part, we do not assume any specific model for the relation between this path loss factor and the transmitter location, thus leaving the first to be an RV. The next parameter in Eq. (20) is the steering vector, $\boldsymbol{a}_l(\boldsymbol{p})$, which is the *l*th array response to a signal transmitted from position $\boldsymbol{p}$. Each entry in this vector represents the relative phase increment experienced by the corresponding antenna element due to the relative additional distance between this element and the transmitter. Under a far field assumption, $\boldsymbol{a}_l(\boldsymbol{p})$ is a function of the signal angle of arrival only. Likewise, if we further assume uniform linear array (ULA) geometry then $\boldsymbol{a}_l(\boldsymbol{p})$ takes the form

$$\boldsymbol{a}_l(\boldsymbol{p}) = \left[1, e^{j2\pi f_c d \cos\theta_l(\boldsymbol{p})/c}, \cdots, e^{j2\pi f_c d (M-1)\cos\theta_l(\boldsymbol{p})/c}\right]^T,$$

where c is the propagation speed, d is the distance between any two adjacent antenna elements, and $\theta_l(\boldsymbol{p})$ is the azimuth angle induced between the *l*th array and the signal location, $\boldsymbol{p}$. It should be mentioned however, that both the CDPD algorithm and its performance analysis are applicable under any type of array configuration and that the ULA assumption will be invoked only in the simulations results part given in Chapter 6. Next in Eq. (20) is $s(t - \tau_l(\boldsymbol{p}) - t_0)$ which is the SOI waveform, transmitted at time t_0 and delayed by $\tau_l(\boldsymbol{p})$. Finally, the vector $\boldsymbol{n}_l(t)$ in Eq. (20) represents a general mixture of two types of signals, each of which with zero mean: a stationary Gaussian noise which is both spatially and temporally white and a cyclostationary interferer whose baud rate is

different from the one of the SOI and any harmonic of this rate. Furthermore, all of the above-mentioned signals, namely, the SOI, AWGN, and cyclostationary interference are assumed to be uncorrelated. It is important to note that due to the existence of a cyclostationary interferer in $\boldsymbol{n}_l(t)$ it will not be temporally white but cyclostationary with the same cycle frequency as the interference.

We conclude from the model in Eq. (20) that the information regarding the transmitter location is captured by two parameters. The first is the steering vector, $\boldsymbol{a}_l(\boldsymbol{p})$, which as mentioned above, depends on the transmitter bearing only, while the second is the signal time of arrival, $\tau_l(\boldsymbol{p})$, which is a function of the distance between the transmitter and the base station only. We remind the reader that since we do not assume any specific relation between the path loss coefficient and the base station-transmitter distance then b_l does not contain information regarding the emitter location.

We next sample the received signal, $\boldsymbol{r}_l(t)$ at times $t = kT_s$ so the discrete time equivalent of Eq. (20) becomes

$$\boldsymbol{r}_l(k) = b_l \boldsymbol{a}_l(\boldsymbol{p}) s_l(k) + \boldsymbol{n}_l(k), \tag{21}$$

where

$$s_l(k) \equiv s(t - \tau_l(\boldsymbol{p}) - t_0)\big|_{t=kT_s}. \tag{22}$$

The sampling rate of the received signal is assumed to be an integral multiple of the baud rate (symbol rate) of the SOI. Likewise, we assume that the baud rate of the SOI is known at the receiver and that we have a total of N_s samples of $\boldsymbol{r}_l(k)$, spreading over a total

observation time of $T' = T_s N_s$. The ratio between the period of the cyclostationary process, T, and the sampling time, T_s, will be henceforth referred to as the over-sampling factor and denoted by OVS.

3 The Cyclic DPD Algorithm

3.1 Introduction

The aim of this study is to develop a localization method for narrowband RF transmitters which will have both superior performance and a relatively low implementation cost and complexity. Before starting the algorithm derivation we shall first motivate this derivation and provide some background as to which categories and classes of localization algorithms the CDPD belongs to.

Generally speaking, location finding methods can be usually classified into two main categories: The spectral-based approach which estimates the emitters' location individually as the global maxima of a certain spectrum function and the parametric approach which performs a multidimensional search for all the emitters' locations simultaneously. Clearly, the complexity of the spectral-based methods is much smaller than the parametric ones where the price for this reduced complexity is some performance degradation of the first class. It should be mentioned however, that since the problem at hand considers a single SOI model, this distinction is obviously irrelevant.

The spectral-based category itself can be further divided into some sub-categories. The most popular among them is the subspace-based class. This class of localization algorithms is based on applying eigenvalue decomposition to the autocorrelation matrix of the received vector and exploiting the eigen-structure of this matrix to exhibit much better estimation performance. The procedure of eigenvalue decomposition of the autocorrelation matrix is applicable to stationary processes. In case of cyclostationary

processes, the “cyclic” counterpart of this class, referred to as cyclic subspace-based methods, applies the eigenvalue decomposition to the cyclic autocorrelation matrix instead. This is the technique used also by the CDPD algorithm.

While the conventional cyclic subspace-based methods estimate the AOA, TOA, or TDOA parameters from which they obtain the emitter location, the CDPD finds this location directly, without intermediate estimations and by applying a search which involves the complete data gathered from all of the base stations. In this sense, it is a derivative of the conventional DPD [25] developed for the stationary case. However, it is important to note that the CDPD is not a simple extension of the conventional DPD but a unique algorithm which shares with the last only the concept of direct multi-base station estimation. While the DPD belongs to the parametric approach and is an implementation of the conditional maximum likelihood (CML) estimation for the problem then the CDPD belongs to the cyclic subspace-based methods which are a branch of the spectral-based approach.

As will be elaborated in the following section, the CDPD algorithm is actually a combination of two estimators, each of which exploits a different property of the propagating signal. The first algorithm, called *Cyclic AOA Direct Position Determination* (CADPD) uses the signal angle of arrival while the second, the *Cyclic TDOA Direct Position Determination* (CTDPD), exploits the time delay of the signal propagation. Nevertheless, they both use exactly the same input, an estimate of the cyclic autocorrelation matrix of the received vector in each sensor array. The estimate of such a matrix, as well as the derivation of each of the above-mentioned algorithms, is given

herein. Thereafter, the optimal choice for the lag parameter of the cyclic autocorrelation matrix is considered. Furthermore, we extend the basic algorithm derivation given for a single lag parameter to handle multiple lag parameters which provide further performance improvement. Finally, we conclude this chapter by studying the ambiguity problem of the CTDPD algorithm and its consequences.

3.2 Algorithm Derivation

3.2.1 Estimating $R^{\alpha}_{\mathbf{r}_l\mathbf{r}_l}(k)$ and its Nonzero Eigenvalue

We start the algorithm derivation in general and the estimation of the cyclic autocorrelation matrix of $\boldsymbol{r}_l(k)$ from Eq. (21) in particular, by calculating the $M \times M$ autocorrelation matrix of the last. This matrix which is associated with the *l*th base station and evaluated at time index *m* and lag parameter *k* is given by

$$R_{\mathbf{r}_l\mathbf{r}_l}(m,k) \equiv E\left\{\boldsymbol{r}_l(m)\boldsymbol{r}_l^H(m-k)\right\} = |b_l|^2 \boldsymbol{a}_l(\boldsymbol{p})\boldsymbol{a}_l^H(\boldsymbol{p})R_{s_l s_l}(m,k) + R_{\mathbf{n}_l\mathbf{n}_l}(m,k), \qquad (23)$$

where

$$R_{s_l s_l}(m,k) \equiv E\left\{s_l(m)s_l^*(m-k)\right\},$$

$$R_{\mathbf{n}_l\mathbf{n}_l}(m,k) \equiv E\left\{\boldsymbol{n}_l(m)\boldsymbol{n}_l^H(m-k)\right\}.$$

The reader should keep in mind that the noise vector, $\boldsymbol{n}_l(k)$, has zero mean and that in addition, the SOI is assumed to be uncorrelated with the two terms constituting this vector, namely, the AWGN and cyclostationary interference. These last two statements thus explain why the cross terms in Eq. (23) between the SOI and noise vector vanish.

Applying the DFS transform at frequency α to both sides of Eq. (23) we obtain the cyclic autocorrelation matrix of the received vector at cycle frequency α

$$R^{\alpha}_{\mathbf{r}_l\mathbf{r}_l}(k) = |b_l|^2 \mathbf{a}_l(\mathbf{p})\mathbf{a}_l^H(\mathbf{p})R^{\alpha}_{s_l s_l}(k) + R^{\alpha}_{\mathbf{n}_l\mathbf{n}_l}(k)\,. \tag{24}$$

Generally speaking, the cycle frequency parameter α may take on all integer multiples of the baud rate. Yet, since more energy of the signal resides in the lower indices of the DFS coefficients, it is most reasonable to choose α to be the first harmonic of the baud rate. Thus, we henceforth set the parameter α as the fundamental cycle frequency, $1/T$, unless otherwise asserted.

Since the AWGN and cyclostationary interference are uncorrelated and neither of them have any component at frequency α according to our model assumptions then we have,

$$R^{\alpha}_{\mathbf{n}_l\mathbf{n}_l}(k) = 0\,, \tag{25}$$

so that Eq. (24) reduces to

$$R^{\alpha}_{\mathbf{r}_l\mathbf{r}_l}(k) = |b_l|^2 \mathbf{a}_l(\mathbf{p})\mathbf{a}_l^H(\mathbf{p})R^{\alpha}_{s_l s_l}(k)\,. \tag{26}$$

Using the shift property of the DFS in Eq. (24), we get

$$R^{\alpha}_{\mathbf{r}_l\mathbf{r}_l}(k) = e^{-j2\pi\alpha(\tau_l(\mathbf{p})+t_0)}|b_l|^2 \mathbf{a}_l(\mathbf{p})\mathbf{a}_l^H(\mathbf{p})R^{\alpha}_{ss}(k)\,, \tag{27}$$

where

$$R^{\alpha}_{ss}(k) = \mathcal{F}\left\{E\left\{s(m)s^*(m-k)\right\}\right\}_{n=1}\,,$$

$$s(m) = s(t)\big|_{t=mT_s}\,.$$

We recall that the signal is assumed to be cycloergodic, so that we can replace the ensemble average with a temporal average in which the number of signal samples tends to infinity. Therefore, Eq. (27) becomes

$$\overline{R}^{\alpha}_{\boldsymbol{r}_l \boldsymbol{r}_l}(k) = e^{-j2\pi\alpha(\tau_l(\boldsymbol{p})+t_0)} \left|b_l\right|^2 \boldsymbol{a}_l(\boldsymbol{p}) \boldsymbol{a}_l^H(\boldsymbol{p}) \overline{R}^{\alpha}_{ss}(k) . \tag{28}$$

We observe that the quantities on the right-hand side of Eq. (28) can be divided into two different kinds of parameters. The first one is the signal parameters which include the transmission instant, t_0, and the cyclic autocorrelation function, $\overline{R}^{\alpha}_{ss}(k)$, while the second type is the system parameters: the path loss factor, b_l, the steering vector, $\boldsymbol{a}_l(\boldsymbol{p})$, and the time delay, $\tau_l(\boldsymbol{p})$. Furthermore, since the information regarding the emitter position is embedded only in the system parameters we gather all these parameters into a single matrix defined as

$$D_l \equiv e^{-j2\pi\alpha\tau_l(\boldsymbol{p})} \left|b_l\right|^2 \boldsymbol{a}_l(\boldsymbol{p}) \boldsymbol{a}_l^H(\boldsymbol{p}) , \tag{29}$$

and rewrite Eq. (28) as follows

$$\overline{R}^{\alpha}_{\boldsymbol{r}_l \boldsymbol{r}_l}(k) = e^{-j2\pi\alpha t_0} D_l \overline{R}^{\alpha}_{ss}(k) . \tag{30}$$

Next, we conclude from the structure of D_l that this matrix is singular and has rank one. This implies that $\overline{R}^{\alpha}_{\boldsymbol{r}_l \boldsymbol{r}_l}(k)$, which is a scaled version of D_l, has also rank one and thus, only a single nonzero eigenvalue. Therefore, this eigenvalue which is further denoted by λ_l can be expressed as,

$$\lambda_l = \text{trace}\left\{\overline{R}^{\alpha}_{\boldsymbol{r}_l \boldsymbol{r}_l}(k)\right\} = e^{-j2\pi\alpha(\tau_l(\boldsymbol{p})+t_0)} M \left|b_l\right|^2 \overline{R}^{\alpha}_{ss}(k)\,, \tag{31}$$

where in the last equality we used the following property of the steering vector which is applicable under any array geometry

$$\left\|\boldsymbol{a}_l(\boldsymbol{p})\right\|^2 = M\,. \tag{32}$$

One should note that the strict equality of Eq. (30) is applicable only to the asymptotic case when the observation time tends to infinity. Specifically, the claim that the cyclic autocorrelation matrix of the observed data is both singular and with rank one holds only theoretically, when averaging an infinite number of samples. In practice, however, the number of samples available is obviously finite so that we can only obtain an estimate for the single nonzero eigenvalue given in Eq. (31). To this end, we first estimate the cyclic autocorrelation matrix of the observed data as the finite observation time version of this matrix. Denoting this estimate by

$$\overline{R}^{N_s}_l(k) \equiv \overline{R}^{\alpha,N_s}_{\boldsymbol{r}_l \boldsymbol{r}_l}(k)\,, \tag{33}$$

we write the finite samples number counterpart of Eq. (30), where the equality of the last is replaced with an approximation

$$\overline{R}^{N_s}_l(k) \cong e^{-j2\pi\alpha t_0} D_l \overline{R}^{\alpha,N_s}_{ss}(k)\,. \tag{34}$$

Typically, the estimated cyclic autocorrelation matrix, $\overline{R}^{N_s}_l(k)$ will be a full rank matrix, namely, all of its eigenvalues will be nonzero. However, for sufficiently long averaging time this matrix rank will approach unity in the sense that a single eigenvalue will be significantly larger than the other eigenvalues. Although it is only an approximation we

will further refer to this eigenvalue as the single nonzero eigenvalue of $\overline{R}_l^{N_s}(k)$. A natural estimate of the nonzero eigenvalue λ_l from Eq. (31) can be then defined as,

$$\hat{\lambda}_l \equiv \text{trace}\left\{\overline{R}_l^{N_s}(k)\right\}, \tag{35}$$

where the reader should keep in mind that $\hat{\lambda}_l$ is a function of the samples number, N_s, and the lag parameter, *k*. Now, substituting Eq. (34) into Eq. (35) and combining the definition of D_l from Eq. (29) leads to,

$$\hat{\lambda}_l \cong e^{-j2\pi\alpha(\tau_l(\boldsymbol{p})+t_0)} M\left|b_l\right|^2 \overline{R}_{ss}^{\alpha,N_s}(k). \tag{36}$$

Eqs. (34) and (36) respectively, introduce expressions for the estimated cyclic autocorrelation matrix and its nonzero eigenvalue, for a given lag parameter choice and a fixed number of samples. These expressions are used hereby for deriving the two constituent algorithms of the CDPD estimator.

3.2.2 The CADPD Estimator

The CADPD estimator is based on exploiting the information embedded in the steering vector, $\boldsymbol{a}_l(\boldsymbol{p})$, regarding the emitter position. First, we notice that according to its definition, the cyclic autocorrelation matrix is not Hermitian in general for any lag choice, unlike the conventional autocorrelation matrix, which is Hermitian for zero lag. Therefore, many desirable and useful properties of Hermitian matrix cannot be applied directly to $\overline{R}_l^{N_s}(k)$. In order to produce a Hermitian matrix, we multiply $\overline{R}_l^{N_s}(k)$ from Eq. (34) by its conjugate transpose

$$\Psi(k) \equiv \left(\overline{R}_l^{N_s}(k)\right)^H \left(\overline{R}_l^{N_s}(k)\right) = \left|\overline{R}_{ss}^{\alpha,N_s}(k)\right|^2 D_l^H D_l = \left|\hat{\lambda}_l\right|^2 \Big/ M \cdot \boldsymbol{a}_l(\boldsymbol{p})\boldsymbol{a}_l^H(\boldsymbol{p}). \qquad (37)$$

Next we recall that any Hermitian matrix, U, has the following decomposition

$$U = V\Lambda V^H,$$

where V is the eigenvectors matrix of U, and Λ is a diagonal matrix with the eigenvalues of U on its main diagonal. The matrix on the left-hand side of Eq. (37), $\Psi(k)$, is Hermitian and like its constructor, $\overline{R}_l^{N_s}(k)$, has rank one. Combining the last observation with the above diagonalization property we conclude that $\boldsymbol{a}_l(\boldsymbol{p})$ is one of the eigenvectors of $\Psi(k)$ which corresponds to the single nonzero eigenvalue of this matrix, $\left|\hat{\lambda}_l\right|^2$. Likewise, it is well known that eigenvectors corresponding to distinct eigenvalues of any Hermitian matrix are orthogonal to each other. Specifically, $\boldsymbol{a}_l(\boldsymbol{p})$ is orthogonal to the $M-1$ eigenvectors corresponding to a zero eigenvalue. Therefore, the cost function that should be minimized and will be here onwards referred to as the CADPD estimator part of the CDPD algorithm is defined as

$$f_{CADPD}(\boldsymbol{p}) \equiv \sum_{l=1}^{L} \left\| E_n^H(l)\boldsymbol{a}_l(\boldsymbol{p}) \right\|^2, \qquad (38)$$

where $E_n(l)$ is an $M \times (M-1)$ matrix containing the noise subspace [19] of the lth base station, i.e., the $M-1$ eigenvectors of the matrix $\Psi(k)$ which correspond to a zero eigenvalue. Typically, this noise subspace is obtained in practice by applying singular value decomposition (SVD) procedure to the original matrix, namely $\overline{R}_l^{N_s}(k)$ and picking the $M-1$ eigenvectors corresponding to the lowest eigenvalues of this matrix.

The CADPD algorithm shown in Eq. (38) is named after another well-known branch in the field of signal array processing called AOA estimation since it can be viewed as a modified version of the Cyclic MUSIC ([6], [17]) used for AOA estimation. However, instead of the conventional AOA optimization applied in the case of Cyclic MUSIC, the CADPD performs its optimization over another parameter of the SOI, the transmitter location. Furthermore, this replacement is possible due to the centralized nature of the CADPD algorithm or specifically, due to the extension of the single base station model considered in the conventional AOA estimation to a multiple base stations model in which the location estimate is obtained using all base stations together.

3.2.3 The CTDPD Estimator

Unlike the CADPD estimator, the CTDPD extracts its information about the transmitter location from another property of the SOI which is the signal propagation delay, $\tau_l(\boldsymbol{p})$. We start the derivation by returning to Eq. (36) and observing that this relation holds for any base station, i.e., for any l. Furthermore, we notice that both sides of Eq. (36) depend on the base station while the scalar $e^{-j2\pi\alpha t_0}\overline{R}_{ss}^{\alpha,N_s}(k)$ on the right-hand side of this equation is a function of the single emitter only. Hence, we divide the nonzero eigenvalue of the l_1 th base station by the corresponding eigenvalue from the l_2 th base station

$$\frac{\hat{\lambda}_{l_1}}{\hat{\lambda}_{l_2}} \cong \frac{\left|b_{l_1}\right|^2}{\left|b_{l_2}\right|^2} e^{-j2\pi\alpha\left(\tau_{l_1}(\boldsymbol{p})-\tau_{l_2}(\boldsymbol{p})\right)}. \tag{39}$$

We observe that while both the magnitude and phase of the term on the left-hand side of Eq. (39) are known at the receiver, only the phase of the right-hand side can be exploited

by the estimator, as the path loss parameter of each base station, b_l, is assumed to be unknown. Therefore, the estimator may use only the phase of the eigenvalue quotient in Eq. (39), unless b_l is estimated for each base station first. Dividing Eq. (39) by the magnitude of its left-hand side yields

$$\frac{\hat{\lambda}_{l_1} / \hat{\lambda}_{l_2}}{\left|\hat{\lambda}_{l_1} / \hat{\lambda}_{l_2}\right|} \cong e^{-j2\pi\alpha\left(\tau_{l_1}(\boldsymbol{p})-\tau_{l_2}(\boldsymbol{p})\right)}. \tag{40}$$

Using the notation

$$\text{phase}\{x\} \equiv x/|x|,$$

the optimization problem can be formulated as the minimization of the following cost function

$$f_{CTDPD}(\boldsymbol{p}) \equiv \sum_{l_1,l_2} \left|\text{phase}\left\{\hat{\lambda}_{l_1} / \hat{\lambda}_{l_2}\right\} - e^{-j2\pi\alpha\left(\tau_{l_1}(\boldsymbol{p})-\tau_{l_2}(\boldsymbol{p})\right)}\right|^2, \tag{41}$$

where the summation in Eq. (41) is performed over all distinct ordered pairs of base stations denoted by the index set of $\{l_1, l_2\}$, and where according to Eq. (31), the quantity $e^{-j2\pi\alpha\left(\tau_{l_1}(\boldsymbol{p})-\tau_{l_2}(\boldsymbol{p})\right)}$ can be equivalently expressed as

$$e^{-j2\pi\alpha\left(\tau_{l_1}(\boldsymbol{p})-\tau_{l_2}(\boldsymbol{p})\right)} = \text{phase}\left\{\lambda_{l_1} / \lambda_{l_2}\right\}. \tag{42}$$

From now on, the cost function in Eq. (41) is referred to as the CTDPD part of the CDPD algorithm. This CTDPD estimator performs a summation of the absolute difference between the estimated and the exact phase of the eigenvalue quotient over all distinct base station pairs. As we already saw, the advantage of a cost function defined in terms of

phases such as the CTDPD method is the fact that no intermediate estimation is required for the path loss coefficient, b_l. Analogously to the CADPD estimator, the CTDPD is named after another conventional signal array processing branch, the TDOA estimation, as it utilizes a phased version of the SOI TDOA. Similarly to the CADPD, the optimization of the CTDPD estimator is carried out over all base stations simultaneously where the conventional optimization argument this time, the signal TDOA, is replaced with the SOI location. However, as opposed to the CADPD method which is a centralized version of the conventional Cyclic MUSIC, the CTDPD is a unique algorithm which is not an extension of any existing method.

3.2.4 The CDPD Estimator

In the last two subsections we derived the cost function of the two estimators which constitute the CDPD algorithm. We now merge these two algorithms into a single cost function. The cost function of the CDPD, $f_{CDPD}(\boldsymbol{p})$, is expressed as a weighted sum of the cost functions of the CADPD and CTDPD given in Eqs. (38) and (41)

$$f_{CDPD}(\boldsymbol{p}) \equiv w_1 f_{CADPD}(\boldsymbol{p}) + w_2 f_{CTDPD}(\boldsymbol{p}) . \tag{43}$$

The weights in Eq. (43) should be determined in order to attain the cost function with the best performance, in the sense that minimizing this cost function results in the minimal MSE of the location estimate. These weights depend on the performance of each of the two estimators constructing the weighted sum of Eq. (43) but also on the transmitter location itself. Since we are mostly interested in the best performance obtained by averaging the MSE over all locations, we have performed extensive Monte Carlo

simulations in which several weight sets were put to the test. According to these simulations, we have found empirically that equal weighting of the two cost functions in Eq. (43) leads to the best total performance of the CDPD estimator. Without loss of generality we thus set both w_1 and w_2 to be 1 so that Eq. (43) reads

$$f_{CDPD}(\boldsymbol{p}) \equiv f_{CADPD}(\boldsymbol{p}) + f_{CTDPD}(\boldsymbol{p}). \tag{44}$$

Hence, the CDPD algorithm finds the position $\boldsymbol{p}$, which minimizes the cost function given in Eq. (44). Clearly, this minimization requires only a *D*-dimensional search. Furthermore, while the conventional DPD needs the entire data batch from the *L* base stations to be transferred into the central processing unit, the CDPD algorithm requires only the nonzero eigenvalue and the noise eigen-subspace obtained in each base station.

3.3 Optimal Lag Choice for $R^{\alpha}_{r_i r_l}(k)$

Till now, the lag parameter, *k*, of the cyclic autocorrelation matrix of the received vector in Eq. (24) was not set to a certain value and assumed to be any integer value. However, it is clear that an appropriate choice for this parameter can improve the algorithm performance while improper setting may severely degrade the last.

As was explained in Section 1.2, the cyclic autocorrelation function and the conventional one have a different behavior in the aspect of their lag parameter. While the magnitude of the conventional autocorrelation function always gains its pick at a lag of $k = 0$ no matter what the signal properties and shape are, the magnitude of the cyclic autocorrelation function often peaks at $k \neq 0$. Thus, the cyclic autocorrelation function does not have a

fixed lag parameter maximizing its magnitude and this value is highly dependent on the signal properties.

In order to demonstrate the dependency of the cyclic autocorrelation function on its lag parameter we shall now examine two different types of signals. The first is a BPSK signal modulated by a rectangular pulse shape while the other is also a BPSK signal shaped this time by a square root raised cosine waveform. In addition, each of the signals is assumed to be over sampled with an over-sampling factor of 8. Clearly, the signal with the rectangular shaping is impractical in real life systems since it has relatively large sidelobes as opposed to the second signal. However, these two kinds of signals were chosen in order to illustrate the different properties of the cyclic autocorrelation function induced by the different signal characteristics. In terms of performance, the most material difference between the two cyclic autocorrelation functions lies in their magnitude which is depicted in Figure 1 and Figure 2.

We observe from these figures that the magnitude of the cyclic autocorrelation function of the rectangular BPSK signal is zero for a zero lag and peaks at a lag equal to half of the over-sampling factor, whereas for the square root raised cosine signal, this magnitude peaks at a zero lag and is a monotonic decreasing function of the lag in the given range. This substantial difference between the magnitudes can be explained as follows. A BPSK signal with a rectangular pulse shape is a constant modulus signal. The cyclic autocorrelation function of a constant modulus signal at a zero lag reduces to a summation over the unity circle of exponential terms with a fixed phase difference between them, which is obviously zero.

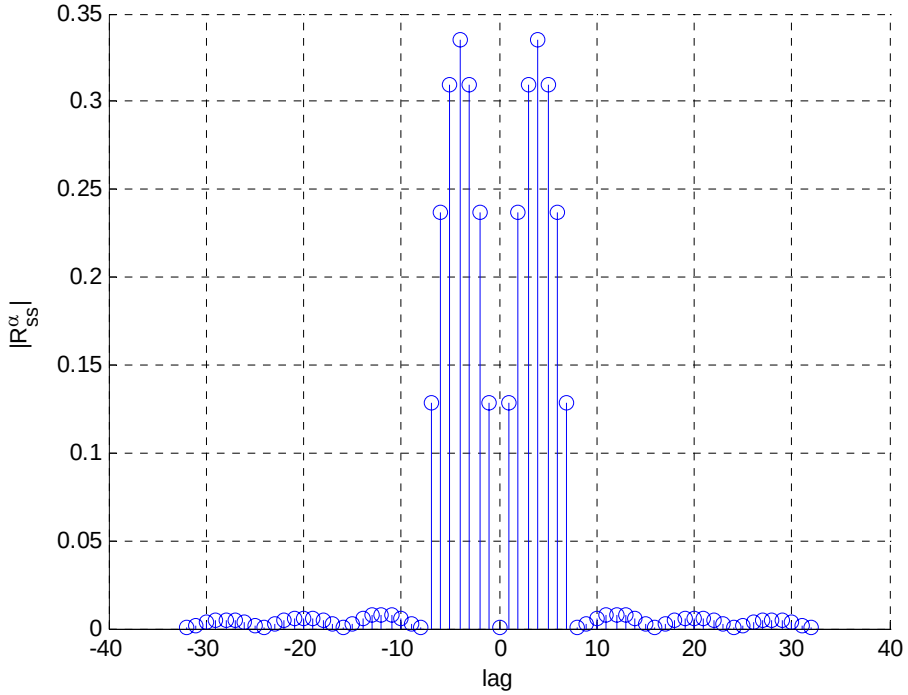

Figure 1. Magnitude of a cyclic autocorrelation function of a BPSK signal shaped by a rectangular waveform.

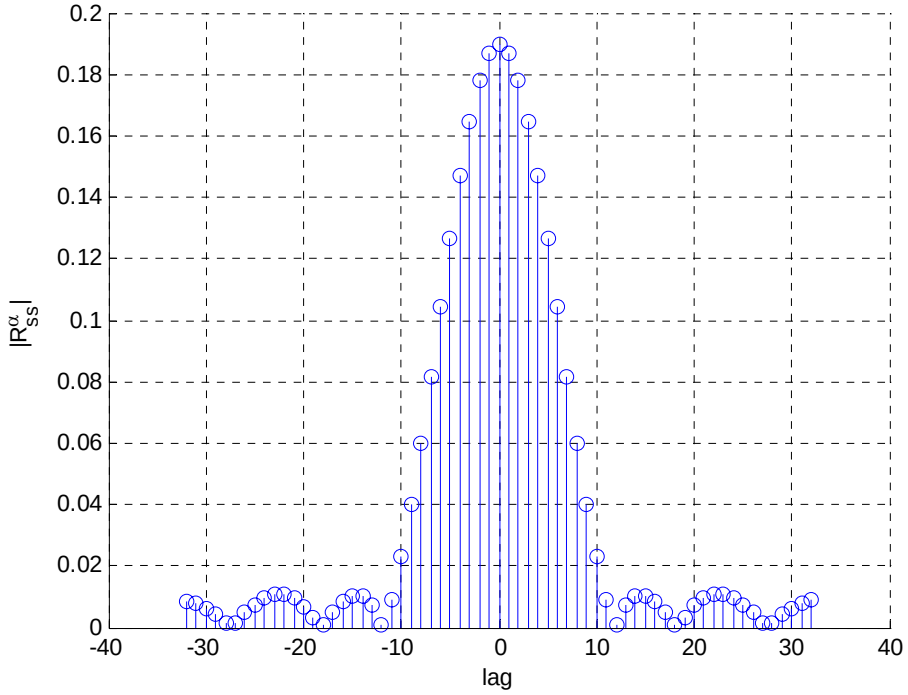

Figure 2. Magnitude of a cyclic autocorrelation function of a BPSK signal shaped by a square root raised cosine waveform.

On the contrary, a square root raised cosine waveform is not a constant modulus signal and gains its maximum magnitude of the cyclic autocorrelation function when all of its phases are aligned, that is, at a zero lag.

Next, we recall that our work deals only with narrowband signals such as raised cosine and squared root raised cosine. Therefore, when a single lag coefficient is considered then in order to maximize the magnitude of the cyclic autocorrelation function of the SOI, $R_{ss}^{\alpha}(k)$, here onwards we set the lag parameter k of $R_{r_i r_l}^{\alpha}(k)$ from Eq. (24) to be zero.

3.4 The Multiple Lag Version of the CDPD Estimator

The previous section was dedicated to the choice of the optimal lag for the cyclic autocorrelation matrix assuming that a single lag coefficient participates in the estimation process. However, this procedure is obviously sub optimal as exploiting more lag coefficients may improve the algorithm performance, since these extra coefficients convey additional information. In order to extend the CDPD, obtained thus far for a single lag parameter, to take into consideration more lag coefficients, we revisit the derivation of the two estimators which constitute this algorithm, namely, the CADPD and CTDPD and introduce their extended counterparts. Then, the multiple lag version of the CDPD method is a straightforward result.

First, we revisit the cost function of the CADPD algorithm given in Eq. (38), where we realize that this cost function utilizes the noise subspace obtained for a given lag choice. That is, $E_n(l)$, although not written explicitly, is a function of the specific lag parameter picked for the empirical version of the cyclic autocorrelation matrix of the received

vector, $\overline{R}_l^{N_s}(k)$. Yet, since Eq. (37) holds for any lag choice, i.e., for any k, we may extend the cost function of Eq. (38) as follows

$$f_{CADPD}^{K}(\boldsymbol{p}) \equiv \sum_{l=1}^{L}\sum_{k=0}^{K-1}\left\|E_n^H(l,k)\boldsymbol{a}_l(\boldsymbol{p})\right\|^2, \tag{45}$$

where the notation $E_n(l)$ from Eq. (38) was replaced with $E_n(l,k)$ in order to underline the dependence of the noise sub space on the lag parameter, and K represents the total number of lag parameters used in the estimation. This parameter is of course a function of the tradeoff between the complexity of the algorithm and the desired performance enhancement. Setting K to a relatively large number entails estimating the cyclic autocorrelation matrix for many lags and applying an SVD procedure to each one of these estimates. Thus, this performance enhancement does not come without a cost which might be sometimes rather high.

Eq. (45) suggests some improvement to the original algorithm given in Eq. (38). However, we can further streamline the former if we note from the previous section that for narrowband signals, the cyclic correlation between two samples is stronger when the lag is smaller. Thus, a weighted averaging between the lags rather than an equally-weighted one as shown in Eq. (45) should exhibit better performance. Applying such averaging to Eq. (45) yields,

$$f_{CADPD}^{K}(\boldsymbol{p}) \equiv \sum_{l=1}^{L}\sum_{k=0}^{K-1}\frac{1}{k+1}\left\|E_n^H(l,k)\boldsymbol{a}_l(\boldsymbol{p})\right\|^2. \tag{46}$$

Next, we return to the CTDPD algorithm and do much of the same we did for the CADPD. First, we recall that similarly to the noise subspace of the CADPD algorithm,

the nonzero eigenvalues appear in the cost function of the CTDPD in Eq. (41) are obtained for a certain lag parameter choice. Furthermore, since this cost function is based on the relation given in Eq. (40) which is true for any lag choice, we generalize the cost function of the CTDPD estimator to several coefficients in the following manner

$$f_{CTDPD}^{K}(\boldsymbol{p}) \equiv \sum_{l_1,l_2}\sum_{k=0}^{K-1}\frac{1}{k+1}\left|\text{phase}\left\{\hat{\lambda}_{l_1}(k)\big/\hat{\lambda}_{l_2}(k)\right\}-e^{-j2\pi\alpha\left(\tau_{l_1}(\boldsymbol{p})-\tau_{l_2}(\boldsymbol{p})\right)}\right|^2, \tag{47}$$

where we used exactly the same weighting as in the case of the CADPD estimator.

Finally, the multiple lag version of the CDPD is given as a sum of the two extended versions of the CADPD and CTDPD, expressed in Eqs. (46) and (47), respectively

$$f_{CDPD}^{K}(\boldsymbol{p}) \equiv f_{CADPD}^{K}(\boldsymbol{p}) + f_{CTDPD}^{K}(\boldsymbol{p}). \tag{48}$$

Clearly, the multiple lag versions of these three considered algorithms given in Eqs. (46)-(48) can be reduced to their original versions by setting K to 1. In the simulation results part given in Chapter 6, we will examine the performance of both the single lag-based estimators and their multiple lag counterparts.

3.5 The Ambiguity Problem of the CTDPD Estimator

We have already seen that the CDPD algorithm in Eq. (44) is actually a combination of two estimators. The first one called CADPD, given in Eq. (38), is a centralized version of a Cyclic AOA while the second, CTDPD, from Eq. (41) is a centralized version of a modified Cyclic TDOA, in the sense that this is a phased version of the last. This section introduces the major drawback of the CTDPD estimator which is ascribed to the inherent ambiguity problem this estimator suffers from. This ambiguity means that there may exist

location coordinates, other than the true ones, resulting in small values of the cost function in Eq. (41). We first explain the cause for the existence of this problem and demonstrate its behavior in terms of the signal-to-noise ratio (SNR) and baud rate. Finally, we conclude this section with the implications of the CTDPD ambiguity on the performance of the CDPD estimator.

3.5.1 Conditions for Ambiguity

The CTDPD given in Eq. (41) is based on finding the minimum phase difference between two terms, namely, the estimated and true eigenvalue quotient. Since any phase term has an ambiguity of 2π radians it readily follows that a cost function based on calculating a phase difference may incur an ambiguity in the estimated emitter location. In order to further formulate this intuition we note that α in Eq. (41) is the baseband SOI baud rate so that its wavelength is given by

$$\lambda_{BB} = \frac{c}{\alpha}, \tag{49}$$

where c is the propagation speed. In addition, $\tau_l(\boldsymbol{p})$ in the same equation is the time delay between the lth base station located at $\boldsymbol{q}_l$ and the transmitter located at position $\boldsymbol{p}$. Therefore, $\tau_l(\boldsymbol{p})$ can be expressed as

$$\tau_l(\boldsymbol{p}) = \left\|\boldsymbol{q}_l - \boldsymbol{p}\right\| / c\,. \tag{50}$$

Using the above-mentioned notation, the exponential term in Eq. (41) can be written as

$$e^{-j\frac{2\pi\alpha}{c}\left(\left\|\boldsymbol{q}_{l_1}-\boldsymbol{p}\right\|-\left\|\boldsymbol{q}_{l_2}-\boldsymbol{p}\right\|\right)}. \tag{51}$$

Now, ambiguity in the exponential term of Eq. (51) occurs when there exist positions $\widetilde{\boldsymbol{p}} \neq \boldsymbol{p}$ such that

$$e^{-j\frac{2\pi\alpha}{c}\left(\left\|\boldsymbol{q}_{l_1}-\widetilde{\boldsymbol{p}}\right\|-\left\|\boldsymbol{q}_{l_2}-\widetilde{\boldsymbol{p}}\right\|\right)} = e^{-j\frac{2\pi\alpha}{c}\left(\left\|\boldsymbol{q}_{l_1}-\boldsymbol{p}\right\|-\left\|\boldsymbol{q}_{l_2}-\boldsymbol{p}\right\|\right)} \ , \forall l_1, l_2 \ . \tag{52}$$

This happens if the following condition is met

$$\left\|\boldsymbol{q}_{l_1}-\widetilde{\boldsymbol{p}}\right\|-\left\|\boldsymbol{q}_{l_2}-\widetilde{\boldsymbol{p}}\right\| = \left\|\boldsymbol{q}_{l_1}-\boldsymbol{p}\right\|-\left\|\boldsymbol{q}_{l_2}-\boldsymbol{p}\right\| + k\lambda_{BB} \ , \forall l_1, l_2 \ , \tag{53}$$

where k is an integer.

Furthermore, if we want to guarantee that no ambiguity occurs, the phase difference associated with any pair of base stations must not exceed π. Specifically, the following condition should hold

$$\left|\Delta\tau_{1,2}\right| \equiv \left|\tau_{l_1}(\boldsymbol{p})-\tau_{l_2}(\boldsymbol{p})\right| = \frac{1}{c}\left|\left\|\boldsymbol{q}_{l_1}-\boldsymbol{p}\right\|-\left\|\boldsymbol{q}_{l_2}-\boldsymbol{p}\right\|\right| < \frac{1}{2\alpha} \ , \forall l_1, l_2, \forall \boldsymbol{p} \in \boldsymbol{P} \ , \tag{54}$$

where $\boldsymbol{P}$ is the set of all points within the search area. Equivalently, Eq. (54) can be expressed as

$$\left|\left\|\boldsymbol{q}_{l_1}-\boldsymbol{p}\right\|-\left\|\boldsymbol{q}_{l_2}-\boldsymbol{p}\right\|\right| < \frac{\lambda_{BB}}{2} \ , \forall l_1, l_2, \forall \boldsymbol{p} \in \boldsymbol{P} \ . \tag{55}$$

The conditions shown in Eqs. (53) and (55) imply that location ambiguity exists in integral multiples of the baseband wavelength, λ_{BB}, and that this problem does not depend on the SNR in which the system operates. Likewise, they suggest that this ambiguity depends on both the SOI wavelength and the system geometry, i.e., the deployment of the base stations and emitter. As long as the distance differences between the various base stations and the transmitter are relatively large compared to the SOI

wavelength, there are more cases in which the condition of Eq. (55) is not met, giving rise to ambiguity in the location estimation. However, when this ratio between the distance differences and the SOI wavelength is rather small, the condition of Eq. (55) may be satisfied so that the ambiguity in the estimates can be avoided.

3.5.2 Experimental Study

In order to study the behavior of the ambiguity problem of the CTDPD algorithm we depart to examine a scenario of a typical cellular system. In this system, we use a baud rate of 0.1 or 0.3 Msym/s as for instance, the data service evolution of the GSM (Global System for Mobile communications), namely, GPRS (General Packet Data Service) and EDGE (Enhanced Data rates for GSM Evolution) cellular technologies use a baud rate of 0.27 Msym/s. Therefore, in our simulations the baud duration, T, is around 0.1/0.3 us, respectively, which yields a baseband wavelength of around 3/1 km. In addition, the system considered herein maintains four base stations placed at the corners of a 4 km $\times$ 4 km square. It is first interesting to plot the contour diagram of the cost function in Eq. (41) for the case in which the emitter is located rather close to one of the base stations. Such a scenario induces relatively large distances between the emitter and the rest of the base stations. Thus, the condition of Eq. (55) is obviously not satisfied and ambiguity should appear. The contours of the cost function for such a case where the emitter is located at coordinates [3101, 2901] meters (marked by a blue asterisk) and the SNR is assumed to be 0 dB are shown in Figure 3. One can observe from this figure that the original contours around the true emitter position are accompanied by additional similar contours in the counter corner of the square. These additional contours are induced due to

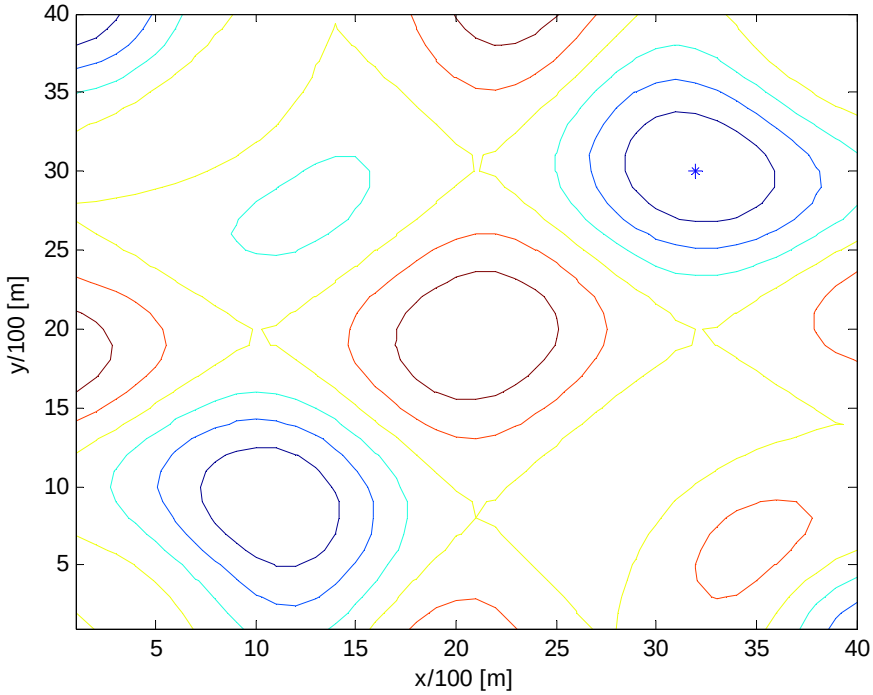

Figure 3. Contour plot of CTDPD for SOI located at [3101, 2901] meters, baud rate of 0.1 MHz, and 0 dB AWGN environment.

the symmetry between the true emitter location and the center of the ambiguous contours with respect to the square center. Specifically, we can see that the induced distances between the true and the ambiguous emitter position to the base stations located at the upper-left and the lower-right corners are much of the same while their distances from the other two base stations have a difference of a single wavelength. This difference results in the ambiguous emitter position as suggested by Eq. (53). When we turn, however, to examine an alternative emitter position, this time at the square center, a different contour plot is obtained as illustrated in Figure 4. This figure demonstrates that for a different location choice there is no ambiguous emitter position in the square area, since this location obeys Eq. (55). Indeed, we do notice the beginning of some contours that may yield ambiguity, however, they are obtained at the square edges and thus, this ambiguity

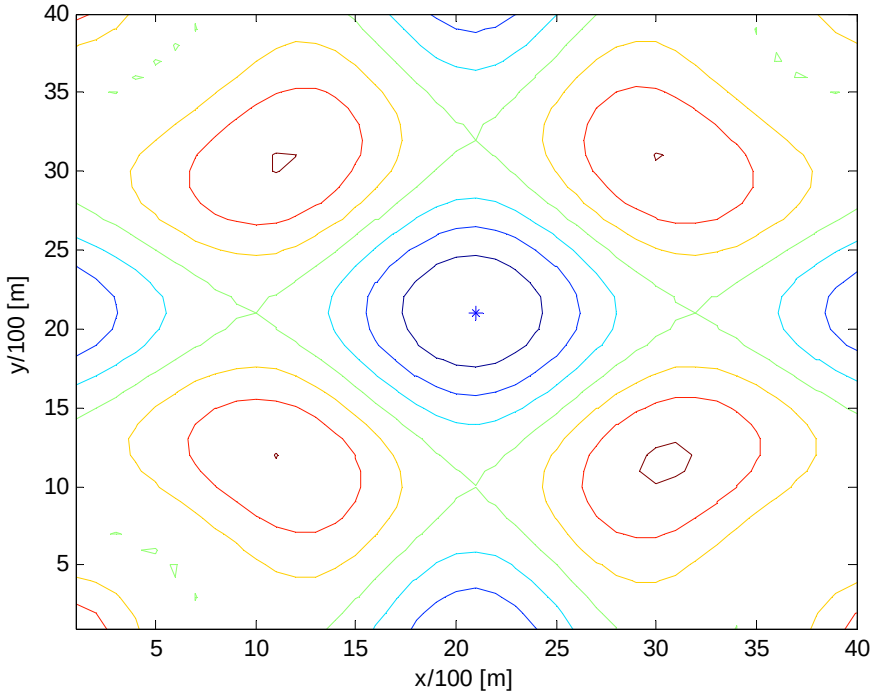

Figure 4. Contour plot of CTDPD for SOI located at [2001, 2001] meters, baud rate of 0.1 MHz, and 0 dB AWGN environment.

may appear in a wider range, outside the square limits.

Another dependency that should be tested is the influence of the SNR on the ambiguity problem. We argued earlier that the considered problem is not SNR dependent so that SNR by itself cannot conceal the ambiguous contours which lead to ambiguous location estimate. To the end of checking this argument, we revisit the scenario of Figure 3 with a slight difference of increasing the SNR to be 100 dB instead of 0 dB. The cost function contours obtained for this new test case are given in Figure 5. As expected, the contour plot remains more of the same for 100 dB AWGN environment as in 0 dB environment and the ambiguity problem is not mitigated. This empirical observation thus corroborates our analytical conclusion.

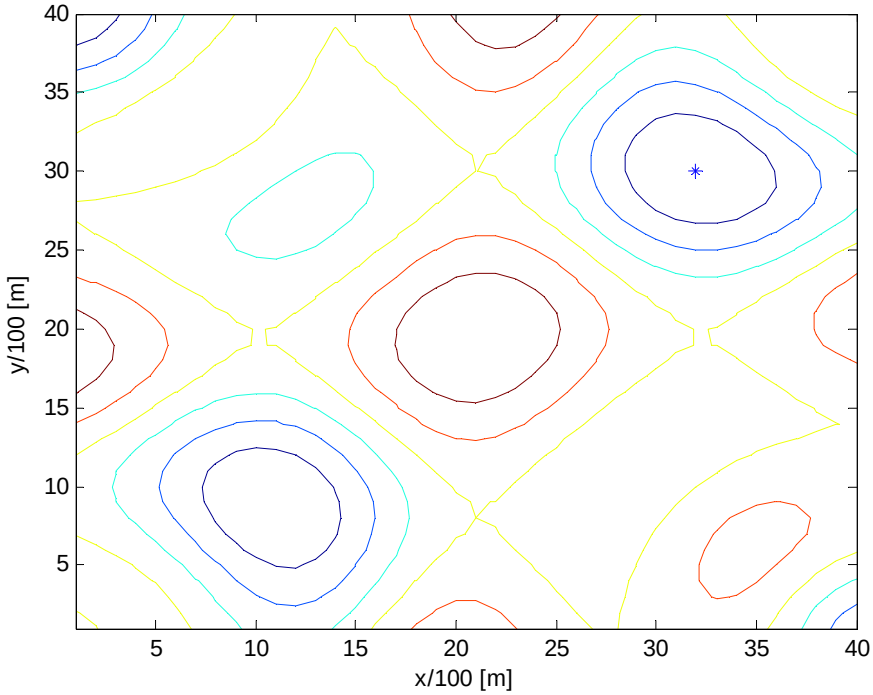

Figure 5. Contour plot of CTDPD for SOI located at [3101, 2901] meters, baud rate of 0.1 MHz, and 100 dB AWGN environment.

While the SNR is found to be irrelevant to the problem at hand, the SOI baud rate, or equivalently its wavelength, does play a major role in the contours behavior as demonstrated by Figure 6 and Figure 7. These figures depict the contours of the cost function for the same scenarios shown in Figure 3 and Figure 4, respectively, but this time the baud rate was tripled so that the SOI wavelength was three-fold smaller. We infer from the last two figures that the contours become much denser when the SOI wavelength is decreased and therefore the ambiguity problem is aggravated dramatically. This aggravation is ascribed to the fact that the smaller the wavelength, the harder is to satisfy Eq. (55). Equivalently, there are now more ambiguous locations, available within the square borders, which satisfy Eq. (53).

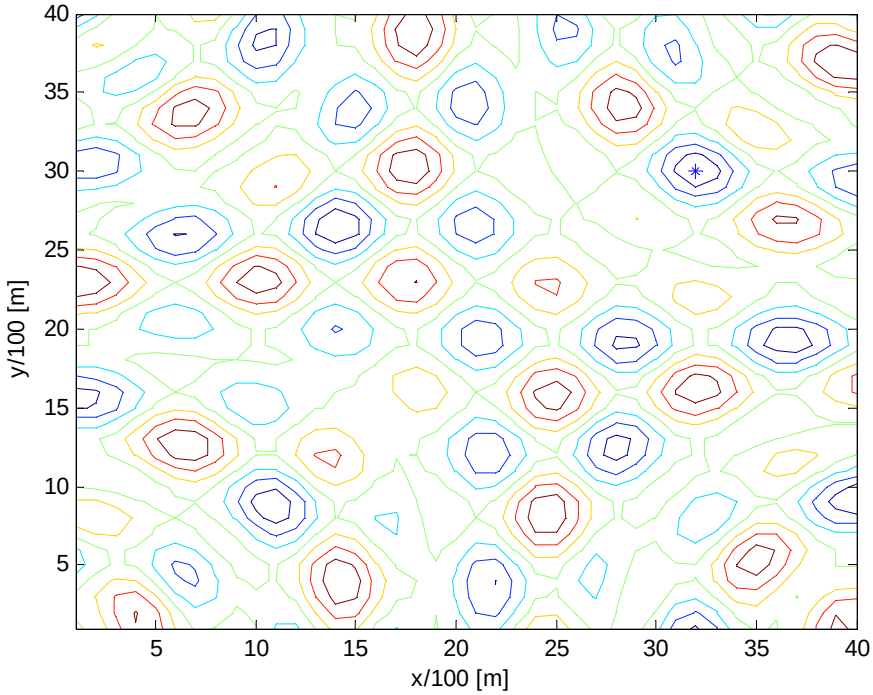

Figure 6. Contour plot of CTDPD for SOI located at [3101, 2901] meters, baud rate of 0.3 MHz, and 0 dB AWGN environment.

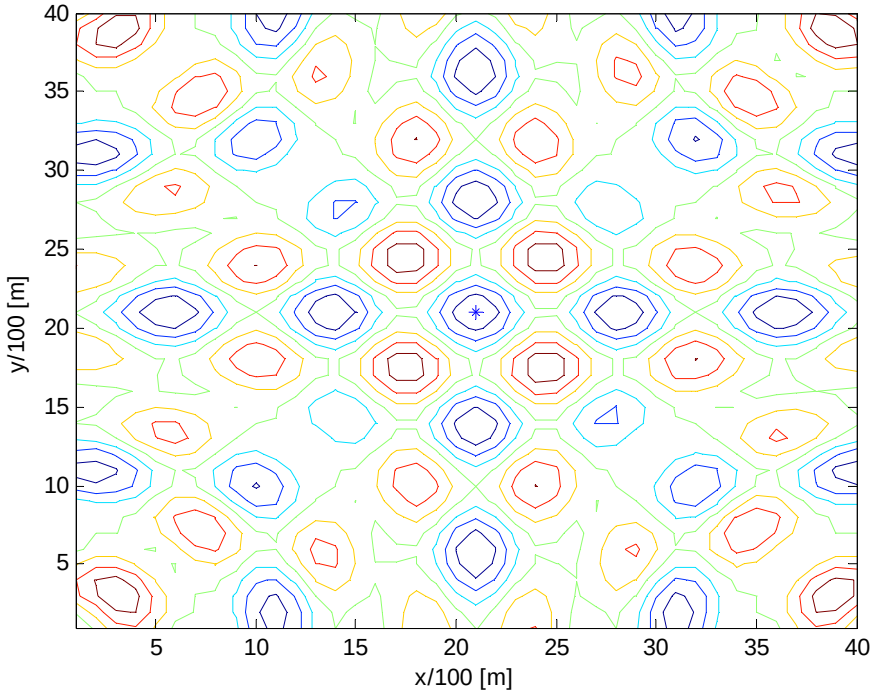

Figure 7. Contour plot of CTDPD for SOI located at [2001, 2001] meters, baud rate of 0.3 MHz, and 0 dB AWGN environment.

3.5.3 Implications of the CTDPD Ambiguity on the CDPD Estimator

When we turn to evaluate the practical consequences of the considered problem we should bear in mind that while the CTDPD estimator does suffer from ambiguity problem, the CDPD algorithm does not use this estimator alone but rather in conjunction with the CADPD algorithm as described in Eq. (44). Therefore, it is first necessary to examine the influence of the additional cost function on the contours obtained for the CDPD estimator. To this end, we revisit the scenarios of Figure 6 and Figure 7, and plot the contours of both the CADPD and CDPD estimators. These plots are given in Figure 8-Figure 11.

We observe from these two figure sets that as opposed to the CTDPD algorithm, the CADPD method enjoys monotonic decreasing contours around the true emitter position. Likewise, it is readily seen from these figures that the ambiguity problem is indeed resolved for the CDPD algorithm by combining the cost function of the CADPD with the one of the CTDPD. Thus, the final conclusion is that in general, the CDPD estimator does not share the problem of ambiguous location estimate. There may be, however, some rare cases obtained in a very low SNR environment in which ambiguity might crop up also for the CDPD estimator. For these cases the recommendation should be to perform first a coarse search over the square grid using the CADPD estimator alone. Then, after the search on the coarse grid has generated an initial location estimate, the CDPD can be applied in this neighborhood with a fine grid search.

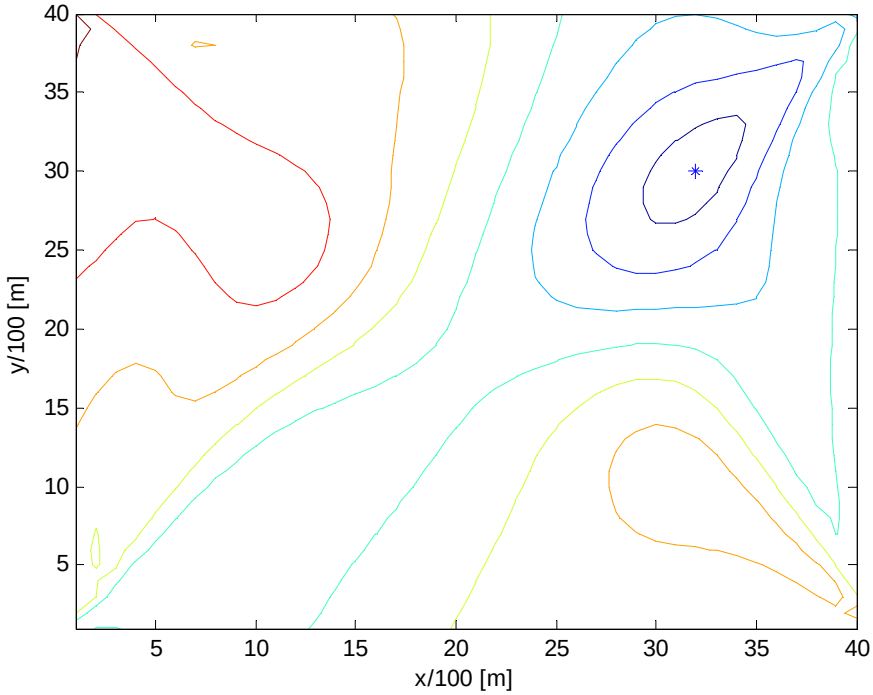

Figure 8. Contour plot of CADPD for SOI located at [3101, 2901] meters, baud rate of 0.3 MHz, and 0 dB AWGN environment.

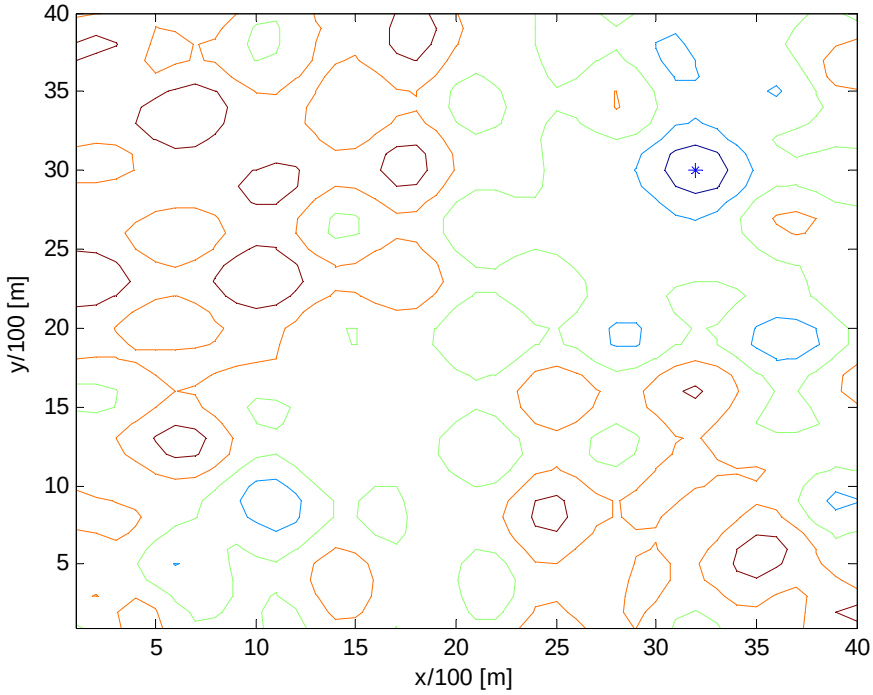

Figure 9. Contour plot of CDPD for SOI located at [3101, 2901] meters, baud rate of 0.3 MHz, and 0 dB AWGN environment.

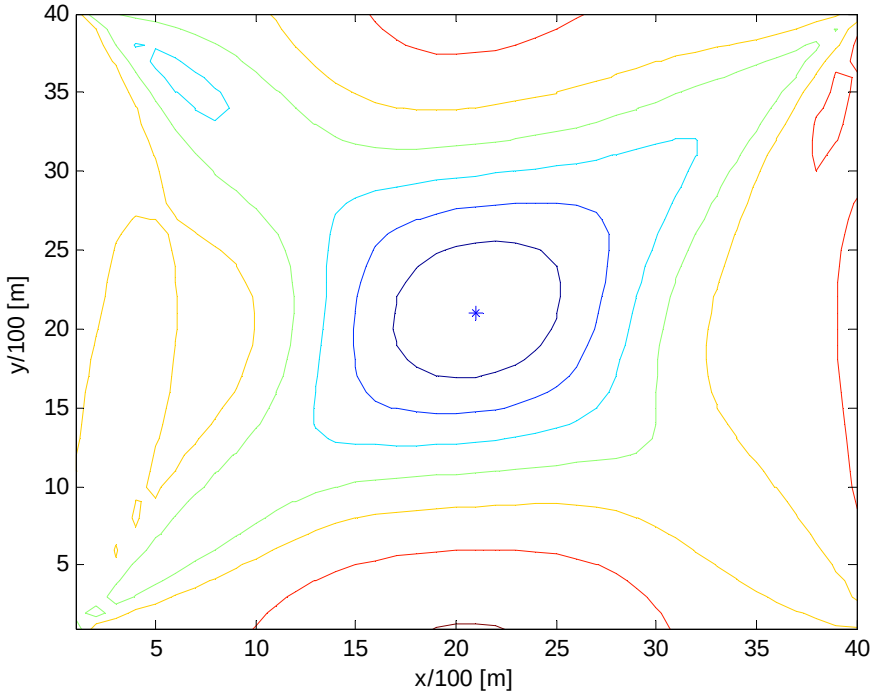

Figure 10. Contour plot of CADPD for SOI located at [2001, 2001] meters, baud rate of 0.3 MHz, and 0 dB AWGN environment.

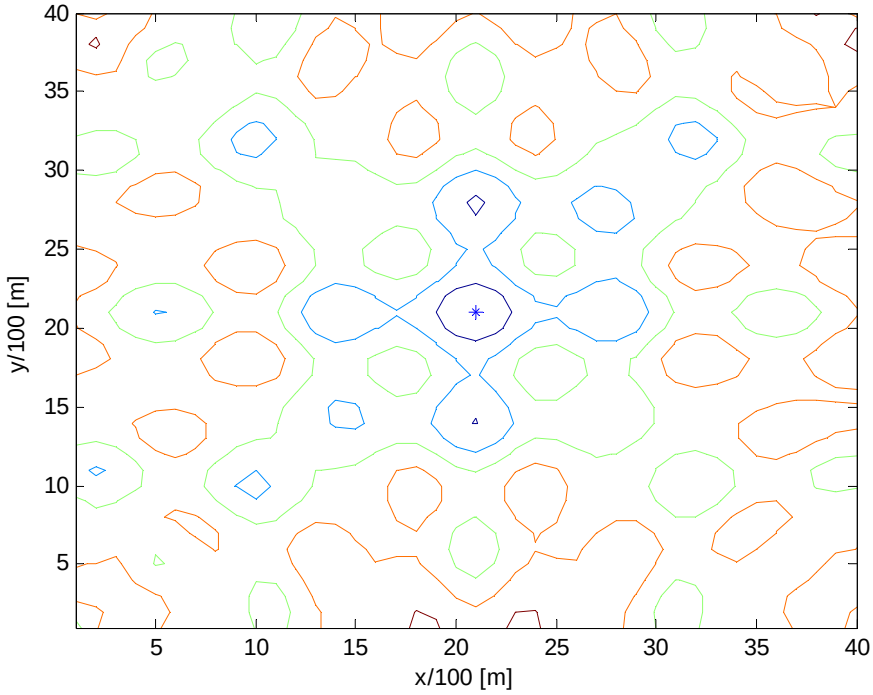

Figure 11. Contour plot of CDPD for SOI located at [2001, 2001] meters, baud rate of 0.3 MHz, and 0 dB AWGN environment.

4 Performance Analysis

4.1 Introduction

The most prevalent figure of merit for an estimator is its MSE which can be then compared to the standard benchmark for unbiased estimators – the CRLB. The goal of this chapter is hence to derive a closed-form expression for the MSE of the CDPD algorithm. The analytical expression obtained in this chapter can be used to predict the MSE of this algorithm without the need of simulations or experiments, under the assumption of small errors. Later, in the simulation results chapter the analytical performance is compared to the empirical one in order to demonstrate their compliance.

Before we start with the analysis itself we should first outline its content. We already saw in Chapter 3 that the CDPD algorithm is a combination of two estimators, the CADPD and CTDPD. The CADPD estimator is found to be a modified version of the conventional Cyclic MUSIC method where the optimization argument of the latter, namely the signal AOA, is replaced with the transmitter location and the optimization procedure in the case of CADPD is performed simultaneously over all base stations that participate in the estimation process. The performance of the conventional Cyclic MUSIC in the case of a Gaussian cyclostationary SOI was already studied by some papers (e.g., [16]). Clearly, the analysis derived in these papers cannot be applied directly to the CADPD algorithm since the estimated parameters are different for the two methods and the SOI in our study is assumed to be non Gaussian. However, due to the high resemblance between these two algorithms we skip the MSE derivation of the CADPD. Instead, this chapter will focus only on the performance analysis of the CTDPD estimator

which is not a modified version of an existing algorithm so that its performance analysis is obviously not available or can be deduced using some extensions.

In order to facilitate the performance analysis of the CTDPD algorithm, we assume that the transmitted signal, $s(k)$, is a BPSK signal with an arbitrary pulse shape, and treat the path loss coefficients merely as unknown parameters rather than RVs. Furthermore, we henceforth assume that the noise vector in each base station, $\boldsymbol{n}_l(k)$, consists only of a circular symmetric complex Gaussian noise which is spatially and temporally white, uncorrelated with the SOI, and with zero mean. In addition, the analysis introduced here is a small error analysis (SEA) based on sufficiently large observation time and high SNR. The consequence is that during the derivation, only first order terms of the noise will be handled while second or higher order terms will be neglected. Likewise, terms that are $o(N_s^{-1})$ will be neglected as well.

Since the cost function in Eq. (41) which is a summation of the phase difference between the estimated and the true eigenvalue quotient over all base stations is quite involved, the derivation of the CTDPD MSE will be split into several stages. We shall now outline the main contents of these stages:

- Section 4.2 obtains a simplified version, $\widetilde{f}(\boldsymbol{p})$, of the original cost function of Eq. (41). Similarly to the original cost function, $\widetilde{f}(\boldsymbol{p})$ is an explicit function of the estimated phase of the eigenvalue quotients from all of the base stations. Thereafter, the covariance matrix of the location error is expressed in terms of the first and second derivatives of $\widetilde{f}(\boldsymbol{p})$.

- In Section 4.3, the first and second derivatives of $\widetilde{f}(\boldsymbol{p})$ are calculated as a function of the estimated phase of the eigenvalue quotients.
- Section 4.4 computes the additive noise corrupting the estimated phase of the eigenvalue quotient of each base station pair so that the last is expressed as a sum of this noise and the true phase.
- Section 4.5 obtains an expression for the covariance matrix of the first derivative of $\widetilde{f}(\boldsymbol{p})$ in terms of the covariance of the phase error found in Section 4.4.
- Finally, Section 4.6 derives the covariance of the phase error found in Section 4.4 in terms of the system parameters. Afterwards, this covariance is substituted back into the covariance matrix of the location error obtained in Section 4.2 and a closed-form expression of the latter ensues.

4.2 Expression for the Error Covariance Matrix

We start by calculating the covariance matrix of the estimation error vector under the framework of SEA. This matrix is obtained in terms of the covariance of the first derivative of $f_{CTDPD}(\boldsymbol{p})$ which is defined in Eq. (41). Here onwards, for notational convenience, we will omit the subscript from the cost function name and will denote it simply by $f(\boldsymbol{p})$:

$$f(\boldsymbol{p}) = \sum_{l_1,l_2} \left| \text{phase}\left\{ \hat{\lambda}_{l_1} / \hat{\lambda}_{l_2} \right\} - e^{-j2\pi\alpha\left(\tau_{l_1}(\boldsymbol{p}) - \tau_{l_2}(\boldsymbol{p})\right)} \right|^2 .$$

Now the estimated emitter location, $\hat{\boldsymbol{p}}$ is obtained as the location $\boldsymbol{p}$ which minimizes the cost function $f(\boldsymbol{p})$. Thus, the first derivative of this cost function with respect to $\boldsymbol{p}$ should be zero when evaluated at $\hat{\boldsymbol{p}}$. That is

$$f'(\hat{\boldsymbol{p}}) = 0 . \tag{56}$$

Since $f(\boldsymbol{p})$ is a scalar function of a vector $\boldsymbol{p}$ then differentiating it with respect to this vector results in a vector also. Specifically, this derivative is given as

$$f'(\boldsymbol{p}) \equiv \left[\frac{\partial f(\boldsymbol{p})}{\partial \boldsymbol{p}_x}, \frac{\partial f(\boldsymbol{p})}{\partial \boldsymbol{p}_y} \right]^T , \tag{57}$$

where $\boldsymbol{p}_x$ and $\boldsymbol{p}_y$ are the x and y coordinates of $\boldsymbol{p}$, respectively, that is

$$\boldsymbol{p} \equiv \left[\boldsymbol{p}_x, \boldsymbol{p}_y \right]^T . \tag{58}$$

Next, we expand the left-hand side of Eq. (56) to a Taylor series around the true value of the emitter location which is denoted by $\boldsymbol{p}_0$ to avert ambiguous notation. Since the analysis is valid for small errors where the number of samples is sufficiently large and the system is operated in the high SNR regime then second and higher-order terms of the Taylor series expansion are considered as a residual term and can be neglected. Thus, we are left with a first order expansion that yields the following approximation

$$f'(\boldsymbol{p}_0) \cong -f''(\boldsymbol{p}_0) \cdot \boldsymbol{\varepsilon}_p , \tag{59}$$

where $\boldsymbol{\varepsilon}_p$ is the vector of estimation error defined as

$$\boldsymbol{\varepsilon}_{\boldsymbol{p}} \equiv \hat{\boldsymbol{p}} - \boldsymbol{p}_0 \,, \tag{60}$$

and where the second derivative of $f(\boldsymbol{p})$ w.r.t. $\boldsymbol{p}$ equals the following Hessian matrix

$$f''(\boldsymbol{p}) \equiv \begin{bmatrix} \dfrac{\partial^2 f(\boldsymbol{p})}{\partial \boldsymbol{p}_x^2} & \dfrac{\partial^2 f(\boldsymbol{p})}{\partial \boldsymbol{p}_x \partial \boldsymbol{p}_y} \\ \dfrac{\partial^2 f(\boldsymbol{p})}{\partial \boldsymbol{p}_x \partial \boldsymbol{p}_y} & \dfrac{\partial^2 f(\boldsymbol{p})}{\partial \boldsymbol{p}_y^2} \end{bmatrix}. \tag{61}$$

We now rewrite Eq. (59) as follows

$$f'(\boldsymbol{p}_0) \cong -f''(\boldsymbol{p}_0)\big|_{\hat{\lambda}_l = \lambda_l} \cdot \boldsymbol{\varepsilon}_{\boldsymbol{p}} - \left[f''(\boldsymbol{p}_0) - f''(\boldsymbol{p}_0)\big|_{\hat{\lambda}_l = \lambda_l} \right] \cdot \boldsymbol{\varepsilon}_{\boldsymbol{p}} \,. \tag{62}$$

Since $\left[f''(\boldsymbol{p}_0) - f''(\boldsymbol{p}_0)\big|_{\hat{\lambda}_l = \lambda_l} \right] \cdot \boldsymbol{\varepsilon}_{\boldsymbol{p}}$ is actually a second order noise term and can be thus neglected then Eq. (62) boils down to

$$f'(\boldsymbol{p}_0) \cong -f''(\boldsymbol{p}_0)\big|_{\hat{\lambda}_l = \lambda_l} \cdot \boldsymbol{\varepsilon}_{\boldsymbol{p}} \,. \tag{63}$$

Therefore, the estimation error $\boldsymbol{\varepsilon}_{\boldsymbol{p}}$ can be finally approximated as

$$\boldsymbol{\varepsilon}_{\boldsymbol{p}} \cong -\left[f''(\boldsymbol{p}_0)\big|_{\hat{\lambda}_l = \lambda_l} \right]^{-1} \cdot f'(\boldsymbol{p}_0) \,. \tag{64}$$

Consequently, the covariance matrix of the estimation error takes the form

$$E\left\{ \boldsymbol{\varepsilon}_{\boldsymbol{p}} \boldsymbol{\varepsilon}_{\boldsymbol{p}}^H \right\} \cong \left[f''(\boldsymbol{p}_0)\big|_{\hat{\lambda}_l = \lambda_l} \right]^{-1} \cdot E\left\{ f'(\boldsymbol{p}_0) \cdot f'(\boldsymbol{p}_0)^T \right\} \cdot \left[f''(\boldsymbol{p}_0)\big|_{\hat{\lambda}_l = \lambda_l} \right]^{-1}, \tag{65}$$

where in Eq. (65) we used both that $f(\boldsymbol{p})$ and hence also its derivatives are all real-valued functions and that $f''(\boldsymbol{p})\big|_{\hat{\lambda}_l = \lambda_l}$ is a Hessian matrix and therefore Hermitian in general and symmetric in particular.

Before evaluating the terms on the right-hand side of Eq. (65) we shall first introduce some simplifications to the original cost function, $f(\boldsymbol{p})$. Applying some simple algebraic manipulations to this cost function yields

$$\begin{aligned} f(\boldsymbol{p}) = \sum_{l_1,l_2} 2 - e^{j2\pi\alpha\left(\tau_{l_1}(\boldsymbol{p})-\tau_{l_2}(\boldsymbol{p})\right)} \cdot \text{phase}\left\{\hat{\lambda}_{l_1} / \hat{\lambda}_{l_2}\right\} \\ - e^{-j2\pi\alpha\left(\tau_{l_1}(\boldsymbol{p})-\tau_{l_2}(\boldsymbol{p})\right)} \cdot \text{phase}^{*}\left\{\hat{\lambda}_{l_1} / \hat{\lambda}_{l_2}\right\}. \end{aligned} \tag{66}$$

It is clear that the minimization of $f(\boldsymbol{p})$ from Eq. (66) is equivalent to the maximization of the following cost function

$$\widetilde{f}(\boldsymbol{p}) = \sum_{l_1,l_2} \text{Re}\left\{e^{j2\pi\alpha\left(\tau_{l_1}(\boldsymbol{p})-\tau_{l_2}(\boldsymbol{p})\right)} \cdot \text{phase}\left\{\hat{\lambda}_{l_1} / \hat{\lambda}_{l_2}\right\}\right\}. \tag{67}$$

Now, since all of the formulation obtained so far for the original cost function, $f(\boldsymbol{p})$ holds also for the modified cost function, $\widetilde{f}(\boldsymbol{p})$ (up to negation) then the covariance matrix of the estimation error can be expressed instead as

$$E\left\{\boldsymbol{\varepsilon}_{\boldsymbol{p}}\boldsymbol{\varepsilon}_{\boldsymbol{p}}^{H}\right\} \cong \left[\widetilde{f}''(\boldsymbol{p}_0)\Big|_{\hat{\lambda}_l=\lambda_l}\right]^{-1} \cdot E\left\{\widetilde{f}'(\boldsymbol{p}_0)\cdot\widetilde{f}'(\boldsymbol{p}_0)^{T}\right\}\cdot\left[\widetilde{f}''(\boldsymbol{p}_0)\Big|_{\hat{\lambda}_l=\lambda_l}\right]^{-1}. \tag{68}$$

In order to complete the SEA we need to obtain a closed-form expression for the terms on the right-hand side of Eq. (68). For these expressions we shall first need to compute the derivatives of the modified cost function, $\widetilde{f}(\boldsymbol{p})$ with respect to the emitter position, $\boldsymbol{p}$. These derivatives are given hereby.

4.3 Expression for the Derivatives of $\widetilde{f}(\boldsymbol{p})$

Taking the first and second derivatives of Eq. (67) with respect to the transmitter location, $\boldsymbol{p}$, yields

$$\widetilde{f}'(\boldsymbol{p}) = -2\pi\alpha \sum_{l_1,l_2} \left(\tau'_{l_1}(\boldsymbol{p}) - \tau'_{l_2}(\boldsymbol{p})\right) \cdot \mathrm{Im}\left\{ e^{j2\pi\alpha\left(\tau_{l_1}(\boldsymbol{p}) - \tau_{l_2}(\boldsymbol{p})\right)} \cdot \mathrm{phase}\left\{ \hat{\lambda}_{l_1} / \hat{\lambda}_{l_2} \right\} \right\}, \tag{69}$$

and

$$\begin{aligned} \widetilde{f}''(\boldsymbol{p}) = -2\pi\alpha \sum_{l_1,l_2} \Big[& \mathrm{Im}\left\{ e^{j2\pi\alpha\left(\tau_{l_1}(\boldsymbol{p}) - \tau_{l_2}(\boldsymbol{p})\right)} \cdot \mathrm{phase}\left\{ \hat{\lambda}_{l_1} / \hat{\lambda}_{l_2} \right\} \right\} \cdot \left(\tau''_{l_1}(\boldsymbol{p}) - \tau''_{l_2}(\boldsymbol{p})\right) \\ & + 2\pi\alpha \cdot \mathrm{Re}\left\{ e^{j2\pi\alpha\left(\tau_{l_1}(\boldsymbol{p}) - \tau_{l_2}(\boldsymbol{p})\right)} \cdot \mathrm{phase}\left\{ \hat{\lambda}_{l_1} / \hat{\lambda}_{l_2} \right\} \right\} \cdot \Gamma_{l_1 l_2, l_1 l_2}(\boldsymbol{p}) \Big], \end{aligned} \tag{70}$$

where

$$\Gamma_{l_1 l_2, l_3 l_4}(\boldsymbol{p}) \equiv \left(\tau'_{l_1}(\boldsymbol{p}) - \tau'_{l_2}(\boldsymbol{p})\right) \cdot \left(\tau'_{l_3}(\boldsymbol{p}) - \tau'_{l_4}(\boldsymbol{p})\right)^T . \tag{71}$$

Next, we observe that the derivative terms in Eq. (68) are evaluated at the true emitter position, $\boldsymbol{p}_0$ and that in the case of the second derivative we should also replace the estimated phase with the true one. First, setting $\boldsymbol{p}$ to be $\boldsymbol{p}_0$ for both derivatives, then combining Eq. (42), and finally replacing $\mathrm{phase}\left\{ \hat{\lambda}_{l_1} / \hat{\lambda}_{l_2} \right\}$ with $\mathrm{phase}\left\{ \lambda_{l_1} / \lambda_{l_2} \right\}$ in the second derivative, results

$$\widetilde{f}'(\boldsymbol{p}_0) = -2\pi\alpha \sum_{l_1,l_2} \mathrm{Im}\left\{ \mathrm{phase}\left\{ \lambda_{l_2} / \lambda_{l_1} \right\} \cdot \mathrm{phase}\left\{ \hat{\lambda}_{l_1} / \hat{\lambda}_{l_2} \right\} \right\} \cdot \left(\tau'_{l_1}(\boldsymbol{p}_0) - \tau'_{l_2}(\boldsymbol{p}_0)\right), \tag{72}$$

and

$$\widetilde{f}''(\boldsymbol{p}_0)\Big|_{\hat{\lambda}_l=\lambda_l} = -4\pi^2\alpha^2 \sum_{l_1,l_2} \Gamma_{l_1 l_2, l_1 l_2}(\boldsymbol{p}_0)\,. \tag{73}$$

We conclude from Eq. (72) that our next step should be obtaining an expression for the estimated phase of the eigenvalue quotient in terms of the true phase. This derivation is carried out in the next section.

4.4 Expression for the Phase Error of the Eigenvalue Quotient

4.4.1 Introduction

In this section, we derive a closed-form expression for the additive noise corrupting the phase of the eigenvalue quotient in Eq. (41). Clearly, in the asymptotic case, where the number of samples is arbitrarily large, the estimated eigenvalue quotient coincides with the theoretical one at the true emitter location so that the cost function in Eq. (41) reduces to zero. However, in the presence of finite number of samples the noise does not vanish any longer, and thus there is some difference between the estimated and theoretical eigenvalue quotient. The aim of this section is to develop an expression for this difference. To this end, we first obtain a SEA expression for the estimated nonzero eigenvalue in each base station. Then, we compute a SEA term for the estimated eigenvalue quotient of a base station pair, and finally, we calculate the real and imaginary parts of this eigenvalue quotient from which we eventually produce both its magnitude and phase.

4.4.2 Expression for the Eigenvalue Quotient

In this subsection, we provide an expression for the estimate of the single nonzero eigenvalue of $\overline{R}^{\alpha}_{\boldsymbol{r}_l\boldsymbol{r}_l}(k)$ in terms of the corresponding actual eigenvalue. We recall that the estimated nonzero eigenvalue was obtained as the trace of $\overline{R}^{N_s}_{l}(k)$, the estimated cyclic autocorrelation matrix of the received signal at the *l*th base station. For convenience, we revisit the definition of this matrix from Eq. (33)

$$\overline{R}^{N_s}_{l}(k) \equiv \overline{R}^{\alpha,N_s}_{\boldsymbol{r}_l\boldsymbol{r}_l}(k) .$$

The received signal $\boldsymbol{r}_l(k)$ is corrupted by the additive noise $\boldsymbol{n}_l(k)$ as described in Eq. (21), so that $\overline{R}^{N_s}_{l}(k)$ can be expressed as follows

$$\begin{aligned}\overline{R}^{N_s}_{l}(k) = {} & |b_l|^2 \boldsymbol{a}_l(\boldsymbol{p})\boldsymbol{a}_l^H(\boldsymbol{p})\overline{R}^{\alpha,N_s}_{s_l s_l}(k) + b_l \boldsymbol{a}_l(\boldsymbol{p})\overline{R}^{\alpha,N_s}_{s_l \boldsymbol{n}_l}(k) \\ & + b_l^* \overline{R}^{\alpha,N_s}_{\boldsymbol{n}_l s_l}(k)\boldsymbol{a}_l^H(\boldsymbol{p}) + \overline{R}^{\alpha,N_s}_{\boldsymbol{n}_l \boldsymbol{n}_l}(k) .\end{aligned} \tag{74}$$

The nonzero eigenvalue of the estimated cyclic autocorrelation matrix, $\overline{R}^{N_s}_{l}(k)$, was already defined in Eq. (35). Combining this definition with Eq. (74) yields

$$\begin{aligned}\hat{\lambda}_l = {} & M|b_l|^2 \overline{R}^{\alpha,N_s}_{s_l s_l}(k) + b_l \text{trace}\left\{\boldsymbol{a}_l(\boldsymbol{p})\overline{R}^{\alpha,N_s}_{s_l \boldsymbol{n}_l}(k)\right\} \\ & + b_l^* \text{trace}\left\{\overline{R}^{\alpha,N_s}_{\boldsymbol{n}_l s_l}(k)\boldsymbol{a}_l^H(\boldsymbol{p})\right\} + \text{trace}\left\{\overline{R}^{\alpha,N_s}_{\boldsymbol{n}_l \boldsymbol{n}_l}(k)\right\}.\end{aligned} \tag{75}$$

We now simplify Eq. (75) using one of the basic trace properties. Let $\boldsymbol{x}$ and $\boldsymbol{y}$ be two column vectors. Then, the following equalities hold

$$\text{trace}\left\{\boldsymbol{x} \cdot \boldsymbol{y}^H\right\} = \text{trace}\left\{\boldsymbol{y}^H \cdot \boldsymbol{x}\right\} = \boldsymbol{y}^H \cdot \boldsymbol{x} .$$

Using this property we rewrite Eq. (75) as

$$\hat{\lambda}_l = M\left|b_l\right|^2 \overline{R}_{s_l s_l}^{\alpha,N_s}(k) + b_l \overline{R}_{s_l \boldsymbol{n}_l}^{\alpha,N_s}(k)\boldsymbol{a}_l(\boldsymbol{p}) + b_l^* \boldsymbol{a}_l^H(\boldsymbol{p})\overline{R}_{\boldsymbol{n}_l s_l}^{\alpha,N_s}(k) + \text{trace}\left\{\overline{R}_{\boldsymbol{n}_l \boldsymbol{n}_l}^{\alpha,N_s}(k)\right\}. \tag{76}$$

Comparing the expression above for the estimated eigenvalue, $\hat{\lambda}_l$ with the actual (asymptotic) eigenvalue, λ_l given in (31) we conclude that

$$\hat{\lambda}_l = \lambda_l + \varepsilon_{s_l s_l} + \varepsilon_{\boldsymbol{n}_l s_l} + \varepsilon_{\boldsymbol{n}_l \boldsymbol{n}_l}\ , \tag{77}$$

where,

$$\varepsilon_{s_l s_l} \equiv M\left|b_l\right|^2 \left(\overline{R}_{s_l s_l}^{\alpha,N_s}(k) - \overline{R}_{s_l s_l}^{\alpha}(k)\right), \tag{78}$$

$$\varepsilon_{\boldsymbol{n}_l s_l} \equiv b_l \overline{R}_{s_l \boldsymbol{n}_l}^{\alpha,N_s}(k)\boldsymbol{a}_l(\boldsymbol{p}) + b_l^* \boldsymbol{a}_l^H(\boldsymbol{p})\overline{R}_{\boldsymbol{n}_l s_l}^{\alpha,N_s}(k)\ , \tag{79}$$

$$\varepsilon_{\boldsymbol{n}_l \boldsymbol{n}_l} \equiv \text{trace}\left\{\overline{R}_{\boldsymbol{n}_l \boldsymbol{n}_l}^{\alpha,N_s}(k)\right\}. \tag{80}$$

One should note that all the noise terms defined in Eqs. (78)-(80) are functions of the total number of samples, N_s and the lag parameter, *k*. However, for simplicity of notations we choose to omit this dependence which the reader should keep in mind.

Since we assume that second order terms of the noise are negligible, we have

$$\varepsilon_{\boldsymbol{n}_l \boldsymbol{n}_l} \cong 0\ , \tag{81}$$

so that Eq. (77) reduces to

$$\hat{\lambda}_l \cong \lambda_l + \varepsilon_{s_l s_l} + \varepsilon_{\boldsymbol{n}_l s_l}\ . \tag{82}$$

We conclude from Eq. (82) that under the framework of SEA, the eigenvalue computed by the CDPD in Eq. (35) is corrupted by two terms. The first, $\varepsilon_{s_l s_l}$, represents the difference between the estimated and the asymptotic cyclic autocorrelation of the SOI

while the second, $\varepsilon_{\boldsymbol{n}_l s_l}$, is ascribed to the measurement noise experienced by the antenna array. Specifically, $\varepsilon_{\boldsymbol{n}_l s_l}$ consists of the estimated cyclic cross correlation between the noise, $\boldsymbol{n}_l(k)$ and the SOI. Clearly, since $\boldsymbol{n}_l(k)$ is uncorrelated with the SOI and has zero mean then their cross correlation, as well as their cyclic cross correlation, are both zeros. However, this is true only asymptotically, when the number of samples, N_s, tends to infinity. In this case, all of the estimated quantities in the terms $\varepsilon_{s_l s_l}$ and $\varepsilon_{\boldsymbol{n}_l s_l}$ coincide with the corresponding true ones so that these two terms reduce to zero. Likewise, the approximation done in Eq. (81) becomes a strict equality under asymptotic conditions since $\boldsymbol{n}_l(k)$ is assumed to be a purely stationary process meaning that its cyclic autocorrelation is zero when evaluated at the cycle frequency of the SOI, α. The last observations imply that $\hat{\lambda}_l$ tends to λ_l when averaging an infinite number of samples so that the estimator is claimed to be a consistent estimator of the emitter location. It should be clear however that the derivation presented here accounts for any distortion exists due to a finite block size. In particular, $\varepsilon_{s_l s_l}$ and $\varepsilon_{\boldsymbol{n}_l s_l}$ are obviously non-zero terms under non-asymptotic conditions.

After determining the basic quantity used by the suggested estimator we move to the first manipulation done on this quantity, namely, obtaining the eigenvalue quotient. The ratio between the estimated eigenvalues associated with any two base stations is given by,

$$\frac{\hat{\lambda}_{l_1}}{\hat{\lambda}_{l_2}} = \frac{\lambda_{l_1} + \varepsilon_{s_{l_1} s_{l_1}} + \varepsilon_{\boldsymbol{n}_{l_1} s_{l_1}}}{\lambda_{l_2} + \varepsilon_{s_{l_2} s_{l_2}} + \varepsilon_{\boldsymbol{n}_{l_2} s_{l_2}}}. \tag{83}$$

Under the assumption that both noise terms $\varepsilon_{s_l s_l}$ and $\varepsilon_{\boldsymbol{n}_l s_l}$ are sufficiently small we apply the following approximation to Eq. (83)

$$\frac{1}{1+\delta} \approx 1-\delta \text{, for } |\delta| << 1 .$$

Thus, Eq. (83) can be approximated as follows

$$\frac{\hat{\lambda}_{l_1}}{\hat{\lambda}_{l_2}} \cong \frac{\lambda_{l_1} + \varepsilon_{s_{l_1} s_{l_1}} + \varepsilon_{\boldsymbol{n}_{l_1} s_{l_1}}}{\lambda_{l_2}} \left(1 - \frac{\varepsilon_{s_{l_2} s_{l_2}} + \varepsilon_{\boldsymbol{n}_{l_2} s_{l_2}}}{\lambda_{l_2}} \right). \tag{84}$$

Rearranging the terms in (84) and omitting second order noise terms we get

$$\frac{\hat{\lambda}_{l_1}}{\hat{\lambda}_{l_2}} \cong \frac{\lambda_{l_1}}{\lambda_{l_2}} \left(1 + \frac{\varepsilon_{s_{l_1} s_{l_1}} + \varepsilon_{\boldsymbol{n}_{l_1} s_{l_1}}}{\lambda_{l_1}} - \frac{\varepsilon_{s_{l_2} s_{l_2}} + \varepsilon_{\boldsymbol{n}_{l_2} s_{l_2}}}{\lambda_{l_2}} \right). \tag{85}$$

4.4.3 Expression for the Magnitude of the Eigenvalue Quotient

The last step of the algorithm is to divide the eigenvalue quotient by its absolute value given by,

$$\left| \frac{\hat{\lambda}_{l_1}}{\hat{\lambda}_{l_2}} \right| = \sqrt{ \mathrm{Im}^2 \left\{ \frac{\hat{\lambda}_{l_1}}{\hat{\lambda}_{l_2}} \right\} + \mathrm{Re}^2 \left\{ \frac{\hat{\lambda}_{l_1}}{\hat{\lambda}_{l_2}} \right\} } . \tag{86}$$

To this end, we should first compute the real and imaginary parts of Eq. (85)

$$\begin{aligned} \mathrm{Re}\left\{ \frac{\hat{\lambda}_{l_1}}{\hat{\lambda}_{l_2}} \right\} \cong \mathrm{Re}\left\{ \frac{\lambda_{l_1}}{\lambda_{l_2}} \right\} \cdot \left(1 + \mathrm{Re}\left\{ \frac{\varepsilon_{s_{l_1} s_{l_1}} + \varepsilon_{\boldsymbol{n}_{l_1} s_{l_1}}}{\lambda_{l_1}} \right\} - \mathrm{Re}\left\{ \frac{\varepsilon_{s_{l_2} s_{l_2}} + \varepsilon_{\boldsymbol{n}_{l_2} s_{l_2}}}{\lambda_{l_2}} \right\} \right) \\ - \mathrm{Im}\left\{ \frac{\lambda_{l_1}}{\lambda_{l_2}} \right\} \cdot \left(\mathrm{Im}\left\{ \frac{\varepsilon_{s_{l_1} s_{l_1}} + \varepsilon_{\boldsymbol{n}_{l_1} s_{l_1}}}{\lambda_{l_1}} \right\} - \mathrm{Im}\left\{ \frac{\varepsilon_{s_{l_2} s_{l_2}} + \varepsilon_{\boldsymbol{n}_{l_2} s_{l_2}}}{\lambda_{l_2}} \right\} \right), \end{aligned} \tag{87}$$

and,

$$\begin{aligned}\mathrm{Im}\left\{\frac{\hat{\lambda}_{l_1}}{\hat{\lambda}_{l_2}}\right\} \cong \mathrm{Im}\left\{\frac{\lambda_{l_1}}{\lambda_{l_2}}\right\}\cdot\left(1+\mathrm{Re}\left\{\frac{\varepsilon_{s_{l_1}s_{l_1}}+\varepsilon_{\boldsymbol{n}_{l_1}s_{l_1}}}{\lambda_{l_1}}\right\}-\mathrm{Re}\left\{\frac{\varepsilon_{s_{l_2}s_{l_2}}+\varepsilon_{\boldsymbol{n}_{l_2}s_{l_2}}}{\lambda_{l_2}}\right\}\right)\\ +\mathrm{Re}\left\{\frac{\lambda_{l_1}}{\lambda_{l_2}}\right\}\cdot\left(\mathrm{Im}\left\{\frac{\varepsilon_{s_{l_1}s_{l_1}}+\varepsilon_{\boldsymbol{n}_{l_1}s_{l_1}}}{\lambda_{l_1}}\right\}-\mathrm{Im}\left\{\frac{\varepsilon_{s_{l_2}s_{l_2}}+\varepsilon_{\boldsymbol{n}_{l_2}s_{l_2}}}{\lambda_{l_2}}\right\}\right).\end{aligned} \tag{88}$$

Now using the following approximation

$$(1+\delta)^2 \approx 1+2\delta\ ,\ \text{for}\ |\delta| << 1\ ,$$

the squared value of the real and imaginary parts of the eigenvalue quotient can be approximated as,

$$\begin{aligned}\mathrm{Re}^2\left\{\frac{\hat{\lambda}_{l_1}}{\hat{\lambda}_{l_2}}\right\} \cong \mathrm{Re}^2\left\{\frac{\lambda_{l_1}}{\lambda_{l_2}}\right\}\cdot\left(1+2\,\mathrm{Re}\left\{\frac{\varepsilon_{s_{l_1}s_{l_1}}+\varepsilon_{\boldsymbol{n}_{l_1}s_{l_1}}}{\lambda_{l_1}}\right\}-2\,\mathrm{Re}\left\{\frac{\varepsilon_{s_{l_2}s_{l_2}}+\varepsilon_{\boldsymbol{n}_{l_2}s_{l_2}}}{\lambda_{l_2}}\right\}\right)\\ -2\,\mathrm{Re}\left\{\frac{\lambda_{l_1}}{\lambda_{l_2}}\right\}\mathrm{Im}\left\{\frac{\lambda_{l_1}}{\lambda_{l_2}}\right\}\cdot\left(\mathrm{Im}\left\{\frac{\varepsilon_{s_{l_1}s_{l_1}}+\varepsilon_{\boldsymbol{n}_{l_1}s_{l_1}}}{\lambda_{l_1}}\right\}-\mathrm{Im}\left\{\frac{\varepsilon_{s_{l_2}s_{l_2}}+\varepsilon_{\boldsymbol{n}_{l_2}s_{l_2}}}{\lambda_{l_2}}\right\}\right),\end{aligned} \tag{89}$$

and,

$$\begin{aligned}\mathrm{Im}^2\left\{\frac{\hat{\lambda}_{l_1}}{\hat{\lambda}_{l_2}}\right\} \cong \mathrm{Im}^2\left\{\frac{\lambda_{l_1}}{\lambda_{l_2}}\right\}\cdot\left(1+2\,\mathrm{Re}\left\{\frac{\varepsilon_{s_{l_1}s_{l_1}}+\varepsilon_{\boldsymbol{n}_{l_1}s_{l_1}}}{\lambda_{l_1}}\right\}-2\,\mathrm{Re}\left\{\frac{\varepsilon_{s_{l_2}s_{l_2}}+\varepsilon_{\boldsymbol{n}_{l_2}s_{l_2}}}{\lambda_{l_2}}\right\}\right)\\ +2\,\mathrm{Re}\left\{\frac{\lambda_{l_1}}{\lambda_{l_2}}\right\}\mathrm{Im}\left\{\frac{\lambda_{l_1}}{\lambda_{l_2}}\right\}\cdot\left(\mathrm{Im}\left\{\frac{\varepsilon_{s_{l_1}s_{l_1}}+\varepsilon_{\boldsymbol{n}_{l_1}s_{l_1}}}{\lambda_{l_1}}\right\}-\mathrm{Im}\left\{\frac{\varepsilon_{s_{l_2}s_{l_2}}+\varepsilon_{\boldsymbol{n}_{l_2}s_{l_2}}}{\lambda_{l_2}}\right\}\right).\end{aligned} \tag{90}$$

Substituting Eqs. (89) and (90) into (86) we get,

$$\left|\frac{\hat{\lambda}_{l_1}}{\hat{\lambda}_{l_2}}\right| \cong \left|\frac{\lambda_{l_1}}{\lambda_{l_2}}\right| \cdot \left(1 + 2\,\mathrm{Re}\left\{\frac{\varepsilon_{s_{l_1}s_{l_1}} + \varepsilon_{\boldsymbol{n}_{l_1}s_{l_1}}}{\lambda_{l_1}}\right\} - 2\,\mathrm{Re}\left\{\frac{\varepsilon_{s_{l_2}s_{l_2}} + \varepsilon_{\boldsymbol{n}_{l_2}s_{l_2}}}{\lambda_{l_2}}\right\}\right)^{1/2}. \tag{91}$$

4.4.4 Expression for the Phase of the Eigenvalue Quotient

Finally, the phase of the eigenvalue quotient is defined as

$$\mathrm{phase}\left\{\frac{\hat{\lambda}_{l_1}}{\hat{\lambda}_{l_2}}\right\} \equiv \left|\frac{\hat{\lambda}_{l_2}}{\hat{\lambda}_{l_1}}\right| \cdot \frac{\hat{\lambda}_{l_1}}{\hat{\lambda}_{l_2}}. \tag{92}$$

In order to compute this term we first provide an approximate expression for the denominator of (92). To this end, we use the following approximation

$$(1+\delta)^{-1/2} \approx 1 - \delta/2, \text{ for } |\delta| << 1.$$

Plugging the above approximation into Eq. (91) leads to

$$\left|\frac{\hat{\lambda}_{l_1}}{\hat{\lambda}_{l_2}}\right|^{-1} \cong \left|\frac{\lambda_{l_1}}{\lambda_{l_2}}\right|^{-1} \cdot \left(1 - \mathrm{Re}\left\{\frac{\varepsilon_{s_{l_1}s_{l_1}} + \varepsilon_{\boldsymbol{n}_{l_1}s_{l_1}}}{\lambda_{l_1}}\right\} + \mathrm{Re}\left\{\frac{\varepsilon_{s_{l_2}s_{l_2}} + \varepsilon_{\boldsymbol{n}_{l_2}s_{l_2}}}{\lambda_{l_2}}\right\}\right). \tag{93}$$

Substituting Eqs. (85) and (93) into Eq. (92) and neglecting second-order noise terms yields

$$\mathrm{phase}\left\{\frac{\hat{\lambda}_{l_1}}{\hat{\lambda}_{l_2}}\right\} \cong \left(1 + j(w_{l_1,l_2} + v_{l_1,l_2})\right) \cdot \mathrm{phase}\left\{\frac{\lambda_{l_1}}{\lambda_{l_2}}\right\}. \tag{94}$$

where

$$w_{l_1,l_2} \equiv \mathrm{Im}\left\{\frac{\varepsilon_{s_{l_1}s_{l_1}}}{\lambda_{l_1}} - \frac{\varepsilon_{s_{l_2}s_{l_2}}}{\lambda_{l_2}}\right\}, \tag{95}$$

and

$$v_{l_1,l_2} \equiv \mathrm{Im}\left\{\frac{\varepsilon_{\boldsymbol{n}_{l_1}s_{l_1}}}{\lambda_{l_1}} - \frac{\varepsilon_{\boldsymbol{n}_{l_2}s_{l_2}}}{\lambda_{l_2}}\right\}. \tag{96}$$

Next, we return to the definition of $\varepsilon_{s_l s_l}$ from Eq. (78). According to this definition, the expression for the true eigenvalue, λ_l given in Eq. (31), and the following relation which holds for any base station

$$\overline{R}^{\alpha}_{s_l s_l}(k) = e^{-j2\pi\alpha(\tau_l(\boldsymbol{p})+t_0)}\overline{R}^{\alpha}_{ss}(k), \tag{97}$$

we obtain that,

$$\begin{aligned} w_{l_1,l_2} &= \mathrm{Im}\left\{\frac{\overline{R}^{\alpha,N_s}_{s_{l_1}s_{l_1}}(k)}{\overline{R}^{\alpha}_{s_{l_1}s_{l_1}}(k)} - \frac{\overline{R}^{\alpha,N_s}_{s_{l_2}s_{l_2}}(k)}{\overline{R}^{\alpha}_{s_{l_2}s_{l_2}}(k)}\right\} \\ &= \mathrm{Im}\left\{\frac{e^{j2\pi\alpha t_0}}{\overline{R}^{\alpha}_{ss}(k)}\left(e^{j2\pi\alpha\tau_{l_1}(\boldsymbol{p})}\overline{R}^{\alpha,N_s}_{s_{l_1}s_{l_1}}(k) - e^{j2\pi\alpha\tau_{l_2}(\boldsymbol{p})}\overline{R}^{\alpha,N_s}_{s_{l_2}s_{l_2}}(k)\right)\right\}. \end{aligned} \tag{98}$$

We then recall from the model definition in Eq. (22) that $s_l(m)$ is a delayed version of the transmitted signal $s(m)$. Specifically,

$$s_{l_2}(m) = s\left((m+\xi_{l_{1,2}})\cdot T_s + [\tau_{l_1}(\boldsymbol{p}) - \tau_{l_2}(\boldsymbol{p})] \bmod T_s - \tau_{l_1}(\boldsymbol{p}) - t_0\right), \tag{99}$$

where

$$\xi_{l_{1,2}} \equiv \left\lfloor \frac{\tau_{l_1}(\boldsymbol{p}) - \tau_{l_2}(\boldsymbol{p})}{T_s} \right\rfloor. \tag{100}$$

Under the reasonable assumption that the time shift $[\tau_{l_1}(\boldsymbol{p}) - \tau_{l_2}(\boldsymbol{p})] \bmod T_s$ is negligible for narrowband signal then Eq. (99) becomes,

$$s_{l_2}(m) \cong s_{l_1}(m + \xi_{l_{1,2}}) . \tag{101}$$

Thus, after a simple change in the summation index we have the following approximation,

$$e^{j2\pi\alpha\tau_{l_2}(\boldsymbol{p})} \overline{R}^{\alpha,N_s}_{s_{l_2}s_{l_2}}(k) \cong e^{j2\pi\alpha\tau_{l_1}(\boldsymbol{p})} \frac{1}{N_s} \sum_{m=\xi_{l_{1,2}}}^{N_s+\xi_{l_{1,2}}-1} s_{l_1}(m) s_{l_1}(m-k) e^{-j2\pi\alpha m T_s} . \tag{102}$$

Substituting Eq. (102) into Eq. (98) yields

$$\begin{aligned} w_{l_1,l_2} \cong \frac{1}{N_s} \mathrm{Im}\Bigg\{ \frac{e^{j2\pi\alpha(\tau_{l_1}(\boldsymbol{p})+t_0)}}{\overline{R}^{\alpha}_{ss}(k)} \Bigg(& \sum_{m=0}^{\xi_{l_{1,2}}-1} s_{l_1}(m) s_{l_1}(m-k) e^{-j2\pi\alpha m T_s} \\ & - \sum_{m=N_s}^{N_s+\xi_{l_{1,2}}-1} s_{l_1}(m) s_{l_1}(m-k) e^{-j2\pi\alpha m T_s} \Bigg) \Bigg\} , \end{aligned} \tag{103}$$

which implies that

$$E\left\{ w_{l_1,l_2} w_{l_3,l_4} \right\} = O(N_s^{-2}) \cong 0 . \tag{104}$$

Furthermore, since the noise has zero mean and is statistically independent of the SOI then

$$E\left\{ w_{l_1,l_2} v_{l_3,l_4} \right\} = 0 . \tag{105}$$

Therefore, we conclude that the term w_{l_1,l_2} does not have any contribution to the covariance of the phase of the estimated eigenvalue quotient under SEA assumption. This observation suggests that Eq. (94) can be rewritten as

$$\text{phase}\left\{\frac{\hat{\lambda}_{l_1}}{\hat{\lambda}_{l_2}}\right\} \cong \left(1 + j v_{l_1,l_2}\right) \cdot \text{phase}\left\{\frac{\lambda_{l_1}}{\lambda_{l_2}}\right\}. \tag{106}$$

We conclude from Eq. (106) that we have managed to express the estimated phase of the eigenvalue quotient as a sum of the true (asymptotic) phase and a noise term. This noise term can be expressed as a multiplication of the exact phase of the eigenvalue quotient and another factor which is a function of both the AWGN and SOI. Clearly, since the noise term is a function of the phase of the eigenvalue quotient then it is also a function of the emitter location, $\boldsymbol{p}$, and the deployment of the base stations.

After developing a closed-form expression for the noise corrupting the estimated phase of the eigenvalue quotient of the estimator in Eq. (41) we return to the evaluation of the estimator MSE by handling to the last missing piece in Eq. (68) – the correlation matrix of $\widetilde{f}'(\boldsymbol{p}_0)$, $E\left\{\widetilde{f}'(\boldsymbol{p}_0)\cdot\widetilde{f}'(\boldsymbol{p}_0)^T\right\}$.

4.5 Expression for $E\left\{\widetilde{f}'(\boldsymbol{p}_0)\cdot\widetilde{f}'(\boldsymbol{p}_0)^T\right\}$

In this section, we obtain an explicit expression for the correlation matrix $E\left\{\widetilde{f}'(\boldsymbol{p}_0)\cdot\widetilde{f}'(\boldsymbol{p}_0)^T\right\}$ by exploiting the statistical properties of the two signals involved, namely the SOI and the noise. According to Eqs. (72) and (106) we have

$$E\left\{\widetilde{f}'(\boldsymbol{p}_0)\cdot\widetilde{f}'(\boldsymbol{p}_0)^T\right\} = 4\pi^2\alpha^2 \sum_{l_1,l_2}\sum_{l_3,l_4} E\left\{v_{l_1,l_2} v_{l_3,l_4}\right\}\cdot\Gamma_{l_1l_2,l_3l_4}(\boldsymbol{p}_0). \tag{107}$$

We now use the definition of v_{l_1,l_2} in Eq. (96) to write

$$
\begin{aligned}
E\left\{v_{l_1,l_2}v_{l_3,l_4}\right\} = E\Bigg\{\Bigg(&\mathrm{Im}\left\{\frac{1}{\lambda_{l_1}}\right\}\cdot\frac{\varepsilon_{\boldsymbol{n}_{l_1}s_{l_1}}+\varepsilon^{*}_{\boldsymbol{n}_{l_1}s_{l_1}}}{2}+\mathrm{Re}\left\{\frac{1}{\lambda_{l_1}}\right\}\cdot\frac{\varepsilon_{\boldsymbol{n}_{l_1}s_{l_1}}-\varepsilon^{*}_{\boldsymbol{n}_{l_1}s_{l_1}}}{2j}\\
&-\mathrm{Im}\left\{\frac{1}{\lambda_{l_2}}\right\}\cdot\frac{\varepsilon_{\boldsymbol{n}_{l_2}s_{l_2}}+\varepsilon^{*}_{\boldsymbol{n}_{l_2}s_{l_2}}}{2}-\mathrm{Re}\left\{\frac{1}{\lambda_{l_2}}\right\}\cdot\frac{\varepsilon_{\boldsymbol{n}_{l_2}s_{l_2}}-\varepsilon^{*}_{\boldsymbol{n}_{l_2}s_{l_2}}}{2j}\Bigg)\\
&\cdot\Bigg(\mathrm{Im}\left\{\frac{1}{\lambda_{l_3}}\right\}\cdot\frac{\varepsilon_{\boldsymbol{n}_{l_3}s_{l_3}}+\varepsilon^{*}_{\boldsymbol{n}_{l_3}s_{l_3}}}{2}+\mathrm{Re}\left\{\frac{1}{\lambda_{l_3}}\right\}\cdot\frac{\varepsilon_{\boldsymbol{n}_{l_3}s_{l_3}}-\varepsilon^{*}_{\boldsymbol{n}_{l_3}s_{l_3}}}{2j}\\
&-\mathrm{Im}\left\{\frac{1}{\lambda_{l_4}}\right\}\cdot\frac{\varepsilon_{\boldsymbol{n}_{l_4}s_{l_4}}+\varepsilon^{*}_{\boldsymbol{n}_{l_4}s_{l_4}}}{2}-\mathrm{Re}\left\{\frac{1}{\lambda_{l_4}}\right\}\cdot\frac{\varepsilon_{\boldsymbol{n}_{l_4}s_{l_4}}-\varepsilon^{*}_{\boldsymbol{n}_{l_4}s_{l_4}}}{2j}\Bigg)\Bigg\}.
\end{aligned}
\tag{108}
$$

From Eq. (108) we conclude that in order to proceed with the derivation, we should first compute $E\left\{\varepsilon_{\boldsymbol{n}_{l_1}s_{l_1}}\varepsilon^{*}_{\boldsymbol{n}_{l_2}s_{l_2}}\right\}$ and $E\left\{\varepsilon_{\boldsymbol{n}_{l_1}s_{l_1}}\varepsilon_{\boldsymbol{n}_{l_2}s_{l_2}}\right\}$.

4.5.1 Expression for $E\left\{\varepsilon_{\boldsymbol{n}_{l_1}s_{l_1}}\varepsilon^{*}_{\boldsymbol{n}_{l_2}s_{l_2}}\right\}$ and $E\left\{\varepsilon_{\boldsymbol{n}_{l_1}s_{l_1}}\varepsilon_{\boldsymbol{n}_{l_2}s_{l_2}}\right\}$

In order to determine both $E\left\{\varepsilon_{\boldsymbol{n}_{l_1}s_{l_1}}\varepsilon_{\boldsymbol{n}_{l_2}s_{l_2}}\right\}$ and $E\left\{\varepsilon_{\boldsymbol{n}_{l_1}s_{l_1}}\varepsilon_{\boldsymbol{n}_{l_2}s_{l_2}}\right\}$, we note that the noise vector $\boldsymbol{n}_l(k)$ is assumed to be circular symmetric Gaussian noise which is both spatially and temporally uncorrelated so that,

$$
\begin{aligned}
&E\left\{\boldsymbol{n}_{l_1}(k_1)\boldsymbol{n}^{H}_{l_2}(k_2)\right\}=0\ ,\forall l_1\neq l_2\bigcup\forall k_1\neq k_2\ ,\\
&E\left\{\boldsymbol{n}_{l_1}(k_1)\boldsymbol{n}^{T}_{l_2}(k_2)\right\}=0\ ,\forall l_1,l_2,k_1,k_2\ .
\end{aligned}
\tag{109}
$$

Since $\boldsymbol{n}_l(k)$ is circular symmetric, its real and imaginary parts have the same variance (see, e.g., [15]) which will be denoted by $\frac{\sigma_n^2}{2}$, or equivalently

$$E\left\{\boldsymbol{n}_l(k)\boldsymbol{n}_l^H(k)\right\}=\sigma_n^2 I_{M\times M}\ . \tag{110}$$

Furthermore, since $\boldsymbol{n}_l(k)$ is also statistically independent of the SOI, $s_l(k)$, and has zero mean then

$$\begin{aligned}
&E\left\{s_{l_1}(k_1)s_{l_2}(k_2)\boldsymbol{n}_{l_1}(k_3)\boldsymbol{n}_{l_2}^H(k_4)\right\}=E\left\{s_{l_1}(k_1)s_{l_2}(k_2)\right\}E\left\{\boldsymbol{n}_{l_1}(k_3)\boldsymbol{n}_{l_2}^H(k_4)\right\},\\
&\qquad\forall l_1,l_2,k_1,k_2,k_3,k_4\ ,\\
&E\left\{s_{l_1}(k_1)s_{l_2}(k_2)\boldsymbol{n}_{l_1}(k_3)\boldsymbol{n}_{l_2}^T(k_4)\right\}=E\left\{s_{l_1}(k_1)s_{l_2}(k_2)\right\}E\left\{\boldsymbol{n}_{l_1}(k_3)\boldsymbol{n}_{l_2}^T(k_4)\right\}=0\ ,\\
&\qquad\forall l_1,l_2,k_1,k_2,k_3,k_4\ .
\end{aligned} \tag{111}$$

Next, we write an explicit expression for $E\left\{\varepsilon_{\boldsymbol{n}_{l_1}s_{l_1}}\varepsilon_{\boldsymbol{n}_{l_2}s_{l_2}}\right\}$ by substituting the definition of $\varepsilon_{\boldsymbol{n}_l s_l}$ from Eq. (79)

$$\begin{aligned}
E\left\{\varepsilon_{\boldsymbol{n}_{l_1}s_{l_1}}\varepsilon_{\boldsymbol{n}_{l_2}s_{l_2}}\right\}=\frac{1}{N_s^2}\sum_{m_1=0}^{N_s-1}\sum_{m_2=0}^{N_s-1}e^{-j2\pi\alpha(m_1+m_2)T_s}&\\
\cdot\Big(b_{l_1}b_{l_2}\boldsymbol{a}_{l_1}^T(\boldsymbol{p})E\left\{s_{l_1}(m_1)s_{l_2}(m_2)\boldsymbol{n}_{l_1}^*(m_1-k)\boldsymbol{n}_{l_2}^H(m_2-k)\right\}\boldsymbol{a}_{l_2}(\boldsymbol{p})&\\
+b_{l_1}b_{l_2}^*\boldsymbol{a}_{l_1}^T(\boldsymbol{p})E\left\{s_{l_1}(m_1)s_{l_2}(m_2-k)\boldsymbol{n}_{l_1}^*(m_1-k)\boldsymbol{n}_{l_2}^T(m_2)\right\}\boldsymbol{a}_{l_2}^*(\boldsymbol{p})&\\
+b_{l_1}^*b_{l_2}\boldsymbol{a}_{l_1}^H(\boldsymbol{p})E\left\{s_{l_1}(m_1-k)s_{l_2}(m_2)\boldsymbol{n}_{l_1}(m_1)\boldsymbol{n}_{l_2}^H(m_2-k)\right\}\boldsymbol{a}_{l_2}(\boldsymbol{p})&\\
+b_{l_1}^*b_{l_2}^*\boldsymbol{a}_{l_1}^H(\boldsymbol{p})E\left\{s_{l_1}(m_1-k)s_{l_2}(m_2-k)\boldsymbol{n}_{l_1}(m_1)\boldsymbol{n}_{l_2}^T(m_2)\right\}\boldsymbol{a}_{l_2}^*(\boldsymbol{p})\Big)\ .&
\end{aligned} \tag{112}$$

Combining Eqs. (109) and (111) together with Eq. (112) implies that

$$E\left\{\varepsilon_{\boldsymbol{n}_{l_1}s_{l_1}}\varepsilon_{\boldsymbol{n}_{l_2}s_{l_2}}\right\}=0\ ,\forall l_1\neq l_2\ , \tag{113}$$

and by similar arguments we also conclude that

$$E\left\{\varepsilon_{\boldsymbol{n}_{l_1}s_{l_1}}\varepsilon^{*}_{\boldsymbol{n}_{l_2}s_{l_2}}\right\}=0\,,\forall l_1\neq l_2\,. \tag{114}$$

Finally, we observe from Eqs. (113) and (114) that the only terms that are left to determine in Eq. (108) are those which are limited to a single base station, i.e., $E\left\{\varepsilon^2_{\boldsymbol{n}_l s_l}\right\}$ and $E\left\{\left|\varepsilon_{\boldsymbol{n}_l s_l}\right|^2\right\}$.

4.5.2 Expression for $E\left\{\varepsilon^2_{\boldsymbol{n}_l s_l}\right\}$ and $E\left\{\left(\varepsilon^{*}_{\boldsymbol{n}_l s_l}\right)^2\right\}$

We start the computation of $E\left\{\varepsilon^2_{\boldsymbol{n}_l s_l}\right\}$ by doing much of the same we did for $E\left\{\varepsilon_{\boldsymbol{n}_{l_1}s_{l_1}}\varepsilon_{\boldsymbol{n}_{l_2}s_{l_2}}\right\}$ in Eq. (112)

$$\begin{aligned}E\left\{\varepsilon^2_{\boldsymbol{n}_l s_l}\right\}=\frac{1}{N_s^2}\sum_{m_1=0}^{N_s-1}\sum_{m_2=0}^{N_s-1}e^{-j2\pi\alpha(m_1+m_2)T_s}\\ \cdot\Big(b_l^2\boldsymbol{a}_l^T(\boldsymbol{p})E\left\{s_l(m_1)s_l(m_2)\boldsymbol{n}_l^*(m_1-k)\boldsymbol{n}_l^H(m_2-k)\right\}\boldsymbol{a}_l(\boldsymbol{p})\\ +\left|b_l\right|^2\boldsymbol{a}_l^T(\boldsymbol{p})E\left\{s_l(m_1)s_l(m_2-k)\boldsymbol{n}_l^*(m_1-k)\boldsymbol{n}_l^T(m_2)\right\}\boldsymbol{a}_l^*(\boldsymbol{p})\\ +\left|b_l\right|^2\boldsymbol{a}_l^H(\boldsymbol{p})E\left\{s_l(m_1-k)s_l(m_2)\boldsymbol{n}_l(m_1)\boldsymbol{n}_l^H(m_2-k)\right\}\boldsymbol{a}_l(\boldsymbol{p})\\ +(b_l^*)^2\boldsymbol{a}_l^H(\boldsymbol{p})E\left\{s_l(m_1-k)s_l(m_2-k)\boldsymbol{n}_l(m_1)\boldsymbol{n}_l^T(m_2)\right\}\boldsymbol{a}_l^*(\boldsymbol{p})\Big).\end{aligned} \tag{115}$$

Again, combining Eqs. (109)-(111), and (32) together with Eq. (115) suggests that the last expression amounts to

$$E\left\{\varepsilon^2_{\boldsymbol{n}_l s_l}\right\}=\frac{2M\left|b_l\right|^2\sigma_n^2}{N_s^2}\sum_{m=0}^{N_s-1}e^{-j2\pi\alpha(2m+k)T_s}E\left\{s_l(m+k)s_l(m-k)\right\}. \tag{116}$$

Likewise, it can be easily verified that similarly to Eqs. (115) and (116) we have

$$E\left\{\left(\varepsilon^{*}_{\mathbf{n}_l s_l}\right)^2\right\} = E^{*}\left\{\varepsilon^{2}_{\mathbf{n}_l s_l}\right\} = \frac{2M\left|b_l\right|^2\sigma_n^2}{N_s^2}\sum_{m=0}^{N_s-1} e^{j2\pi\alpha(2m+k)T_s} E\left\{s_l(m+k)s_l(m-k)\right\}. \tag{117}$$

Before we continue with the simplification of Eq. (116), we need first to introduce some useful notations. Since the transmitted signal $s(m)$ is assumed to be a BPSK signal whose shaping is accomplished by an arbitrary pulse then the following representation is considered for this signal

$$s(m) = \sum_{n=-\infty}^{\infty} d\left(\left\lfloor \frac{m}{OVS} \right\rfloor + n\right)\cdot q(n\cdot OVS + m \bmod OVS), \tag{118}$$

where $d(m)$ is a series of i.i.d. RVs drawn from a binary symmetric distribution, $q(m)$ is an arbitrary pulse shape with limited bandwidth, and OVS is the over-sampling factor defined as the number of sampling times per a single symbol

$$OVS \equiv T/T_s = (\alpha T_s)^{-1}. \tag{119}$$

The transmitted signal $s(m)$ is then delayed by a different time delay in each base station as suggested by Eq. (22) so that the formulation above can be adjusted to the delayed signal of the *l*th base station, $s_l(m)$, by writing

$$s_l(m) = \sum_{n=-\infty}^{\infty} d_l\left(\left\lfloor \frac{m}{OVS} \right\rfloor + n\right)\cdot q_l(n\cdot OVS + m \bmod OVS), \tag{120}$$

where $d_l(m)$ and $q_l(m)$ are delayed versions of $d(m)$ and $q(m)$, respectively, with the corresponding delay associated with the *l*th base station:

$$q_l(m) = q(t-\tau_l(\boldsymbol{p})-t_0)\big|_{t=mT_s}, \tag{121}$$

$$d_l(m) = d(t - \tau_l(\boldsymbol{p}) - t_0)\big|_{t=mT_s} .$$

We substitute Eq. (120) into Eq. (116) to get

$$\begin{aligned} E\left\{\varepsilon^2_{\boldsymbol{n}_l s_l}\right\} = & \frac{2M|b_l|^2\sigma_n^2}{N_s^2}\sum_{m=0}^{N_s-1} e^{-j2\pi\alpha(2m+k)T_s} \\ & \cdot \sum_{n_1=-\infty}^{\infty}\sum_{n_2=-\infty}^{\infty} E\left\{ d_l\left(\left\lfloor \frac{m+k}{OVS} \right\rfloor + n_1\right) d_l\left(\left\lfloor \frac{m-k}{OVS} \right\rfloor + n_2\right)\right\} \\ & \cdot q_l(n_1 \cdot OVS + (m+k) \bmod OVS) \cdot q_l(n_2 \cdot OVS + (m-k) \bmod OVS) . \end{aligned} \tag{122}$$

As the information symbols, $d_l(m)$ are i.i.d. and with a unity variance, their second moment is given by

$$E\{d_l(m_1)d_l(m_2)\} = \delta_{m_1,m_2} , \tag{123}$$

where δ_{m_1,m_2} is the Kronecker delta function. We substitute Eq. (123) into Eq. (122) so the latter reads

$$E\left\{\varepsilon^2_{\boldsymbol{n}_l s_l}\right\} = \frac{2M|b_l|^2\sigma_n^2}{N_s^2}\sum_{m=0}^{N_s-1} e^{-j2\pi\alpha(2m+k)T_s} Q_l(m,k) , \tag{124}$$

where

$$\begin{aligned} Q_l(m,k) \equiv & \sum_{n=-\infty}^{\infty} q_l\left(\left(n - \left\lfloor \frac{m+k}{OVS} \right\rfloor + \left\lfloor \frac{m-k}{OVS} \right\rfloor\right) \cdot OVS + (m+k) \bmod OVS\right) \\ & \cdot q_l(n \cdot OVS + (m-k) \bmod OVS) . \end{aligned} \tag{125}$$

It is clear from the definition of $Q_l(m,k)$ that this function is periodic in *m* with period OVS. Bearing this in mind and utilizing the relation from Eq. (119), we can simplify Eq. (124) as follows

$$E\left\{\varepsilon^2_{\mathbf{n}_l s_l}\right\} = \frac{2M|b_l|^2\sigma_n^2}{N_s \cdot OVS}\sum_{m=0}^{OVS-1} e^{-j2\pi\alpha(2m+k)T_s} Q_l(m,k). \tag{126}$$

For simplicity, we henceforth assume that the over-sampling factor, OVS, is even. Under this assumption, rearranging the summation in Eq. (126), we get

$$\begin{aligned} E\left\{\varepsilon^2_{\mathbf{n}_l s_l}\right\} &= \frac{2M|b_l|^2\sigma_n^2}{N_s \cdot OVS}\sum_{m=0}^{OVS/2-1}\Big[e^{-j2\pi\alpha(2m+k)T_s} Q_l(m,k) \\ &\qquad + e^{-j2\pi\alpha[2(m+OVS/2)+k]T_s} Q_l(m+OVS/2,k)\Big], \qquad (127) \\ &= \frac{2M|b_l|^2\sigma_n^2}{N_s \cdot OVS}\sum_{m=0}^{OVS/2-1} e^{-j2\pi\alpha(2m+k)T_s}\left[Q_l(m,k)+ Q_l(m+OVS/2,k)\right]. \end{aligned}$$

The expression obtained in Eq. (127) is quite involved for the general case. However, we can further streamline this expression if we use the following property, proved in Appendix A, of a band limited pulse shape whose bandwidth is bounded above by half of its sampling rate: Under the choice $k=0$ or $k=OVS/2$ the sum of two values of the function $Q_l(m,k)$, evaluated at times m and $m+OVS/2$ which results in samples of $q_l(m)$ at the Nyquist rate, is independent of m, that is,

$$\left[Q_l(m,k)+Q_l(m+OVS/2,k)\right] = g_l(k), \forall m, k \in [0, OVS/2]. \tag{128}$$

Therefore, Eq. (127) reduces to

$$E\left\{\varepsilon^2_{\mathbf{n}_l s_l}\right\} = \frac{2e^{-j2\pi\alpha kT_s}M|b_l|^2\sigma_n^2}{N_s \cdot OVS} g_l(k)\sum_{m=0}^{OVS/2-1} e^{-j4\pi\alpha mT_s}, k \in [0, OVS/2]. \tag{129}$$

Clearly, since the summation above over the $OVS/2$ exponential terms on the unity circle is zero we get

$$E\left\{\varepsilon_{\boldsymbol{n}_l s_l}^2\right\}=0\,,\ k\in[0,\,OVS/2]. \tag{130}$$

Therefore, according to Eq. (117) and the last relation we have also that

$$E\left\{\left(\varepsilon_{\boldsymbol{n}_l s_l}^*\right)^2\right\}=0\,,\ k\in[0,\,OVS/2]. \tag{131}$$

We already saw in Section 3.3 that the optimal lag choice for the narrowband signals considered in this work is $k=0$. Thus, we may always use the reduced expressions for $E\left\{\varepsilon_{\boldsymbol{n}_l s_l}^2\right\}$ and $E\left\{\left(\varepsilon_{\boldsymbol{n}_l s_l}^*\right)^2\right\}$ obtained in Eqs. (130) and (131), respectively, rather than the general and somewhat lengthy relation from Eq. (127). Our next step in the derivation is to develop an expression for the term $E\left\{\left|\varepsilon_{\boldsymbol{n}_l s_l}\right|^2\right\}$ by similar means to those applied in the calculation of $E\left\{\varepsilon_{\boldsymbol{n}_l s_l}^2\right\}$. This derivation is given in the next subsection.

4.5.3 Expression for $E\left\{\left|\varepsilon_{\boldsymbol{n}_l s_l}\right|^2\right\}$

Toward the end of determining $E\left\{\left|\varepsilon_{\boldsymbol{n}_l s_l}\right|^2\right\}$, we write the corresponding counterpart of Eq. (115) for the case of $\left|\varepsilon_{\boldsymbol{n}_l s_l}\right|^2$

$$\begin{aligned}E\left\{\left|\varepsilon_{\boldsymbol{n}_l s_l}\right|^2\right\}=\frac{1}{N_s^2}\sum_{m_1=0}^{N_s-1}\sum_{m_2=0}^{N_s-1}e^{-j2\pi\alpha(m_1-m_2)T_s}\\ \cdot\Big(|b_l|^2\,\boldsymbol{a}_l^T(\boldsymbol{p})E\left\{s_l(m_1)s_l(m_2)\boldsymbol{n}_l^*(m_1-k)\boldsymbol{n}_l^T(m_2-k)\right\}\boldsymbol{a}_l^*(\boldsymbol{p})\\ +b_l^2\,\boldsymbol{a}_l^T(\boldsymbol{p})E\left\{s_l(m_1)s_l(m_2-k)\boldsymbol{n}_l^*(m_1-k)\boldsymbol{n}_l^H(m_2)\right\}\boldsymbol{a}_l(\boldsymbol{p})\\ +(b_l^*)^2\,\boldsymbol{a}_l^H(\boldsymbol{p})E\left\{s_l(m_1-k)s_l(m_2)\boldsymbol{n}_l(m_1)\boldsymbol{n}_l^T(m_2-k)\right\}\boldsymbol{a}_l^*(\boldsymbol{p})\\ +|b_l|^2\,\boldsymbol{a}_l^H(\boldsymbol{p})E\left\{s_l(m_1-k)s_l(m_2-k)\boldsymbol{n}_l(m_1)\boldsymbol{n}_l^H(m_2)\right\}\boldsymbol{a}_l(\boldsymbol{p})\Big).\end{aligned} \tag{132}$$

From the same considerations led to the simplification of Eq. (115) to Eq. (116), we may write Eq. (132) as

$$E\left\{\left|\varepsilon_{\mathbf{n}_l s_l}\right|^2\right\}=\frac{M\left|b_l\right|^2\sigma_n^2}{N_s^2}\sum_{m=0}^{N_s-1}\left[E\left\{s_l^2(m)\right\}+E\left\{s_l^2(m-k)\right\}\right]. \tag{133}$$

We then follow exactly the same steps done in the formulation above for $E\left\{\varepsilon_{\mathbf{n}_l s_l}^2\right\}$ to obtain

$$E\left\{\left|\varepsilon_{\mathbf{n}_l s_l}\right|^2\right\}=\frac{M\left|b_l\right|^2\sigma_n^2}{N_s\cdot OVS}\sum_{m=0}^{OVS-1}\left[Q_l(m,0)+Q_l(m-k,0)\right]. \tag{134}$$

Likewise, since the averaging over both $Q_l(m,0)$ and $Q_l(m-k,0)$ is actually the power of the arbitrary pulse shape, $q_l(m)$ then

$$\frac{1}{OVS}\sum_{m=0}^{OVS-1}Q_l(m,0)=\frac{1}{OVS}\sum_{m=0}^{OVS-1}Q_l(m-k,0)\,. \tag{135}$$

Next, we recall that $q_l(m)$ is simply a delayed version of the transmitted pulse shape, $q(m)$, of the *l*th base station. This implies that the power of $q_l(m)$ is independent of the base station. Combining the two last observations we conclude that

$$E\left\{\left|\varepsilon_{\mathbf{n}_l s_l}\right|^2\right\}=\frac{2M\left|b_l\right|^2\sigma_s^2\sigma_n^2}{N_s}\,, \tag{136}$$

where

$$\sigma_s^2\equiv\frac{1}{OVS}\sum_{m=0}^{OVS-1}Q_l(m,0)\,,\ \forall l\,. \tag{137}$$

4.6 Final Substitution

First, from Eqs. (113) and (114) we obtain some useful observations regarding Eq. (108) which will be exploited to simplify the last. The first and immediate observation is

$$E\left\{v_{l_1,l_2}v_{l_3,l_4}\right\}=0\,,\ \{l_1,l_2\}\notin\{l_3,l_4\}\,, \tag{138}$$

which means that there is no correlation between two terms of v_{l_1,l_2}, when these terms are evaluated for different base station pairs. However, if one of the base stations in v_{l_1,l_2}, say l_1, coincides with a single base station in the pair of the second term, v_{l_3,l_4}, then we have

$$\begin{aligned}E\left\{v_{l_1,l_2}v_{l_3,l_4}\right\}=\frac{1}{2}\Bigg(&\mathrm{Im}^2\left\{\frac{1}{\lambda_{l_1}}\right\}\cdot\left(E\left\{\left|\varepsilon_{\boldsymbol{n}_{l_1}s_{l_1}}\right|^2\right\}+\mathrm{Re}\left\{E\left\{\varepsilon^2_{\boldsymbol{n}_{l_1}s_{l_1}}\right\}\right\}\right)\\&+\mathrm{Re}^2\left\{\frac{1}{\lambda_{l_1}}\right\}\cdot\left(E\left\{\left|\varepsilon_{\boldsymbol{n}_{l_1}s_{l_1}}\right|^2\right\}-\mathrm{Re}\left\{E\left\{\varepsilon^2_{\boldsymbol{n}_{l_1}s_{l_1}}\right\}\right\}\right)\\&+2\mathrm{Re}\left\{\frac{1}{\lambda_{l_1}}\right\}\cdot\mathrm{Im}\left\{\frac{1}{\lambda_{l_1}}\right\}\cdot\mathrm{Im}\left\{E\left\{\varepsilon^2_{\boldsymbol{n}_{l_1}s_{l_1}}\right\}\right\}\Bigg),\ l_1=l_3,\ l_2\notin\{l_3,l_4\}\,,\end{aligned} \tag{139}$$

and

$$E\left\{v_{l_1,l_2}v_{l_3,l_4}\right\}\Big|_{l_1=l_4,\,l_2\notin\{l_3,l_4\}}=-E\left\{v_{l_1,l_2}v_{l_3,l_4}\right\}\Big|_{l_1=l_3,\,l_2\notin\{l_3,l_4\}}\,, \tag{140}$$

where we used the relation given in Eq. (117). Similarly, the equivalent version of Eqs. (139) and (140) for the case where l_2 coincides with a single base station in the pair of v_{l_3,l_4} is then given by the following equations set

$$E\left\{v_{l_1,l_2}v_{l_3,l_4}\right\}=\frac{1}{2}\Bigg(\mathrm{Im}^2\left\{\frac{1}{\lambda_{l_2}}\right\}\cdot\left(E\left\{\left|\varepsilon_{\boldsymbol{n}_{l_2}s_{l_2}}\right|^2\right\}+\mathrm{Re}\left\{E\left\{\varepsilon^2_{\boldsymbol{n}_{l_2}s_{l_2}}\right\}\right\}\right)$$

$$+\mathrm{Re}^2\left\{\frac{1}{\lambda_{l_2}}\right\}\cdot\left(E\left\{\left|\varepsilon_{\boldsymbol{n}_{l_2}s_{l_2}}\right|^2\right\}-\mathrm{Re}\left\{E\left\{\varepsilon^2_{\boldsymbol{n}_{l_2}s_{l_2}}\right\}\right\}\right) \tag{141}$$

$$+2\mathrm{Re}\left\{\frac{1}{\lambda_{l_2}}\right\}\cdot\mathrm{Im}\left\{\frac{1}{\lambda_{l_1}}\right\}\cdot\mathrm{Im}\left\{E\left\{\varepsilon^2_{\boldsymbol{n}_{l_2}s_{l_2}}\right\}\right\}\Bigg),\ l_2=l_4,\ l_1\notin\{l_3,l_4\},$$

and

$$E\left\{v_{l_1,l_2}v_{l_3,l_4}\right\}\Big|_{l_2=l_3,\,l_1\notin\{l_3,l_4\}}=-E\left\{v_{l_1,l_2}v_{l_3,l_4}\right\}\Big|_{l_2=l_4,\,l_1\notin\{l_3,l_4\}}. \tag{142}$$

The last observation refers to the case in which the base station pair of v_{l_1,l_2} coincides with the pair of the second term so that

$$E\left\{v_{l_1,l_2}v_{l_3,l_4}\right\}\Big|_{l_1=l_3,\,l_2=l_4}=E\left\{v_{l_1,l_2}v_{l_3,l_4}\right\}\Big|_{l_1=l_3,\,l_2\notin\{l_3,l_4\}}+E\left\{v_{l_1,l_2}v_{l_3,l_4}\right\}\Big|_{l_2=l_4,\,l_1\notin\{l_3,l_4\}}. \tag{143}$$

Now using the definition of λ_l given in Eq. (31) and the results obtained in Eqs. (130), (131) and (136), we get

$$E\left\{v_{l_1,l_2}v_{l_3,l_4}\right\}=\frac{\sigma_s^2\sigma_n^2}{N_sM\left|\overline{R}^{\alpha}_{ss}(k)\right|^2\left|b_{l_1}\right|^2},\ l_1=l_3,\ l_2\notin\{l_3,l_4\}, \tag{144}$$

where the expression for $E\left\{v_{l_1,l_2}v_{l_3,l_4}\right\}$ under other settings of l_1, l_2, l_3, and l_4 can be easily obtained using the relations from Eqs. (140), (142), and (143). We bear in mind that according to Eq. (41), the two index sets $\{l_1,l_2\}$ and $\{l_3,l_4\}$ go over exactly the same distinct ordered pairs of base stations. Thus, substituting Eq. (144) into Eq. (107) yields

$$E\left\{\widetilde{f}'(\boldsymbol{p}_0)\cdot\widetilde{f}'(\boldsymbol{p}_0)^T\right\}=\frac{4\pi^2\alpha^2\sigma_s^2\sigma_n^2}{N_sM\left|\overline{R}_{ss}^{\alpha}(k)\right|^2}\cdot\left(\sum_{l_1,l_2}\frac{\left|b_{l_1}\right|^2+\left|b_{l_2}\right|^2}{\left|b_{l_1}\right|^2\left|b_{l_2}\right|^2}\Gamma_{l_1l_2,l_1l_2}(\boldsymbol{p}_0)\right.$$
$$\left.-\sum_{l_1,l_2}\left[\sum_{l_3}\frac{\Gamma_{l_1l_2,l_3l_1}(\boldsymbol{p}_0)}{\left|b_{l_1}\right|^2}+\sum_{l_4}\frac{\Gamma_{l_1l_2,l_2l_4}(\boldsymbol{p}_0)}{\left|b_{l_2}\right|^2}\right]\right), \tag{145}$$

where $\Gamma_{l_1l_2,l_3l_4}(\boldsymbol{p}_0)$ is defined in Eq. (71).

Finally, after the substitution of Eqs. (73) and (145) into Eq. (68), the covariance matrix of the estimation error vector is given by

$$E\left\{\boldsymbol{\varepsilon}_{\boldsymbol{p}}\boldsymbol{\varepsilon}_{\boldsymbol{p}}^H\right\}\cong\frac{\sigma_s^2\sigma_n^2}{4\pi^2\alpha^2N_sM\left|\overline{R}_{ss}^{\alpha}(k)\right|^2}\left[\sum_{l_1,l_2}\Gamma_{l_1l_2,l_1l_2}(\boldsymbol{p}_0)\right]^{-1}$$
$$\cdot\left(\sum_{l_1,l_2}\frac{\left|b_{l_1}\right|^2+\left|b_{l_2}\right|^2}{\left|b_{l_1}\right|^2\left|b_{l_2}\right|^2}\Gamma_{l_1l_2,l_1l_2}(\boldsymbol{p}_0)-\sum_{l_1,l_2}\left[\sum_{l_3}\frac{\Gamma_{l_1l_2,l_3l_1}(\boldsymbol{p}_0)}{\left|b_{l_1}\right|^2}+\sum_{l_4}\frac{\Gamma_{l_1l_2,l_2l_4}(\boldsymbol{p}_0)}{\left|b_{l_2}\right|^2}\right]\right) \tag{146}$$
$$\cdot\left[\sum_{l_1,l_2}\Gamma_{l_1l_2,l_1l_2}(\boldsymbol{p}_0)\right]^{-1}.$$

Equivalently, Eq. (146) can be written in the following representation

$$E\left\{\boldsymbol{\varepsilon}_{\boldsymbol{p}}\boldsymbol{\varepsilon}_{\boldsymbol{p}}^H\right\}\cong\frac{1}{4\pi^2\alpha^2N_sM\left|\rho_{ss}^{\alpha}(k)\right|^2\mathrm{SNR}}\cdot\Omega(\boldsymbol{p}_0,\boldsymbol{b}), \tag{147}$$

where

$$\boldsymbol{b}\equiv[b_1,\cdots,b_L]^T,\quad \mathrm{SNR}\equiv\frac{\sigma_s^2}{\sigma_n^2},\quad \rho_{ss}^{\alpha}(k)\equiv\frac{\overline{R}_{ss}^{\alpha}(k)}{\sigma_s^2}, \tag{148}$$

$$\Omega(\boldsymbol{p}_0,\boldsymbol{b}) \equiv \left[\sum_{l_1,l_2}\Gamma_{l_1l_2,l_1l_2}(\boldsymbol{p}_0)\right]^{-1}$$
$$\cdot\left(\sum_{l_1,l_2}\frac{\left|b_{l_1}\right|^2+\left|b_{l_2}\right|^2}{\left|b_{l_1}\right|^2\left|b_{l_2}\right|^2}\Gamma_{l_1l_2,l_1l_2}(\boldsymbol{p}_0)-\sum_{l_1,l_2}\left[\sum_{l_3}\frac{\Gamma_{l_1l_2,l_3l_1}(\boldsymbol{p}_0)}{\left|b_{l_1}\right|^2}+\sum_{l_4}\frac{\Gamma_{l_1l_2,l_2l_4}(\boldsymbol{p}_0)}{\left|b_{l_2}\right|^2}\right]\right)$$
$$\cdot\left[\sum_{l_1,l_2}\Gamma_{l_1l_2,l_1l_2}(\boldsymbol{p}_0)\right]^{-1}.$$

The magnitude of $\rho_{ss}^{\alpha}(k)$ is sometimes referred to as the *feature strength* of the signal $s(m)$ at cycle frequency α and lag *k*. The feature strength can be viewed as the squared ratio between the power gained by the SOI at cycle frequency α and lag *k* and the signal conventional power, namely, the one obtained at both zero cycle frequency and lag. We mention here that the feature strength of any signal satisfies that $\left|\rho_{ss}^{\alpha}(k)\right|\le 1$ for all α and *k* (see, e.g., [7]), and that the feature strength of most communication signals such as PAM, QAM, and PSK, is around 1/3 or less [16]. The last observation together with Eq. (147) imply that not the entire power of the received signal contributes to a decrease in the estimation error but only a relative part of it, embedded in the corresponding cycle frequency and lag. Likewise, we note that in our model the fading phenomenon experienced by the antenna arrays is captured by the path loss coefficients, b_l, so that any degradation in the algorithm performance in case of fading will be reflected by these factors only. Thus, the definition of the system SNR in Eq. (148) takes no account of any fading and measures the long term average of the signal power.

Furthermore, Eq. (147) shows, as expected, that under SEA, the covariance matrix of the estimation error decreases monotonically with the increase of each of the following four

quantities: the number of samples, N_s, the number of array elements in each base station, M, the SNR in which the system operates, and the baud rate of the SOI, α. Specifically, the matrix $E\left\{\boldsymbol{\varepsilon}_{\boldsymbol{p}}\boldsymbol{\varepsilon}_{\boldsymbol{p}}^{H}\right\}$ is inversely proportional to the first three parameters and to the squared value of the last, where the performance degradation due to a decrease in α is ascribed to the resolution diminution results from the baud duration increase. In addition, the error covariance obviously depends on the geometry of the problem, i.e., on the deployment of the base stations and emitter. This dependency is reflected in terms of the type of $\Gamma_{l_1 l_2, l_3 l_4}(\boldsymbol{p}_0)$. Likewise, $E\left\{\boldsymbol{\varepsilon}_{\boldsymbol{p}}\boldsymbol{\varepsilon}_{\boldsymbol{p}}^{H}\right\}$ is also a function of the path loss factors, b_l, experienced by the different base stations. The smaller these factors are, the larger is the error covariance since any decrease of these factors reduces the effective SNR of the system. Finally, we mention that the observations obtained here analytically will be substantiated empirically using Monte Carlo simulations in Chapter 6.

5 CRLB

This chapter introduces the main concepts of the common benchmark used in the general field of estimation, the Cramér-Rao lower bound (CRLB). The CRLB bounds the error covariance matrix of any unbiased estimate of a real parameters vector. Furthermore, it equals the performance of an efficient estimator if such exists. Therefore, comparing the MSE of a certain unbiased estimator to the CRLB is of much interest when evaluation of the estimator relative efficiency is desired.

We begin this chapter by studying the general formula of the CRLB obtained for a complex Gaussian data and two special cases deduced from it. However, as will be explained in the sequel, the CRLB will not be derived for the certain problem considered in this work as the information that can be extracted from it regarding the problem at hand is very limited.

5.1 General CRLB Formulation

Let $\boldsymbol{\theta}$ be an unknown real parameter vector to be estimated and let $\boldsymbol{r}$ be an observation random vector drawn from a circular symmetric complex Gaussian distribution with parameters

$$\boldsymbol{r} \sim \mathcal{CN}(\boldsymbol{m}(\boldsymbol{\theta}), R(\boldsymbol{\theta})),$$

where $\boldsymbol{m}(\boldsymbol{\theta})$ and $R(\boldsymbol{\theta})$ are the expectation and covariance matrix of $\boldsymbol{r}$, respectively. The i,j entry of the Fisher information matrix (FIM), or equivalently the i,j element of the inverse of the CRLB matrix is given by [24]

$$[(\mathbf{FIM})]_{ij} \equiv [(\mathbf{CRLB})^{-1}]_{ij} = \text{trace}\left\{ R^{-1}(\boldsymbol{\theta}) \frac{\partial R(\boldsymbol{\theta})}{\partial \theta_i} R^{-1}(\boldsymbol{\theta}) \frac{\partial R(\boldsymbol{\theta})}{\partial \theta_j} \right\} + 2\,\text{Re}\left\{ \frac{\partial \boldsymbol{m}^*(\boldsymbol{\theta})}{\partial \theta_i} R^{-1}(\boldsymbol{\theta}) \frac{\partial \boldsymbol{m}(\boldsymbol{\theta})}{\partial \theta_j} \right\}. \quad (149)$$

The general formula given in Eq. (149) provides the CRLB on the covariance matrix of any unbiased estimate of $\boldsymbol{\theta}$ assuming that the observation vector $\boldsymbol{r}$ has a complex Gaussian distribution. However, in order to apply this formula to the estimation problem of interest herein, we should make some modifications in the problem formulation presented in Chapter 2. These modifications are set forth in the following section.

5.2 The CRLB Model

To the end of determining the exact adjustments needed in the current data model for the application of the CRLB formula, we revisit the problem formulation given in Eq. (21). There we observe that although this model equation holds for any *l*, where $l = 1,..,L$, it is written separately for each base station so that Eq. (149) cannot be applied directly to the observation vector of Eq. (21), $\boldsymbol{r}_l(k)$. Hence, we should convert the existing model representation into a compound form in which a single observation vector contains the samples from all of the base stations. The most straightforward way to obtain such an observation vector is to transform the existing model into the frequency domain using a DFT procedure [23]. Applying a DFT of length N_s to Eq. (21) yields

$$\bar{\boldsymbol{r}}_l(k) = b_l \boldsymbol{a}_l(\boldsymbol{p}) \bar{s}(k) e^{-j\frac{2\pi k}{N_s T_s}(\tau_l(\boldsymbol{p}) - t_0)} + \bar{\boldsymbol{n}}_l(k), \quad (150)$$

where $\bar{\boldsymbol{r}}_l(k)$, $\bar{s}(k)$, and $\bar{\boldsymbol{n}}_l(k)$ are the kth DFT coefficients of the received vector, SOI, and noise vector of the lth array, respectively, and where the kth DFT coefficient is defined as [14]

$$\bar{s}(k) \equiv \frac{1}{\sqrt{N_s}} \sum_{n=0}^{N_s-1} s(n) e^{-\frac{j2\pi nk}{N_s}}.$$

Finally, concatenating the DFT coefficients given in Eq. (150) from all of the L base stations into a single observation vector leads to the following compound model representation

$$\bar{\boldsymbol{r}}(k) = \tilde{\boldsymbol{a}}(k, \boldsymbol{p}, \boldsymbol{b}) \bar{s}'(k) + \bar{\boldsymbol{n}}(k), \tag{151}$$

where we used the following notations

$$\begin{aligned}
&\bar{\boldsymbol{r}}(k) \equiv \left[\bar{\boldsymbol{r}}_1^T(k), \cdots, \bar{\boldsymbol{r}}_L^T(k)\right]^T, \\
&\tilde{\boldsymbol{a}}(k, \boldsymbol{p}, \boldsymbol{b}) \equiv \left[b_1 e^{-j\frac{2\pi k}{N_s T_s}\tau_1(\boldsymbol{p})} \boldsymbol{a}_1^T(\boldsymbol{p}), \cdots, b_L e^{-j\frac{2\pi k}{N_s T_s}\tau_L(\boldsymbol{p})} \boldsymbol{a}_L^T(\boldsymbol{p}) \right]^T, \\
&\bar{s}'(k) \equiv \bar{s}(k) e^{-j\frac{2\pi k}{N_s T_s} t_0}, \\
&\bar{\boldsymbol{n}}(k) \equiv \left[\bar{\boldsymbol{n}}_1^T(k), \cdots, \bar{\boldsymbol{n}}_L^T(k)\right]^T.
\end{aligned} \tag{152}$$

Eq. (151) introduces a new model representation which is equivalent to the one from Eq. (21). This frequency domain model treats the L distinct base stations, each equipped with M-element array, as a single equivalent base station with ML array elements. Likewise, each M array elements of the same base station experience the same path loss factor, b_l and the same time delay, $e^{-j\frac{2\pi k}{N_s T_s}(\tau_l(\boldsymbol{p}) - t_0)}$. Therefore, using the equivalent model, the

problem of L distinct data models amounts to a single AOA conventional data model, where the emitter angle of arrival, θ (see, e.g., [23]) is now replaced with the emitter position, $\boldsymbol{p}$ and the path loss factor is taken this time into account. There is, obviously, an advantage in the compound model of Eq. (151) as it offers a compact and concise representation to the problem at hand – a representation which also coincides with the conventional model in the field of array signal processing. However, this representation has also one drawback. This drawback pertains to the statistical properties of the DFT coefficients of the SOI. While the SOI in the time domain is a cyclostationary signal, its DFT representation is neither cyclostationary, nor stationary. Thus, this transformation is somewhat problematic for a cyclostationary SOI. For a stationary complex white Gaussian SOI which is the typical case in studies on conventional DPD ([25], [11]), this obstacle does not exist since the DFT for such a case is transparent, leaving the frequency domain coefficients with exactly the same statistical properties as their time domain counterparts.

Next, before we can move on to the main part of this chapter, namely obtaining the CRLB for cyclostationary SOI, we should first set the framework under which this CRLB is developed. The two different available frameworks are associated with different CRLB versions, as will be explained in the following discussion.

5.3 Conditional and Unconditional Model

In the literature of CRLB, in particular, and estimation theory, in general, there exist two different types of models [21]. The first one, which is called conditional or deterministic model, assumes that the SOI is nonrandom, meaning that the sequence $\bar{s}'(k)$ in Eq. (151)

represents exactly the same realization for all possible sequences of the observation vector $\bar{\boldsymbol{r}}(k)$, and the only sequence that varies between different realizations of the last is the noise vector, $\bar{\boldsymbol{n}}(k)$. In the second model, which is called unconditional or stochastic model, the SOI is assumed to be a random process, i.e., the sequence $\bar{s}'(k)$ varies from one realization of $\bar{\boldsymbol{r}}(k)$ to another. The substantial difference in the statistical nature of the SOI in these two model types leads to different maximum likelihood (ML) methods termed conditional ML and unconditional ML (UML), respectively. Furthermore, each model assumption obviously entails a different derivation of the CRLB, yielding a different corresponding bound. For notational convenience, the CRLB obtained under conditional model assumption (CMA) will be referred to as CCRLB, and the one corresponding to the unconditional model assumption (UMA) will be denoted by UCRLB. We shall now detail some of the main differences between these two bounds.

The first one is related to the statistical properties assumed regarding the SOI. We recall that in order to apply Eq. (149) to the model given in Eq. (151) $\bar{\boldsymbol{r}}(k)$ is required to have a complex Gaussian distribution. Thus, under CMA only, the noise term $\bar{\boldsymbol{n}}(k)$ should be a complex Gaussian process while the SOI, $\bar{s}'(k)$ is free from constraints on its statistical properties. However, under UMA the SOI and the noise are required to be jointly complex Gaussian which implies that the SOI itself should be drawn from a complex Gaussian distribution.

Another difference between the two CRLB types relates to the vector of nuisance parameters that should be estimated. Although this vector includes many common parameters for both the CCRLB and UCRLB such as the transmitter position, base station

path loss factors, and noise variance, it has a completely different set of SOI parameters under each model assumption. Specifically, under CMA the SOI is nonrandom but represents a single realization and therefore the SOI unknown parameters are the signal data samples, $\bar{s}'(k)$, $k = 1,..,N_s$. Under UMA however, the SOI is random so that the signal unknown parameters comprise the statistical properties of the signal rather than its realization, i.e., the mean and covariance matrix of $\bar{s}'(k)$.

The difference between the two model assumptions does not amount to the above-mentioned changes in the derivation process itself. There is of coarse also a difference in the performance of the two CRLB types. From the general theory of estimation it is well known that under some regularity conditions the ML estimator is found to be asymptotically efficient. In other words, the CRLB which is given as the MSE of the corresponding ML estimator can be attained by this estimator, provided that the ML estimator is consistent. The consistency of the estimator depends on the ratio between the number of data samples and estimated parameters. As long as this ratio remains bounded asymptotically the ML estimator suffers from inconsistency. However, when this ratio tends to infinity when increasing the number of samples, the ML estimate is found to be consistent and thus achieves the CRLB. Therefore, while the UML provides consistent estimation of the emitter position as it suffices to estimate only the statistical properties of the SOI rather than its actual realizations, the CML cannot provide a consistent estimate of the transmitter location. The last observation suggests that the UCRLB is attainable by its corresponding ML estimator, namely the UML, whereas the CCRLB cannot be achieved, even by the CML estimator. This leads to the inevitable conclusion that the

UCRLB is superior to the CCRLB, and whenever applicable, should be preferred as the chosen CRLB.

5.4 CRLB for Cyclostationary SOI

The CRLB for the estimation problems of both AOA and TDOA under the assumption of a cyclostationary SOI was examined in several papers. However, none of these CRLB derivations considered the exact SOI setup which is studied in this work, namely, a cyclostationary non-Gaussian SOI. Such a bound is found to be overly difficult to evaluate. Schell and Gardner computed the UCRLB for a cyclostationary Gaussian SOI [18] and compared it to the performance obtained by the Cyclic MUSIC algorithm for a PAM signal having a Gaussian symbol sequence [16]. As opposed to them, Gardner and Chen have compared their new suggested cyclic TDOA methods to the conventional UCRLB while treating the SOI as a stationary Gaussian signal [10]. This kind of bound can give an indication as for the ultimate performance that can be achieved when both the cyclostationarity and non-Gaussianness of the SOI are not exploited by the estimator which is the inherent situation of conventional methods. Yet, in the range of the observation time considered in this work which is up to 1K samples, the conventional UCRLB is found to be substantially smaller than the MSE obtained for the cyclic TDOA methods in [10]. Therefore, although these methods outperform conventional algorithms that achieve the UCRLB for stationary Gaussian signals, they do not attain this bound for cyclostationary non-Gaussian SOI so that little information can be extracted from the UCRLB.

The discussion above considered previous works which studied the application of the UCRLB to the case of a cyclostationary signal. Specifically, the SOI is inherently assumed to be Gaussian. However, it is well known that most cyclostationary communication signals, especially those having a digital modulation format, are not Gaussian. The justification for using the CRLB under both Gaussianness and cyclostationary assumption is thus the need to determine the effects of cyclostationarity on the estimation performance by comparing existing results which essentially assume only stationary Gaussian SOIs. Likewise, the tractability of the CRLB for Gaussian signals is another argument for using this assumption. We recall however, that since this work considers only a non-Gaussian SOI, it might be more suitable to use instead the CCRLB which was obtained by Stoica and Nehorai [20]. Such a bound is derived under CMA and thus, it is applicable to any type of signal in general, and to a cyclostationary non-Gaussian SOI in particular. Nevertheless, the CCRLB given in [20] has three major drawbacks which put its relevancy in doubt. The first two drawbacks of this CCRLB pertain to the difference between the model assumed in [20] and the one used throughout this work. Specifically, the estimated parameter of the SOI is the signal AOA in the case of [20], whereas in our work this parameter is the transmitter location which is a vector of two or three entries. Furthermore, our model considers the path loss factors experienced by the base stations as additional unknown parameters to be estimated. Thus, the vector of unknown parameters is different in the two studies. Likewise, we note that the CCRLB uses asymptotically an infinite number of signal samples, so that the FIM matrix under CMA has an infinite dimension. Hence, analytical derivation of the CCRLB in [20] was possible only due to the special block structure that the FIM takes under this

certain array model. However, this structure is no longer maintained if the path loss factors are taken into consideration. Thus, if our model formulation remains as is, a closed-form expression for the CCRLB is obviously unavailable unless we use instead a simplified model version in which the path loss factors are assumed to be estimated with zero error. Even under this simplification, we face the third drawback of this bound – the CCRLB is unattainable, even by its corresponding ML estimator. This claim was indeed corroborated by simulation results we performed which are not reported here.

To conclude, the observations brought up in the discussion above lead to the conclusion that currently, no appropriate CRLB is available for the problem at hand. The existing CRLB results are either not applicable to a non-Gaussian SOI or based on a formulation which does not completely comply with the one considered by this work. Furthermore, for a cyclostationary non-Gaussian SOI, the existing CRLB results are found to be substantially loose even for the case of algorithms which achieve the conventional UCRLB or worse, algorithms that outperform them. Therefore, in the simulation results part given in Chapter 6 we skip the comparison between the MSE of the CDPD method and any of the above-mentioned CRLB types and limit the performance comparison to other localization methods, among them the conventional DPD which for stationary Gaussian SOI attains the UCRLB even for a small number of samples and in a relatively low SNR values [11].

6 Simulation Results

In order to assess the performance of the devised algorithm and compare it with previous methods, we carried out an empirical study which simulates a typical cellular system. Such a system was already introduced and studied in the context of the CTDPD ambiguity problem in Subsection 3.5.2. The Monte Carlo simulations were performed in two different kinds of noise environments, AWGN and a mixture of the latter with a cyclostationary interferer having a different cycle frequency than the SOI. The case of additional signal with the same cycle frequency as the SOI is not considered in this chapter as multiple SOIs, all sharing the same cycle frequency, is out of the scope of this work. The concrete setup of each noise environment, as well as the results obtained for it, is reported hereby but first we provide a description of the general setup which is common to both types of simulations. This setup refers mainly to the model description given in Section 2.2.

6.1 General Simulation Setup

The simulations given herein consider four base stations ($L = 4$) placed at the corners of a 4 km $\times$ 4 km square. Each base station is equipped with a ULA of five antenna elements ($M = 5$). The distance, d, between any two adjacent antenna elements of the array is half wavelength. Such an array is depicted in Figure 12. For each trial, the SOI transmitter location is selected at random from a uniform distribution within the square formed by the four base stations. The deployment of the base stations together with the transmitter is illustrated in Figure 13.

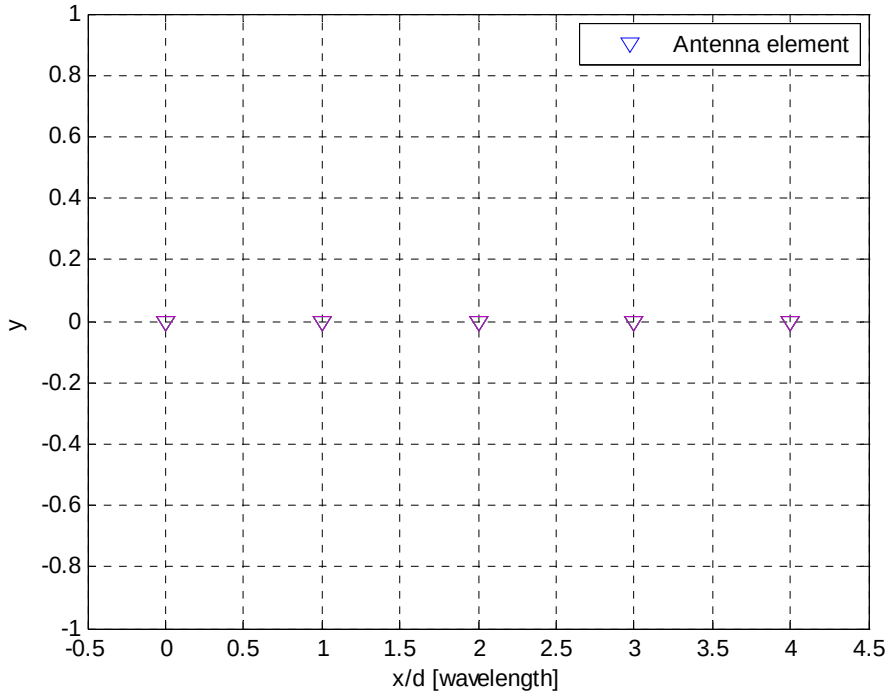

Figure 12. Geometry of a ULA with five antenna elements.

The SOI is a BPSK signal with a square root raised-cosine shaping. Likewise, the carrier frequency of the SOI is assumed to be 900 MHz, and its baud rate is set to be 100 kHz, unless otherwise stated. The over-sampling used in the receiver is 8 ($OVS = 8$), meaning that the sampling rate of the received signal is eight times the baud rate of the SOI. The power of the SOI is given by

$$\sigma_s^2 \equiv \frac{1}{OVS} \sum_{m=0}^{OVS-1} \sum_{n=-\infty}^{\infty} q_{SRRC}^2 (n \cdot OVS + m), \tag{153}$$

where $q_{SRRC}(m)$ is a square root raised-cosine pulse shape

$$q_{SRRC}(m) = \frac{4r}{\pi T} \cdot \left. \frac{\cos\left[(1+r)\pi t/T\right] + (4rt/T)^{-1} \sin\left[(1-r)\pi t/T\right]}{1-(4rt/T)^2} \right|_{t=mT_s},$$

with roll-off factor, r, which is set to 1. In the above equation, T and T_s are defined according to the relation given in Eq. (119).

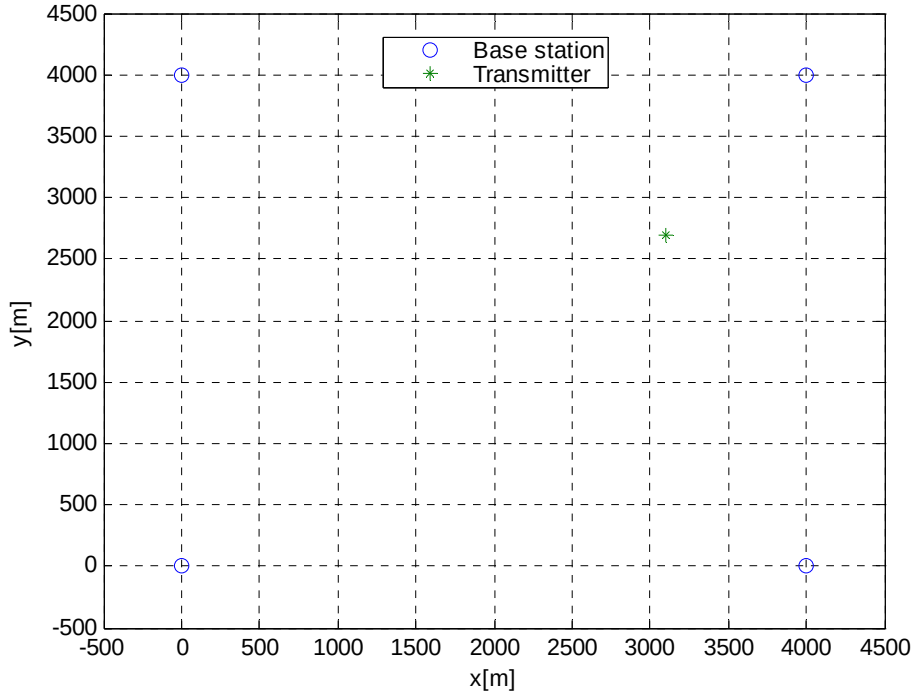

Figure 13. Illustration of base stations and transmitter deployment.

The lag parameter, k, of the cyclic autocorrelation matrix of the received vector in Eq. (23) is set to zero, as the maximum magnitude of the SOI cyclic autocorrelation, $R_{ss}^{\alpha}(k)$, is obtained at this lag value for a shaping of a square root raised cosine waveform (for more details, see Section 3.3).

The AWGN experienced by each antenna array, denoted henceforth by $\boldsymbol{w}_l(k)$, is a complex Gaussian noise which is both spatially and temporally white and has the following distribution

$$\boldsymbol{w}_l(k) \sim \mathcal{CN}(0, \sigma_n^2 I). \tag{154}$$

The path loss factor of each base station is generated once for each trial in the following manner

$$b_l = |b_l| e^{j2\pi\theta_{b_l}}, \qquad |b_l| \sim \mathcal{N}(1, 0.1^2), \quad \theta_{b_l} \sim U(0,1), \tag{155}$$

where $U(0,1)$ is a uniform distribution in the range [0,1].

Five different algorithms were applied in order to locate the SOI in each one of the two environment types:

- Cyclic DPD, including both types of lag versions, namely, the single and multiple lag versions according to Eqs. (44) and (48), respectively, where the multiple lag version used $K = 9$.
- Conventional DPD [25].
- AOA estimation based on Cyclic MUSIC [17] and a least squares location estimation using these AOA estimates as the data. This method is denoted in the plots by CAOA.
- TDOA estimation based on Cross-Correlation [4] between the base station pairs used by the CDPD and a least squares location estimation using these TDOA estimates as the data. This method is denoted in the plots by TDOA.
- TDOA estimation based on Cyclic Cross-Correlation [9] between the base station pairs used by the CDPD and a least squares location estimation using these TDOA estimates as the data. This method is denoted in the plots by CTDOA.

The performance evaluation presented in the following sections is based on the statistics of the miss distance, i.e., the distance between the true emitter position and the estimated one. Likewise, the estimation error in all of the plots of this chapter is given in terms of the root mean square (RMS) value of this miss distance.

6.2 Environment 1: AWGN

In this section, we compare the performance of the various algorithms in the presence of AWGN only, so that the general noise term of Eq. (21), $\boldsymbol{n}_l(k)$, consists of $\boldsymbol{w}_l(k)$ from Eq. (154) alone. Using Monte Carlo simulations, we study the performance of the CDPD algorithm, as well as of other localization methods, in terms of the following parameters:

- Observation time (number of symbols)
- SNR
- Number of antenna elements in each base station
- SOI baud rate

The plots given in the following subsections delineate the RMS error of the location estimation obtained by each one of the methods listed in Section 6.1 for the above-mentioned test cases. For the CDPD method, we report the RMS error of both the final estimator and its two sub estimators, the CADPD and CTDPD. Furthermore, in each one of the four experiments listed above, the predicted performance of the CTDPD algorithm obtained analytically in Chapter 4 is also attached and denoted in the figures by PA (performance analysis). This analytical RMS error is calculated according to Eq. (147) and is found to have an excellent compliance with the empirical one. The main

conclusion arises from the results reported in this section is that the CDPD outperforms all other cyclic methods as well as the TDOA algorithm in an AWGN-only environment. Likewise, this superiority of the CDPD is maintained while exhibiting merely the same performance as the DPD method which is found to achieve the CRLB for this kind of noise environment and a stationary Gaussian SOI. However, as opposed to the DPD, the CDPD offers in addition high robustness to strong narrowband interferences, again, without performance degradation in an AWGN-only environment, relative to the DPD method. The last observation will be demonstrated in detail in Section 6.3.

Finally, we note that for all of the test cases considered in the following subsections the multiple lag version of the CDPD, namely the one using $K = 9$ lag coefficients, does exhibit some performance improvement in comparison with the single lag version. However, this performance improvement is found to be relatively small, especially for high SNR and when using large observation time. The difference between the RMS errors obtained by these two versions gets more material only for low SNR and when averaging a relatively small number of symbols. Therefore, it seems appealing to prefer the multiple lag version of the CDPD over its single lag counterpart mainly in such conditions, since it obviously consumes more computational resources.

6.2.1 Performance vs. Observation Time

This subsection explores the influence of the observation time on the performance of the different algorithms. The effect of the observation time of the SOI utilized by the various methods for the location determination was examined using two SNR values residing in different SNR regimes. For each SNR value the number of symbols varied between 40

and 140 in steps of 20 symbols where at each such step we ran 300 Monte Carlo simulations. For clarity, the results of this simulation are split into two separate figures for each SNR value. Figure 14 and Figure 16 compare the RMS error of the different localization methods for SNR values of 0 dB and 10 dB, respectively, while Figure 15 and Figure 17 focus only on the performance of the CDPD algorithm and its two sub estimators for the above-mentioned SNR values.

We infer from Figure 14 and Figure 16 that the CDPD and DPD methods have similar performance in an AWGN environment for a rather wide range of observation time and in both low and high SNR regimes. The other algorithms, however, exhibit much inferior performance in this type of environment. Specifically, in the presence of AWGN alone, the two other cyclic methods, namely, the CAOA and CTDOA have significantly poor performance relative to the non cyclic methods and the CDPD, especially when using a short observation time.

Another conclusion that can be deduced from Figure 15 and Figure 17 pertains to the error behavior of the CTDPD method as a function of the observation time. According to the analytical SEA given in Eq. (147), the MSE of the CTDPD is inversely proportional to the number of samples. Such behavior is indeed illustrated by the empirical RMS error of the CTDPD. We observe that above a certain value of the observation time, which is around 100 symbols, there is an excellent agreement between the predicted performance derived from the SEA and the empirical one obtained from the Monte Carlo simulations. This observation holds for both low and high SNR regimes.

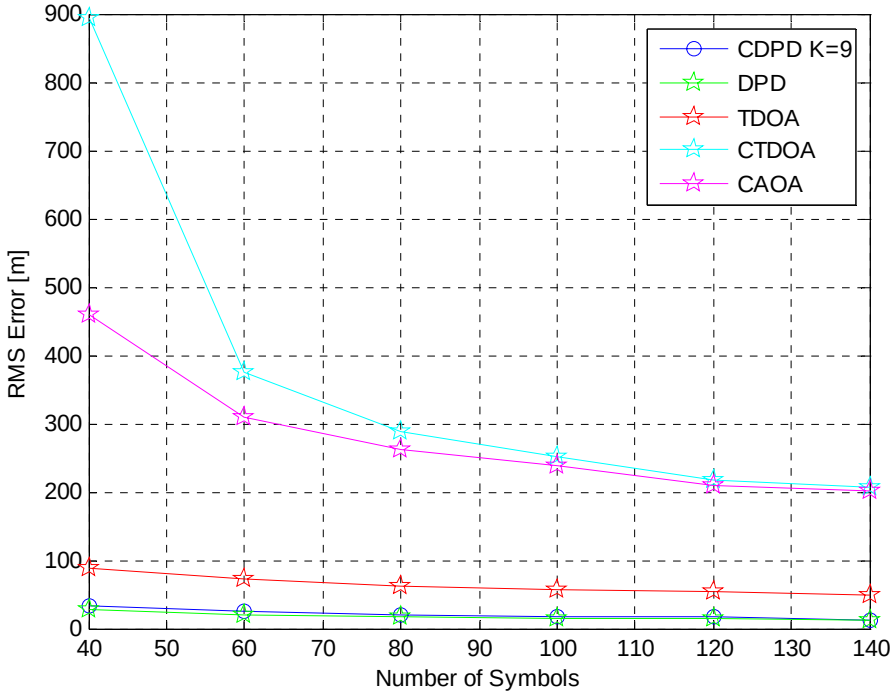

Figure 14. RMS error vs. number of symbols (Part I), SNR = 0 dB, AWGN environment.

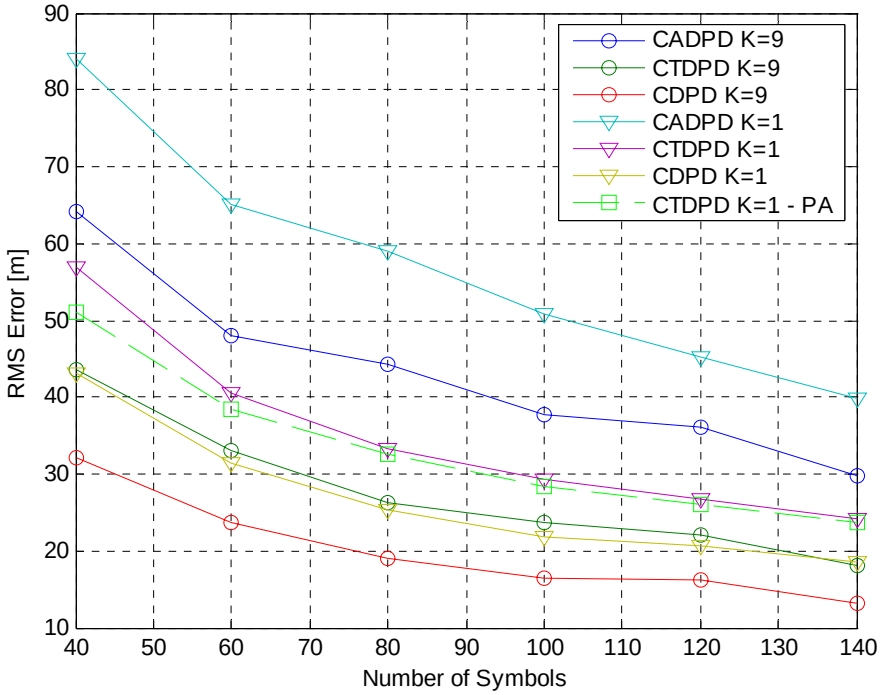

Figure 15. RMS error vs. number of symbols (Part II), SNR = 0 dB, AWGN environment.

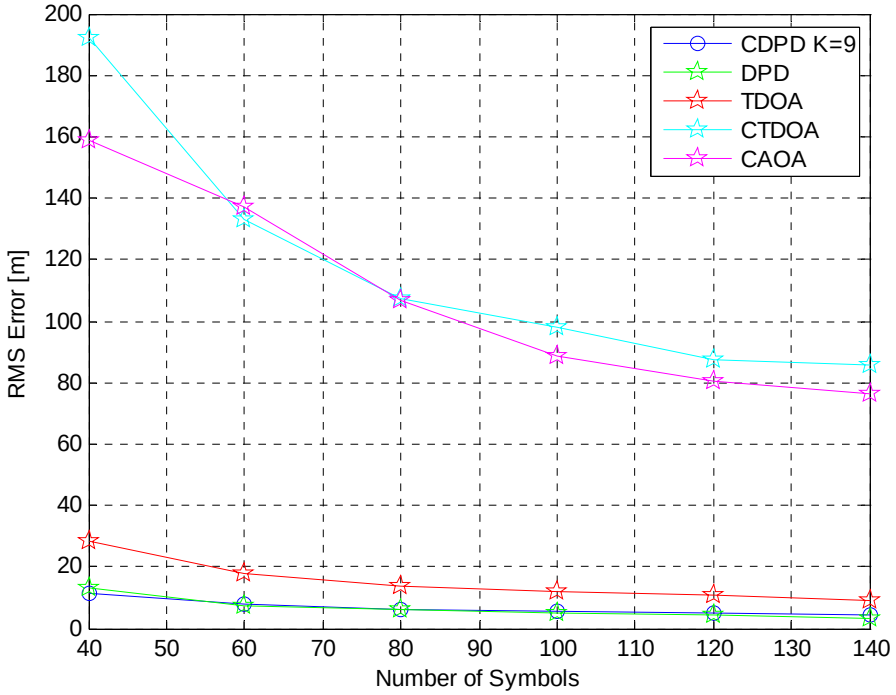

Figure 16. RMS error vs. number of symbols (Part I), SNR = 10 dB, AWGN environment.

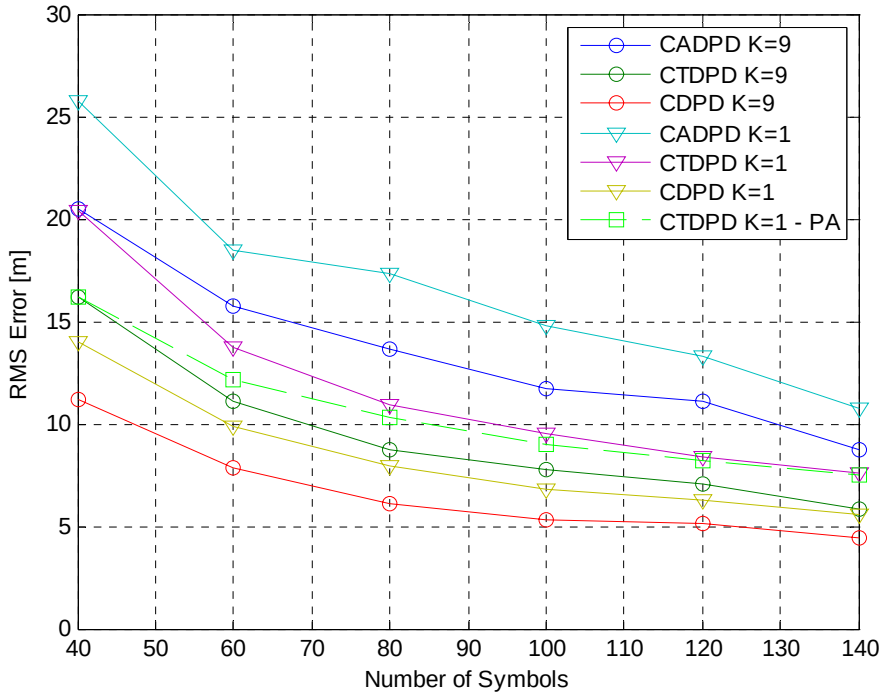

Figure 17. RMS error vs. number of symbols (Part II), SNR = 10 dB, AWGN environment.

6.2.2 Performance vs. SNR

Here we investigate the effect of the system SNR on the performance of the different localization algorithms in general, and the CDPD algorithm in particular. The simulations examined SNR values in the range of [-5, 10] dB in steps of 2.5 dB. At each SNR value, we performed 300 Monte Carlo trials in order to obtain the statistical properties of the performance where each location determination was based on 40 symbols of the SOI, or equivalently, 320 samples of the received signal. The results are shown in Figure 18. Since we already saw in Subsection 6.2.1 that both the CAOA and CTDOA methods exhibit significantly poor performance for a relative short observation time such as the one considered in this subsection, we do not present their performance in this plot. Figure 14 and Figure 16 have already demonstrated the high resemblance between the performance of the CDPD and DPD methods in terms of the observation time for 0 dB and 10 dB, respectively. Similarly to these two figures, Figure 18 shows also similar error behavior of the CDPD and DPD methods in an AWGN-only environment, only this time, in terms of the system SNR. Likewise, the similar performance of these two methods is found to be superior to the one obtained by all the other competing algorithms, including the two cyclic methods CAOA and CTDOA whose RMS error is substantially larger than the error range displayed in this plot for such short observation time. Moreover, Figure 18 also corroborates the analytical performance of the CTDPD method as a function of the SNR. Specifically, the empirical MSE of this method is found to be inversely proportional to the SNR, as predicted by Eq. (147). In addition, we note that the empirical performance converges to the analytical one above a threshold SNR, which is around the

0 dB for the considered observation time. Clearly, for a longer observation time, this threshold SNR should be even smaller, that is, in the negative part of the SNR axis.

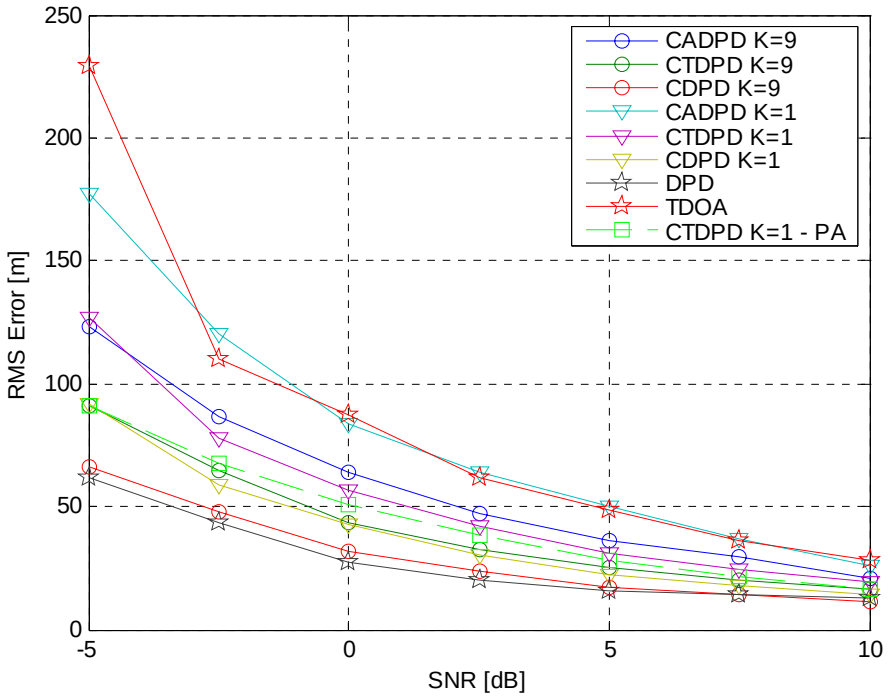

Figure 18. RMS error vs. SNR, AWGN environment.

6.2.3 Performance vs. Number of Antenna Elements

From Eq. (147) we conclude that the MSE of the CTDPD is inversely proportional to the number of sensors in each antenna array. This observation is tested and corroborated empirically in this subsection. The number of elements in each base station was changed from 2 to 5 where for each such value we performed 300 Monte Carlo trials. The SNR was set to 0 dB and the observation time to 120 symbols. The results are shown in Figure 19. Since the conventional DPD substantially outperforms all the other competing methods of the CDPD, this figure compares the RMS error of the CDPD only to the one of the conventional DPD. We observe from Figure 19 that similarly to previous plots, the RMS error of the CDPD and DPD estimators almost coincide for the considered test case.

Furthermore, the empirical performance of the CTDPD algorithm is again well approximated by the predicted performance obtained analytically.

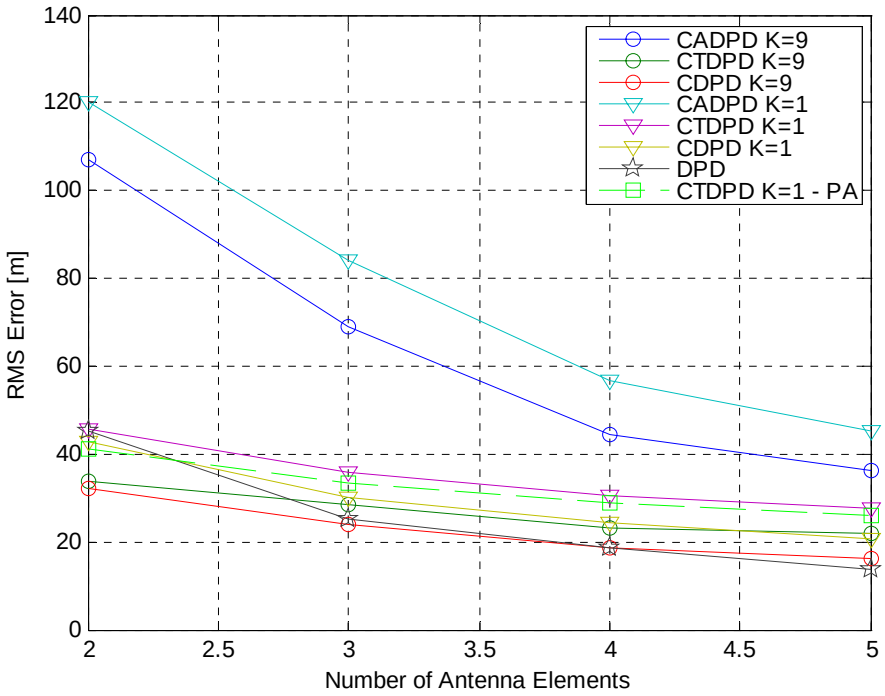

Figure 19. RMS error vs. number of antenna elements, AWGN environment.

6.2.4 Performance vs. SOI Baud Rate

Another observation made according to Eq. (147) is that the MSE of the CTDPD method is inversely proportional to the square SOI baud rate. This subsection is dedicated to validating this observation empirically. To this end, the SOI baud rate is varied between 0.1 and 0.4 MHz in steps of 0.1 MHz where at each such step, 300 Monte Carlo simulations were carried out. In addition, we set the SNR to 5 dB and the observation time to 80 symbols. The results are depicted in Figure 20 where from exactly the same considerations described in Subsection 6.2.3, the performance comparison includes only the CDPD and DPD methods. Again we notice that the CDPD and DPD keep showing much of the same error behavior in an AWGN environment, this time as a function of the

symbol rate. Likewise, the empirical error substantiates the analytical performance of the CTDPD method, i.e., its RMS value increases linearly with the baud duration.

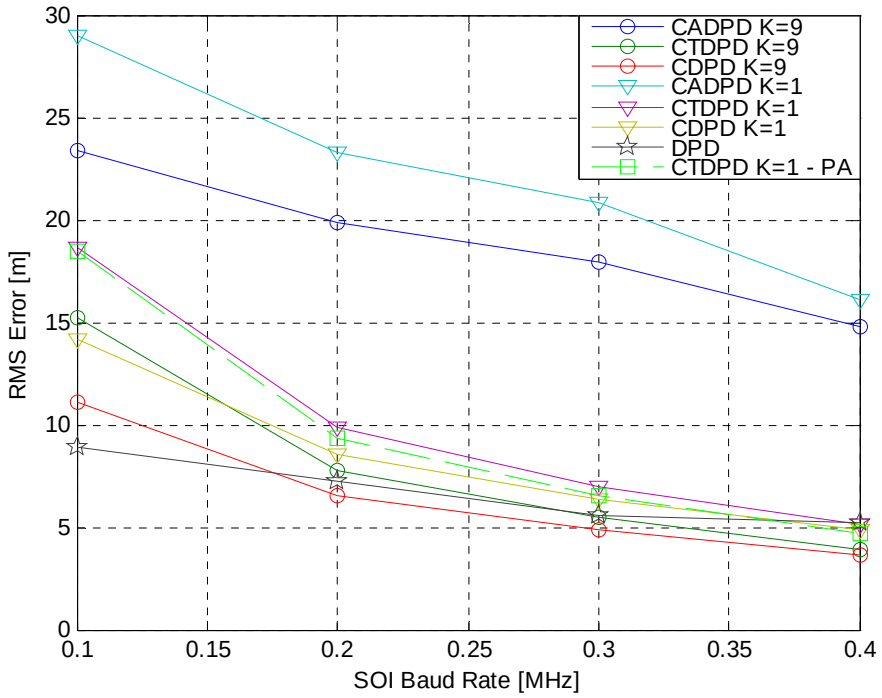

Figure 20. RMS error vs. SOI baud rate, AWGN environment.

6.3 Environment 2: Cyclostationary Interference and AWGN

In Section 6.2 we examined the performance of the CDPD algorithm relative to existing localization methods in an AWGN-only environment. Various simulations were carried out, where each time another system parameter was put to the test. In all of the reported simulations, the CDPD method exhibits similar performance to that obtained by the conventional DPD. Moreover, both methods substantially outperform the other cyclic algorithms, as well as the TDOA method. However, as will be demonstrated in this section, these observations made for an AWGN-only environment do not hold anymore when an additional dominant interference exists in the system. Specifically, the DPD algorithm which had excellent performance in an AWGN-only environment is no longer

a comparable competitor to the CDPD method in the presence of a strong interferer as it provides much larger estimation error than the latter. Similarly to the DPD, dramatic performance degradation is also experienced by the TDOA method for this type of noise. Likewise, the cyclic methods which have poor performance in the presence of AWGN alone become significantly more appealing than the conventional methods such as the DPD when a dominant interference exists. Yet, they still yield a rather large estimation error in comparison with the CDPD for this kind of environment. To conclude, by contrast to the DPD, TDOA, and other cyclic algorithms which gain a relative advantage only in one type of noise environment, the CDPD is found to be an attractive method for an AWGN-only environment as well as in the presence of a strong narrowband interferer.

Next, before we move on to present the results obtained, we shall first describe the exact setup of this noise environment. In this section, the overall noise term in Eq. (21) is a mixture of a narrowband cyclostationary interference and AWGN. Similarly to the SOI, the cyclostationary interferer is also a BPSK signal with a square root raised-cosine shaping. Likewise, both the SOI and the interference have identical carrier frequency, namely, 900 MHz, and the same power so that the signal-to-interference (SIR) ratio is 1. However, the cycle frequency associated with each one of the two signals is different as the baud rate of the SOI is 100 kHz, while the interferer is assumed to posses a symbol rate of 120 kHz. As opposed to the SOI, the location of the interference is fixed for each trial and is set to be [801.8, 1206.4] meters. The Monte Carlo simulations reported in this section include a comparison between the performance of the CDPD and other localization methods as a function of the following parameters:

- Observation time (number of symbols)
- SNR

Thereafter, the excellent robustness of the CDPD algorithm to narrowband interferences is demonstrated using a comparison between contour plots of the CDPD and other localization algorithms. Finally, we mention that all of the simulation results reported hereby consider a single dominant interferer, however, similar results can be obtained also for the case of multiple interferers.

6.3.1 Performance vs. Observation Time

This subsection uses exactly the same setup described in Subsection 6.2.1 and shows the performance obtained by the various algorithms as a function of the observation time for SNR of 0 dB and 10 dB in Figure 21 and Figure 22, respectively. We conclude from these two figures that the CDPD substantially outperforms all other existing methods in the considered noise environment where this conclusion holds for the entire range of the examined observation time and for both low and high SNR regimes. Likewise, the performance of the two non cyclic methods, namely, the TDOA and DPD, does not improve with the increase in either the SNR or the observation time. This behavior is well understood since non cyclic methods cannot distinguish between the SOI and interferer, no matter what the system SNR and number of symbols available are. Thus, any increase in these parameters does not contribute to mitigate the ambiguity problem arises due to the existence of the two sources so that both of them are equally likely to be resolved. By contrast to the non cyclic algorithms, the cyclic methods such as the CTDOA and CAOA

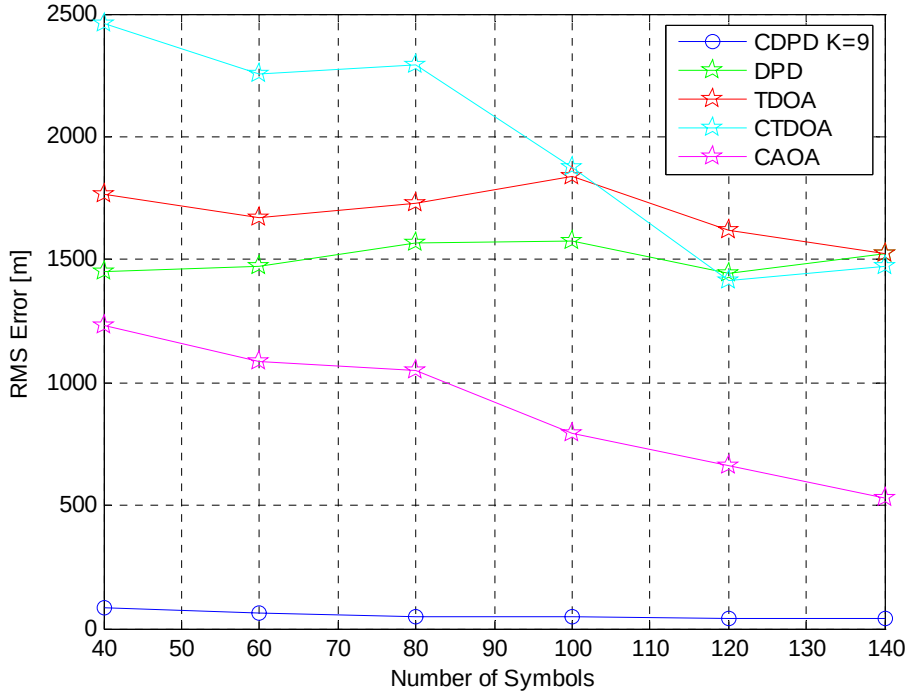

Figure 21. RMS error vs. number of symbols, SNR = 0 dB, interferer and AWGN environment.

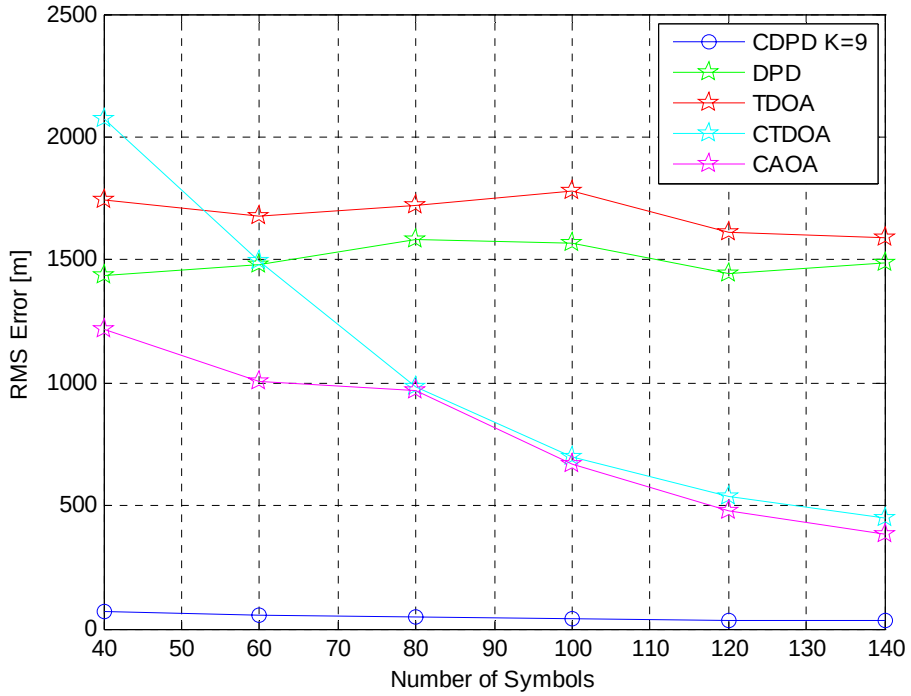

Figure 22. RMS error vs. number of symbols, SNR = 10 dB, interferer and AWGN environment.

do show improvement in their performance with the increase in either the SNR or the observation time, yet they provide much larger errors than the CDPD.

6.3.2 Performance vs. SNR

Here we use exactly the same setup as in Subsection 6.2.2 and plot the results in Figure 23. Again we note that the CDPD has a significant performance advantage relative to all the other competitors through the entire SNR range. Since this subsection considers quite a short observation time then even the cyclic competitors of the CDPD do not have a material superiority over the non cyclic methods. Such methods mitigate the performance degradation caused by interferers better than their corresponding non cyclic methods only when the observation time used for the estimation of the cyclic autocorrelation matrix exceeds the one utilized by the non cyclic methods for the estimation of the conventional autocorrelation matrix (see, e.g., [17]). Likewise, Figure 21 and Figure 22 have already demonstrated that the RMS error of the non cyclic methods does not get smaller with the increase in either the observation time or the SNR. The last two statements thus explain why in the test case considered herein, both the conventional and cyclic methods do not exhibit substantial improvement in their performance while increasing the system SNR.

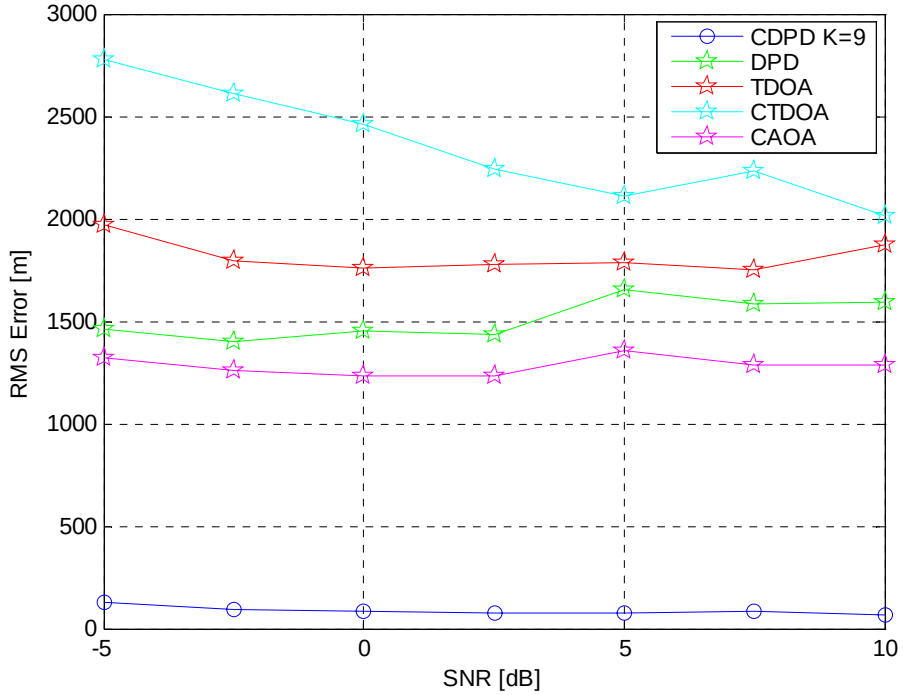

Figure 23. RMS error vs. SNR, interferer and AWGN environment.

6.3.3 Contours Comparison

From the simulation results reported in Subsections 6.3.2 and 6.3.1 we infer that in the presence of a dominant interferer, the CDPD algorithm substantially outperforms traditional estimation algorithms such as the DPD and TDOA methods which do not exploit the cyclostationarity of the SOI. Furthermore, the CDPD is found to outperform also other cyclic methods such as the CAOA and CTDOA. The superior performance of the CDPD is ascribed to its ability to efficiently mitigate interferences which do not share the same cycle frequency as the SOI, namely, having a baud rate different from the one of the SOI. As opposed to existing cyclic methods, this ability is maintained even for a short observation time and in low SNR regime. We next illustrate this ability by plotting the contour diagrams of the CDPD algorithm and its two sub estimators, the CADPD and CTDPD, and comparing them to the ones obtained for both the traditional and cyclic

estimation methods. To this end, we revisit the same two scenarios which were studied in Subsection 3.5.2 and their corresponding contours are plotted in Figure 3 and Figure 4, and simulate them again, this time with an additional cyclostationary interferer positioned at coordinates [1601, 1801] meters. The different location of the SOI in the two above-mentioned figures results in a different relative deployment with the interference. The algorithms contours corresponding to the SOI location of Figure 3 in which the SOI and interferer are distant from one another are given in Figure 24-Figure 30 while the contours corresponding to the SOI location of Figure 4 in which the two emitters are found to be quite close to each other are shown in Figure 31-Figure 37. Furthermore, the interference in the following contours is assumed to have a baud rate of 88 kHz and the SIR is set to 0 dB. The new contours obtained for these modified scenarios are given hereby, where the SOI and interferer locations are marked by blue and red asterisks, respectively. Finally, we mention that these plots are obtained for the single lag version of the CDPD and its two sub estimators, i.e., K in Eq. (48) is set to 1, however, similar plots can be generated also for the multiple lag version.

Figure 24-Figure 37 reveal the reasons behind the great performance differences attained by the various algorithms and the considerable superiority of the CDPD over all examined methods in a noise environment consisting of a strong cyclostationary interferer mixed with AWGN. The traditional methods such as the DPD and TDOA do not exploit the cyclostationarity property of the SOI and thus, cannot distinguish between this signal and the interference. As a result, in the case where the SOI and interference are distant from one another there appear to be two peaks in the cost function contours of the DPD, as shown in Figure 27. The first peak is around the true SOI position whereas the

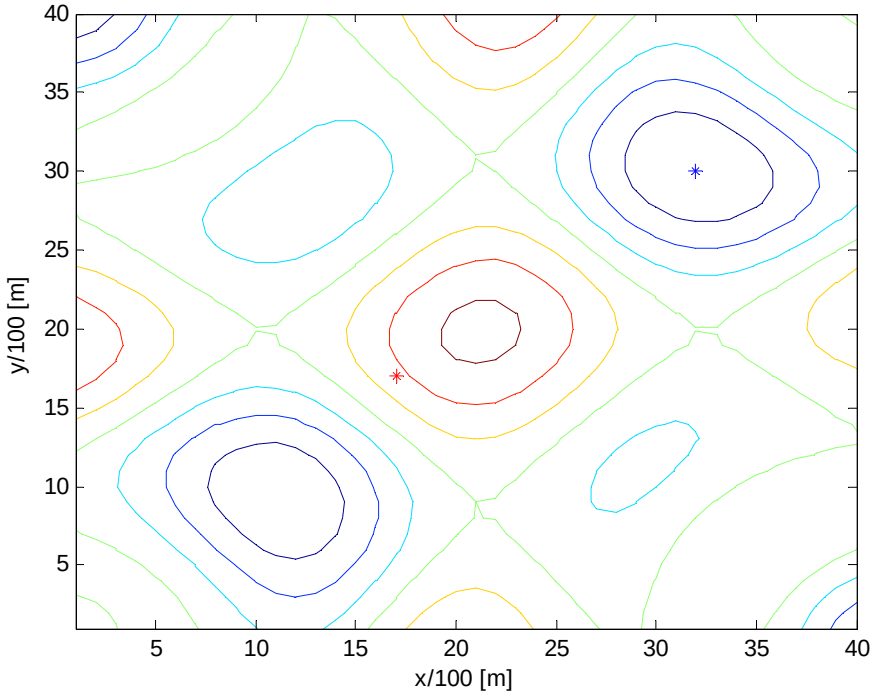

Figure 24. Contour plot of CTDPD for SOI and interferer located at [3101, 2901] and [1601, 1801] meters, respectively.

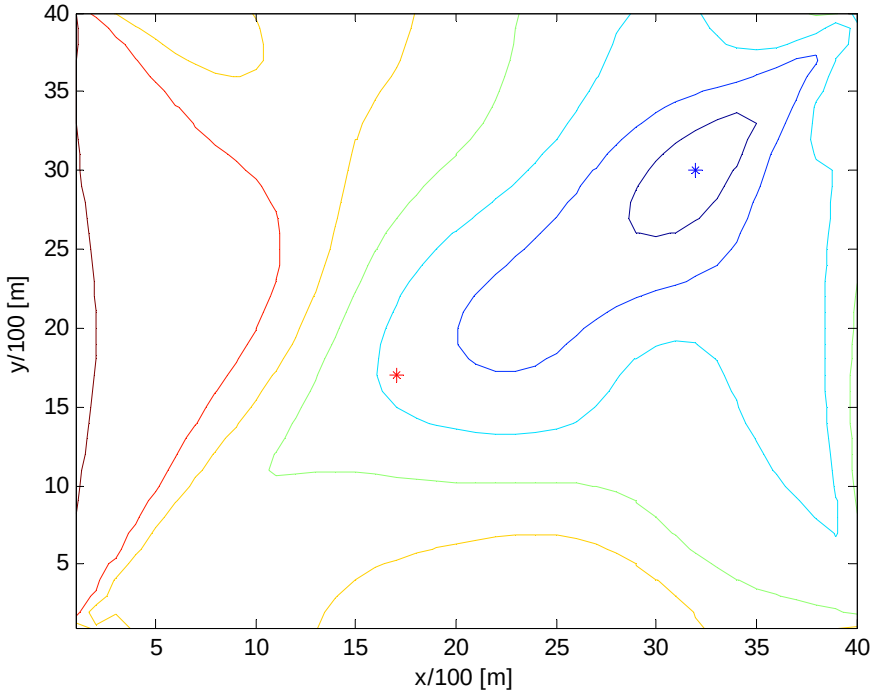

Figure 25. Contour plot of CADPD for SOI and interferer located at [3101, 2901] and [1601, 1801] meters, respectively.

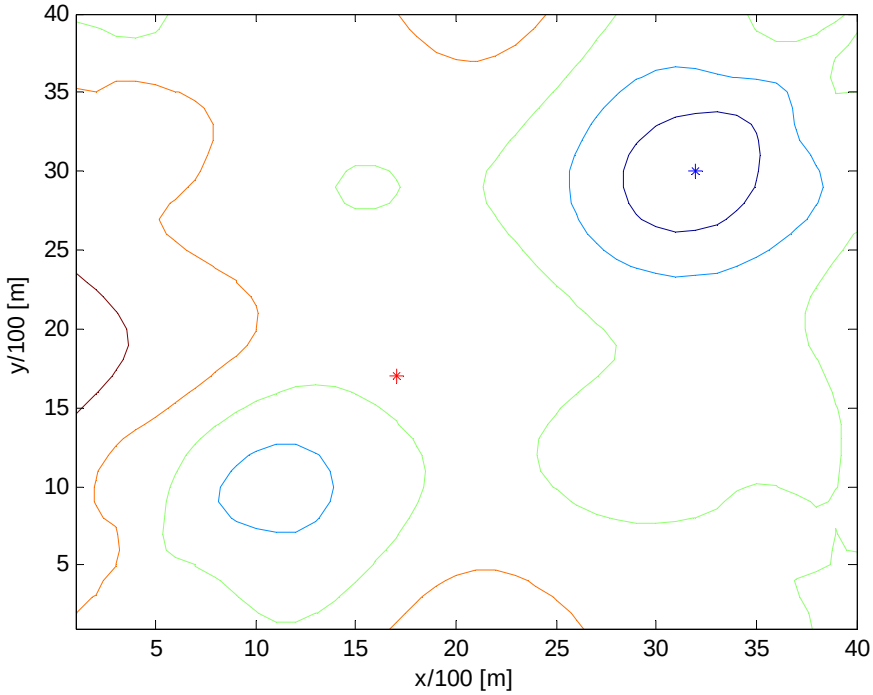

Figure 26. Contour plot of CDPD for SOI and interferer located at [3101, 2901] and [1601, 1801] meters, respectively.

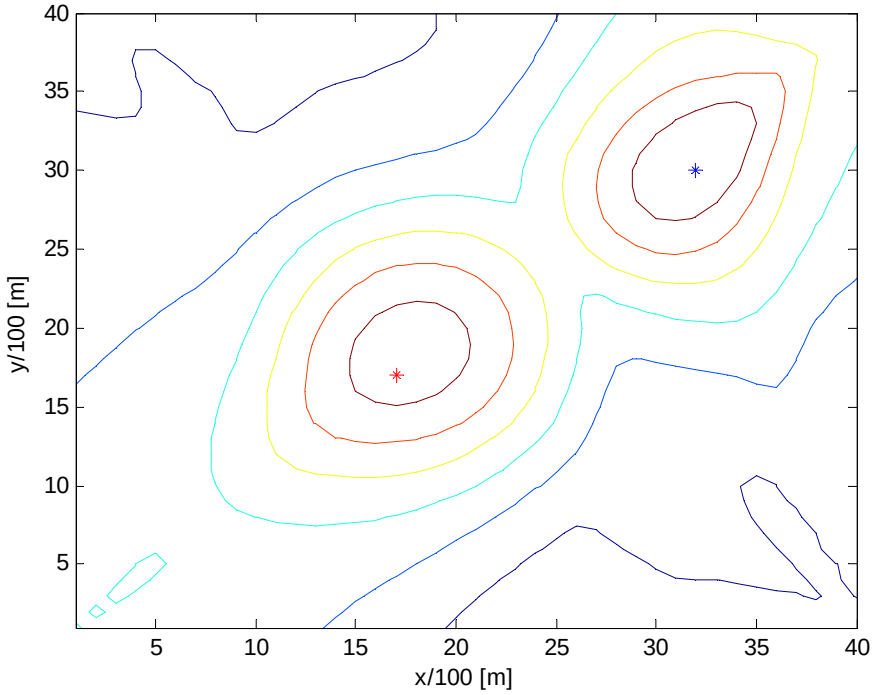

Figure 27. Contour plot of DPD for SOI and interferer located at [3101, 2901] and [1601, 1801] meters, respectively.

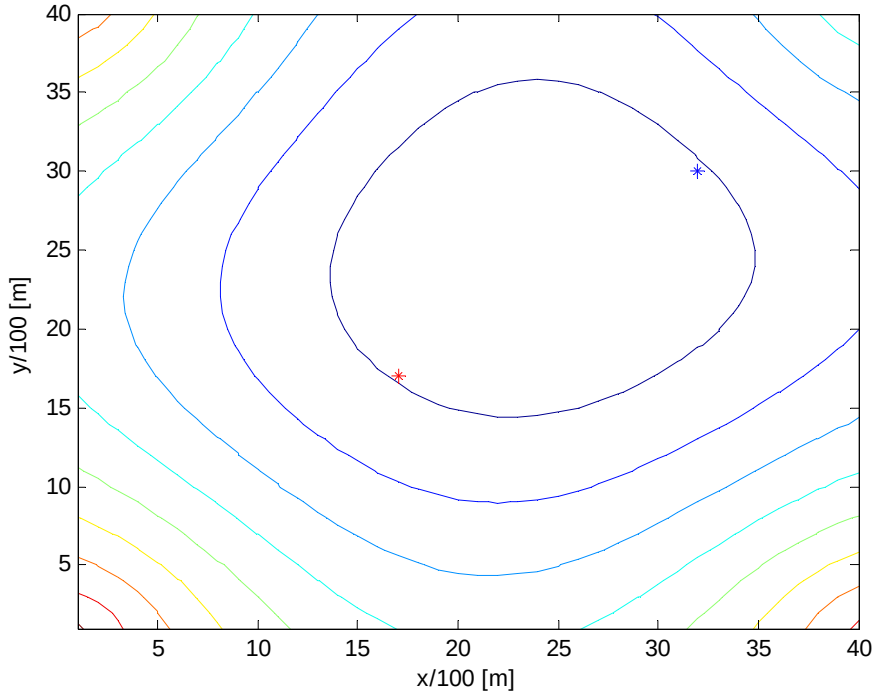

Figure 28. Contour plot of TDOA for SOI and interferer located at [3101, 2901] and [1601, 1801] meters, respectively.

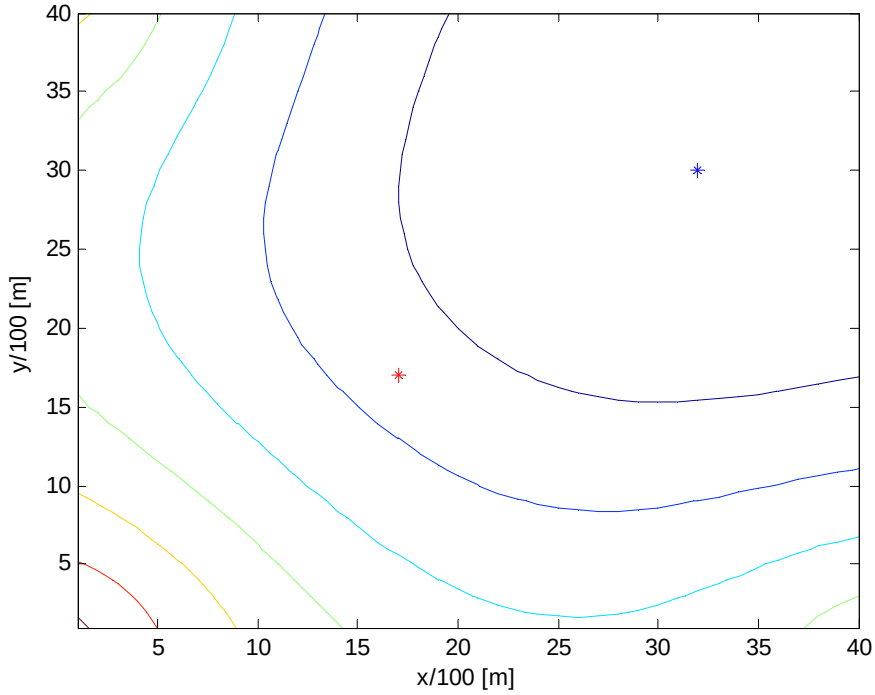

Figure 29. Contour plot of CTDOA for SOI and interferer located at [3101, 2901] and [1601, 1801] meters, respectively.

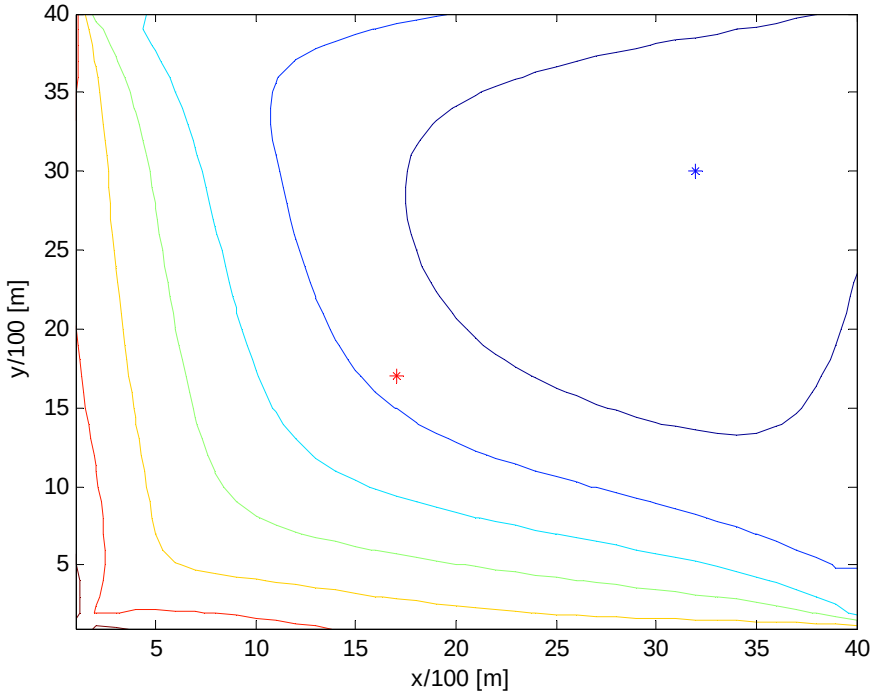

Figure 30. Contour plot of CAOA for SOI and interferer located at [3101, 2901] and [1601, 1801] meters, respectively.

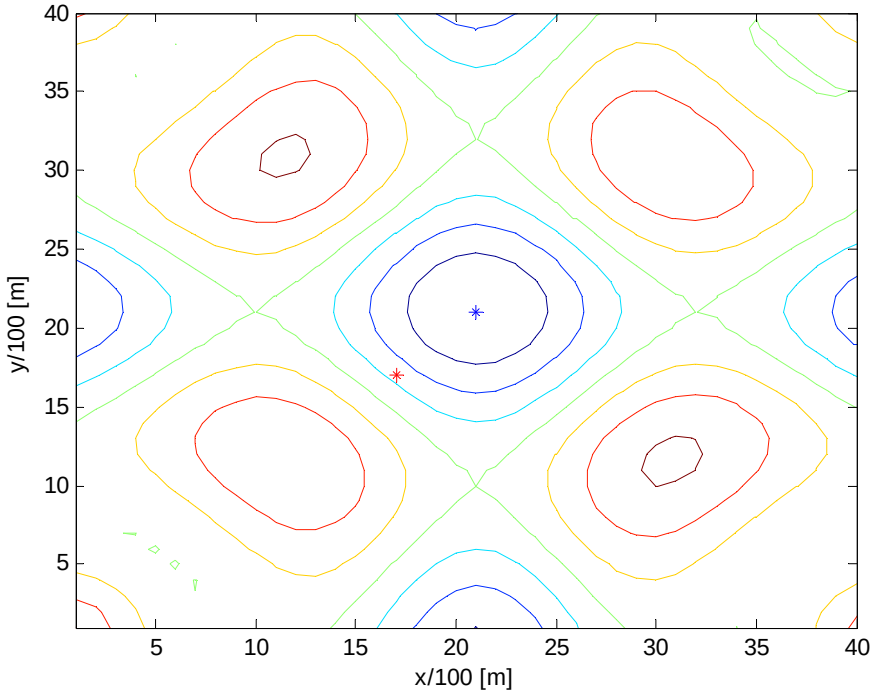

Figure 31. Contour plot of CTDPD for SOI and interferer located at [2001, 2001] and [1601, 1801] meters, respectively.

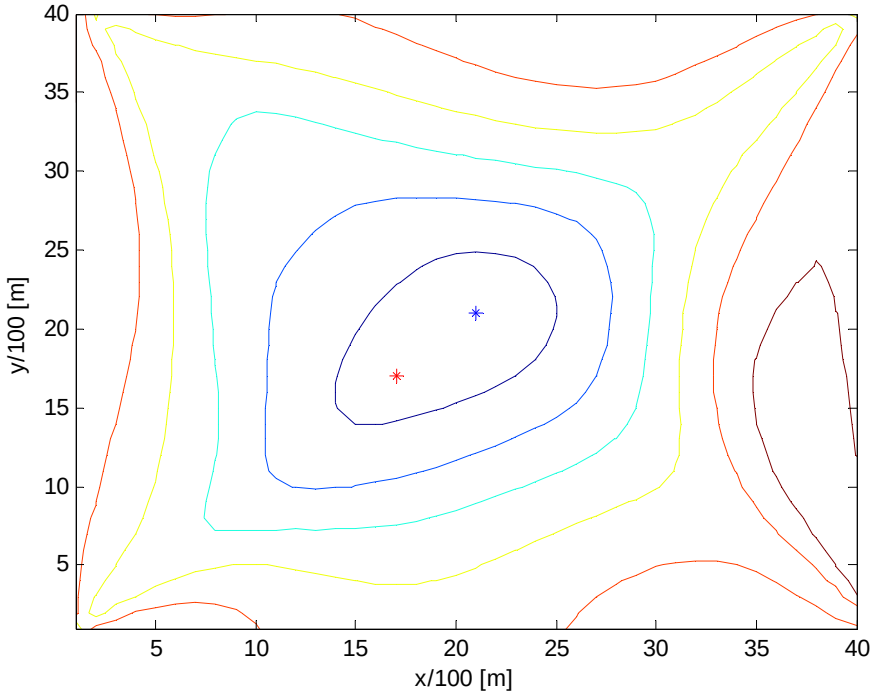

Figure 32. Contour plot of CADPD for SOI and interferer located at [2001, 2001] and [1601, 1801] meters, respectively.

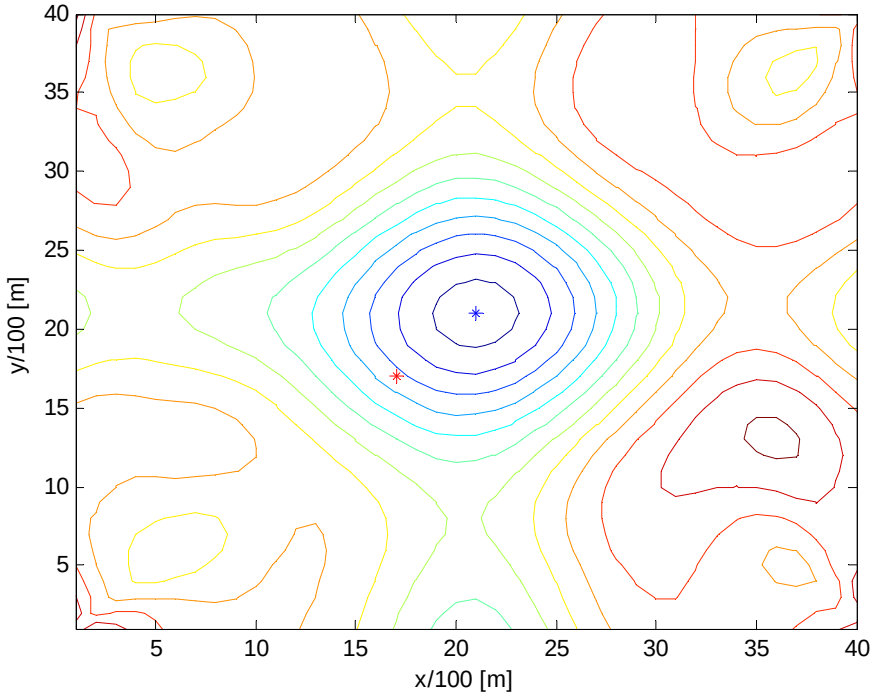

Figure 33. Contour plot of CDPD for SOI and interferer located at [2001, 2001] and [1601, 1801] meters, respectively.

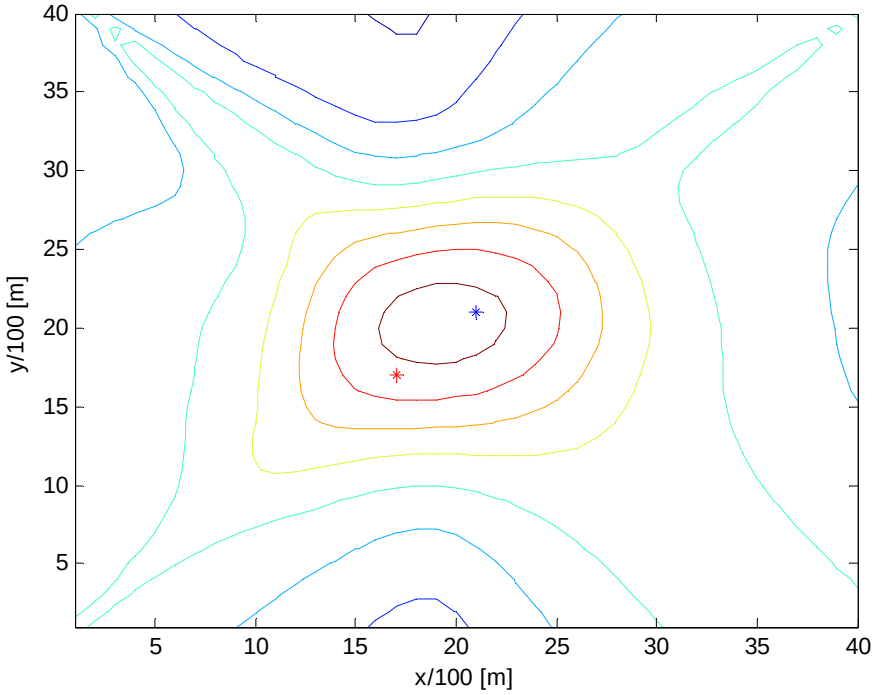

Figure 34. Contour plot of DPD for SOI and interferer located at [2001, 2001] and [1601, 1801] meters, respectively.

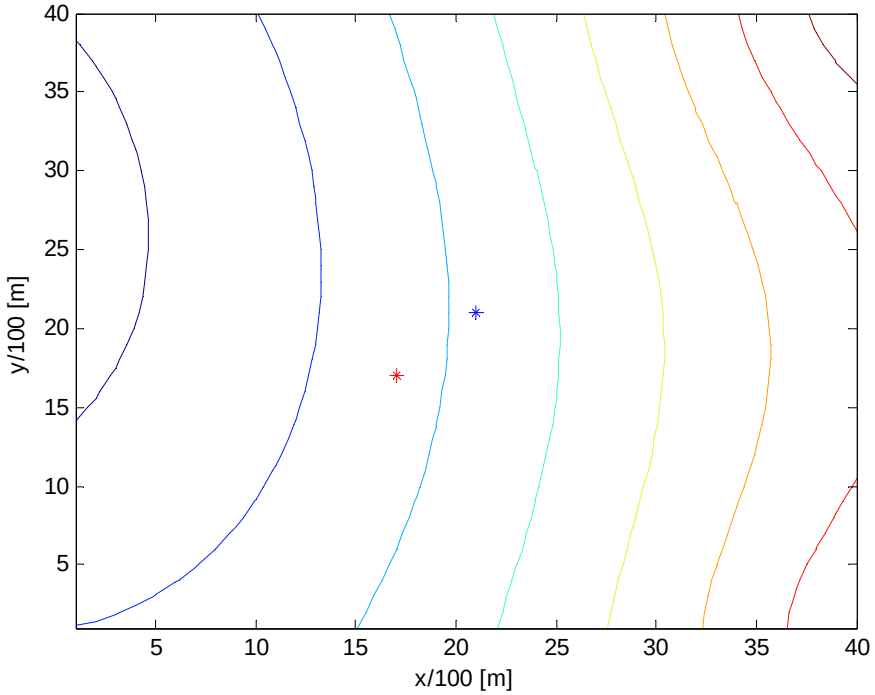

Figure 35. Contour plot of TDOA for SOI and interferer located at [2001, 2001] and [1601, 1801] meters, respectively.

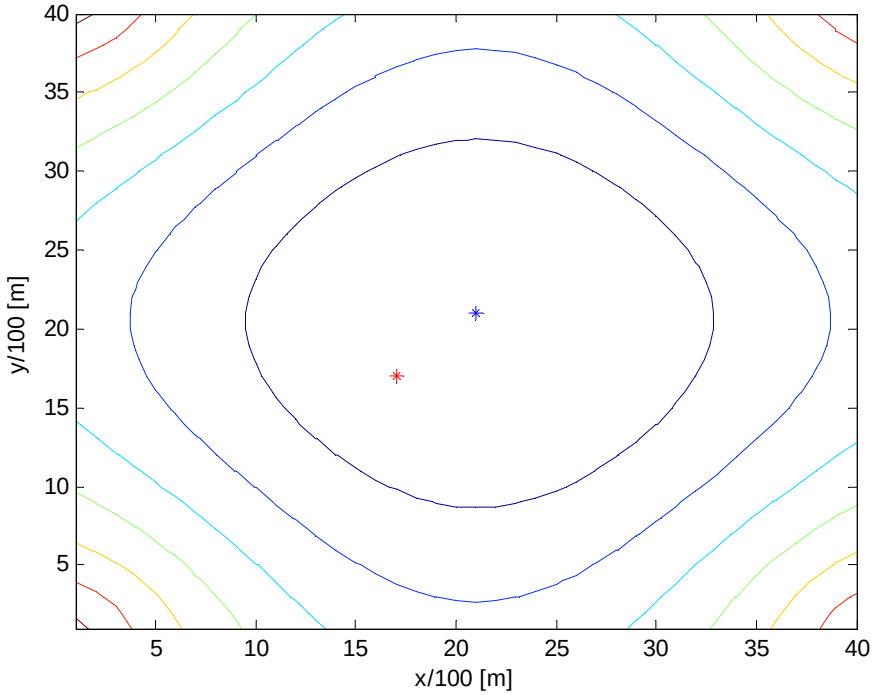

Figure 36. Contour plot of CTDOA for SOI and interferer located at [2001, 2001] and [1601, 1801] meters, respectively.

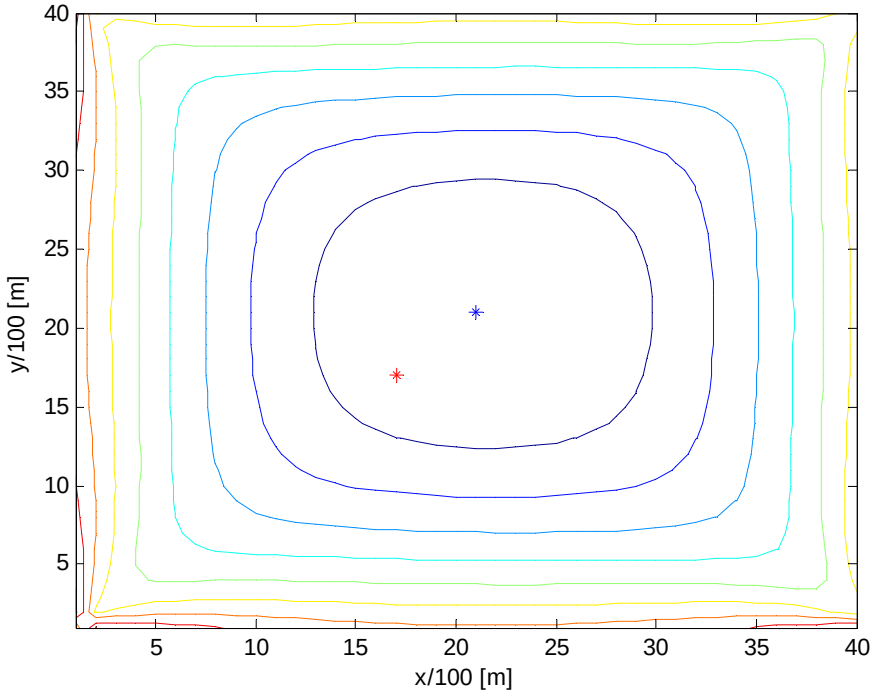

Figure 37. Contour plot of CAOA for SOI and interferer located at [2001, 2001] and [1601, 1801] meters, respectively.

second one is an ambiguous peak, namely, around the interferer location. Therefore, in such a case, the DPD often fails to resolve the SOI position correctly and erroneously prefers the interference location instead. This behavior obviously yields a quite large estimation error as reported in the previous sections of this chapter. For the case where the SOI and interferer are close to each other, which is depicted in Figure 34, there exists only a single peak in the contours of the DPD rather than two peaks as in the previous test case. This plots single peak is obtained in an intermediate point between the two emitter positions which implies that again, the DPD provides a wrong estimate for the SOI position and that this estimate has a significant miss distance. Similarly to the DPD, the TDOA method is also a traditional (non cyclic) method and thus fails to avoid the interference impact. In addition, we observe that the TDOA contours have poor resolution in comparison with the DPD so that for the two examined SOI locations we get only a single peak whose location is neither around the SOI nor the interference, as illustrated in Figure 28 and Figure 35. The considerable distance between the erroneous estimated peak and the true SOI location shown in the last two figures explains the severe performance degradation and the rather large estimation error for this type of noise environment. As opposed to the conventional methods, the CTDOA and CAOA do gain their contours peaks around the true SOI position for the two considered SOI locations, as exemplified by Figure 29, Figure 30, Figure 36, and Figure 37, but their resolution is much worse than the one of the CDPD, which explains their large estimation error after all. Finally, we observe that the contours of the CDPD estimator given in Figure 26 and Figure 33 for the two examined scenarios hardly change their shape in the presence of a narrowband interferer. Specifically, in these two figures we observe the existence of only

one peak around the true SOI location and the absence of both contours smearing and ambiguous peaks which were experienced by the other methods as discussed above. Furthermore, the CDPD contours enjoy much higher resolution relative to the other cyclic methods providing it much lower estimation error than these methods. The last two statements are applicable also to the two sub estimators of the CDPD, i.e., the CTDPD and CADPD whose contour plots are shown in Figure 24, Figure 31, and Figure 25, Figure 32, respectively. Thus, the CDPD succeeds to maintain a complete abolition of the interference even in a low SNR regime and for a short observation time which explains its excellent performance in this type of environment relative to all other methods.

7 Summary and Future Work

In this work, we proposed a novel passive localization method for radio frequency signals called cyclic direct position determination. This method is an extension of the conventional DPD method introduced by Weiss [25] to the case of cyclostationary signals. While the conventional DPD does not make any assumptions on the SOI, the CDPD exploits the *a priori* information it has regarding the cycle frequency of the cyclostationary SOI in order to mitigate strong interferers. Thus, while the conventional DPD exhibits excellent performance in an AWGN-only environment but suffers from an ambiguity problem in the presence of narrowband interferences, the CDPD offers high performance in both types of environments.

The CDPD is constructed from two sub-estimators, the CADPD and CTDPD. Each one of these two algorithms exploits a different property of the SOI, namely, the signal's direction of arrival and propagation delay, respectively. We derived their cost functions and combined them into a single estimator, the CDPD. Next, we explored the optimal choice for the lag parameter of the CDPD algorithm when a single lag is in use and showed how to extend the CDPD cost function to process several lag choices simultaneously for further performance improvement. Furthermore, we considered the ambiguity problem of the CTDPD algorithm and its consequences on the CDPD method.

Subsequently, we presented a SEA for the performance of the CTDPD algorithm in an AWGN environment. The CRLB for the case of cyclostationary SOI for this type of environment was also considered although not derived due the little information it conveys for such a case. Thereafter, the performance of the CDPD was examined using

Monte Carlo simulations and compared to the MSE of other localization methods in the presence of both AWGN and a mixture of the latter with cyclostationary interference. This performance comparison between the different methods was given in terms of several system parameters such as the operational SNR and observation time. In addition, we demonstrated the excellent compliance between the analytical MSE of the CTDPD and the one obtained empirically. Finally, the high robustness of the CDPD method to narrowband interferers was also illustrated by comparing the contour plots of the cost functions of the different localization methods in such a noise environment.

There are, of course, many ideas and aspects of the problem that were left out of the scope of this work. Future work can be thus extended in the following directions:

- The model considered in this work assumes a single emitter possessing the cycle frequency of interest and therefore, the CDPD algorithm was designed to handle only one SOI. Thus, it should be interesting to extend the existing model to include multiple transmitters, all of which sharing the same cycle frequency, and to generalize the CDPD algorithm accordingly.
- Additional extension of the model may be adding a multipath scenario to the basic problem formulation which considered only a single ray reception.
- Another model assumption that was made on the SOI is that its waveform is unknown. Further research can consider the case of a known signal waveform and suggest extension to the existing algorithm which exploits this additional information for further performance enhancement.

- The performance analysis of the CDPD algorithm was made under the assumption of AWGN environment only, i.e., the noise term considered was drawn from a circular symmetric complex white Gaussian distribution. The case of noise environment consisting of a mixture of AWGN and a narrowband cyclostationary interferer with a cycle frequency differing from the one of the SOI was studied empirically using Monte Carlo simulations but was not analytically analyzed. We thus suggest extending the SEA derivation presented in this work to handle also narrowband interferences and comparing this analytical performance with the empirical results.

- In this work, the Monte Carlo simulations were performed assuming certain system parameters such as the SOI modulation type, base station deployment, and geometry of the array sensors. Further research may utilize other system setups and explore their effect on the performance of the CDPD algorithm. Such setups may include different base station configurations, i.e., different number of base stations with different deployments, other array geometries, SOI with *M*-ary modulation, and so on.

Bibliography

[1] A. Amar and A. J. Weiss, "Direct position determination of multiple radio signals," in *Proc. IEEE Int. Conf. Acoust., Speech, Signal Processing* (Piscataway, NJ), May 2004, vol. 2, pp. ii-81-84.

[2] A. B. Baggeroer, W.A. Kuperman, and P. N. Mikhalevsky, "An overview of matched filed methods in ocean acoustics," *IEEE J. of Oceanic Engineering,* vol. 18, no. 4, pp. 401-424, Oct. 1993.

[3] J. J. Caffery and G.L. Stuber, "*Overview of radiolocation in CDMA cellular systems*," *IEEE Commun. Mag*., vol. 36, pp 38-45, Apr. 1998.

[4] G. C. Carter, *Coherence and Time Delay Estimation*, IEEE press, 1993.

[5] W. A. Gardner, *Statistical Spectral Analysis: A Nonprobabilistic Theory*, Englewood Cliffs, NJ: Prentice-Hall, 1987.

[6] ——, "Simplification of MUSIC and ESPRIT by exploitation of cyclostationarity," in *Proc. IEEE*, vol. 76, no. 7, pp. 845-847, July 1988.

[7] ——, *Introduction to Random Processes with Applications to Signals and Systems*, 2nd Ed. New York: McGraw-Hill, 1989.

[8] ——, "Exploitation of spectral redundancy in cyclostationary signals," *IEEE Signal Processing Mag.*, vol. 8, pp. 14-37, Apr. 1991.

[9] W. A. Gardner and C. K. Chen, "Signal-selective time-difference-of-arrival estimation for passive location of man-made signal sources in highly corruptive environments, Part I: Theory and method," *IEEE Trans. Signal Processing*, vol. 40, no. 5, pp. 1168-1184, May 1992.

[10] ——, "Signal-selective time-difference-of-arrival estimation for passive location of man-made signal sources in highly corruptive environments,

Part II: Algorithms and performance," *IEEE Trans. Signal Processing*, vol. 40, no. 5, pp. 1185-1197, May 1992.

[11] Y. Isby, "On the performance of direct position determination," M.Sc. dissertation, Dept. of Elect. Eng., Tel-Aviv Univ., Tel-Aviv, Israel, 2005.

[12] H. Krim and M. Viberg, "Two decades of array signal processing research," *IEEE Signal Processing Mag.*, vol. 13, no. 4, July 1996.

[13] N. Levanon, *Radar Principles*, New York: Wiley, 1988.

[14] A. V. Oppenheim and R. W. Schafer, *Discrete-Time Signal Processing*, Englewood Cliffs, NJ: Prentice-Hall, 1989.

[15] B. Picinbono, "Second-order complex random and normal distribution," *IEEE Trans. Signal Processing*, vol. 44, no. 10, pp. 2637-2640, Oct. 1996.

[16] S. V. Schell, "Performance analysis of the Cyclic MUSIC method of direction estimation for cyclostationary signals," *IEEE Trans. Signal Processing*, vol. 42, no. 11, pp. 3043-3049, Nov. 1994.

[17] S. V. Schell, R. A. Calabretta, W. A. Gardner, and B. G. Agee, "Cyclic MUSIC algorithm for signal-selective DOA estimation," *Proc. IEEE Int. Conf. Acoust., Speech, Signal Processing* (Glasgow, Scotland), May 1989, pp. 2278-2281.

[18] S. V. Schell and W. A. Gardner, "The Cramér-Rao lower bound for directions of arrival of Gaussian cyclostationary signals," *IEEE Trans. Inform. Theory*, vol. 38 pp. 1418-1422, July 1992.

[19] R. O. Schmidt, "Multiple emitter location and signal parameter estimation," *IEEE Trans. Antennas and Propagation,* vol. 34, no. 3, pp. 276-280, Mar. 1986.

[20] P. Stoica and A. Nehorai, "MUSIC, maximum likelihood, and Cramér-Rao bound," *IEEE Trans. Acoust., Speech, Signal Processing*, vol. 37, no. 5, pp. 720-741, May 1989.

[21] ——, "Performance study of conditional and unconditional direction of arrival estimation," *IEEE Trans. Acoust., Speech, Signal Processing*, vol. 38, no. 10, pp. 1783-1795, Oct. 1990.

[22] D. J. Torrieri, "Statistical theory of passive location systems," *IEEE Trans. Aerosp. Electron. Syst.*, vol. AES-20, pp. 184-198, Mar. 1984.

[23] H. L. Van Trees, *Detection, Estimation and Modulation Theory, Part IV*: *Optimum Array Processing*, Wiley & Sons, 2002.

[24] H. Wang and M. Kaveh, "On the statistical sufficiency of the coherently averaged covariance matrix for the estimation of the parameters of wide-band sources," in *Proc. IEEE Int. Conf. Acoust., Speech, Signal Processing* (Dallas, TX), Mar. 1987, pp. 33-36.

[25] A. J. Weiss, "Direct position determination of narrowband radio frequency transmitters," *IEEE Signal Processing Letters*, vol. 11, no. 5, pp. 513-516, May 2004.

[26] J. M. Zagami, S. A. Parl, J. J. Bussgang, and K. D. Melillo, "Providing universal location services using a wireless E911 location network," *IEEE Commun. Mag.*, vol. 36, no. 4, pp. 66-71, Apr. 1998.

Appendix A

In this appendix we prove Eq. (128) given in the performance analysis section. The proof is derived as a corollary of a more general theorem which itself is obtained as a result of a lemma given hereby.

Lemma A.1: Let $s(t)$ be a band limited continuous signal with bandwidth *B*. We sample $s(t)$ with a sampling rate $R_{sam} = 1/T_{sam} \geq 2B$. In this case, the function

$$\rho(f) \equiv \sum_{n=-\infty}^{\infty} s(nT_{sam} - \gamma) e^{j2\pi f(nT_{sam} - \gamma)} \tag{A.1}$$

of the signal samples $s(nT_{sam} - \gamma)$ is independent of γ.

Proof: According to the Nyquist sampling theorem for a band-limited signal we have

$$s(t) = \sum_{n=-\infty}^{\infty} s(nT_{sam}) \frac{\sin\left[\pi(t - nT_{sam})/T_{sam}\right]}{\pi(t - nT_{sam})/T_{sam}}. \tag{A.2}$$

Substituting the relation above into Eq. (A.1), we get

$$\rho(f) = \sum_{n=-\infty}^{\infty} \sum_{k=-\infty}^{\infty} s(kT_{sam}) \frac{\sin\left[\pi\left((n-k)T_{sam} - \gamma\right)/T_{sam}\right]}{\pi\left((n-k)T_{sam} - \gamma\right)/T_{sam}} e^{j2\pi f(nT_{sam} - \gamma)}. \tag{A.3}$$

Rearranging the terms in Eq. (A.3) yields

$$\rho(f) = \sum_{k=-\infty}^{\infty} s(kT_{sam}) e^{j2\pi f(kT_{sam} - \gamma)} \sum_{n=-\infty}^{\infty} \frac{\sin\left[\pi\left((n-k)T_{sam} - \gamma\right)/T_{sam}\right]}{\pi\left((n-k)T_{sam} - \gamma\right)/T_{sam}} e^{j2\pi f(n-k)T_{sam}}. \tag{A.4}$$

If we substitute the following notation

$$m \equiv n - k, \tag{A.5}$$

into Eq. (A.4) then the last one reads

$$\rho(f) = \sum_{k=-\infty}^{\infty} s(kT_{sam}) e^{j2\pi f(kT_{sam}-\gamma)} \sum_{m=-\infty}^{\infty} \frac{\sin\left[\pi\left(mT_{sam}-\gamma\right)/T_{sam}\right]}{\pi\left(mT_{sam}-\gamma\right)/T_{sam}} e^{j2\pi fmT_{sam}} . \tag{A.6}$$

Again we use the sampling theorem to obtain

$$\sum_{m=-\infty}^{\infty} \frac{\sin\left[\pi/T_{sam}\left(mT_{sam}-\gamma\right)\right]}{\pi/T_{sam}\left(mT_{sam}-\gamma\right)} e^{j2\pi fmT_{sam}} = e^{j2\pi f\gamma} , \tag{A.7}$$

which implies that $\rho(f)$ from Eq. (A.6) can be expressed as

$$\rho(f) = \sum_{k=-\infty}^{\infty} s(kT_{sam}) e^{j2\pi fkT_{sam}} . \tag{A.8}$$

From the last expression we observe that $\rho(f)$ is independent of γ which concludes the lemma. □

Theorem A.2: Let $s(t)$ be a continuous signal with bandwidth *B*, then its samples $s(nT_{sam})$ obtained at a sampling rate which satisfies the Nyquist sampling theorem, i.e., $R_{sam} = 1/T_{sam} \geq 2B$, admit the following equality

$$\psi(\tau,\xi) \equiv \sum_{n=-\infty}^{\infty} s(nT_{sam}-\tau)s(nT_{sam}-\tau-\xi) = \psi(\xi) . \tag{A.9}$$

Stated in words, we say that $\psi(\tau,\xi)$ is independent of τ and is a function of ξ only.

Proof: According to the inverse Fourier transform we have,

$$s(nT_{sam}-\tau) = \int_{-B}^{B} S(f) e^{j2\pi f(nT_{sam}-\tau)} df , \tag{A.10}$$

so that $\psi(\tau,\xi)$ from Eq. (A.9) can be written as

$$\psi(\tau,\xi)=\sum_{n=-\infty}^{\infty}\int_{-B}^{B}S(f)s(nT_{sam}-\tau-\xi)e^{j2\pi f(nT_{sam}-\tau-\xi)}e^{j2\pi f\xi}df\ . \tag{A.11}$$

Replacing the summation and integral order in Eq. (A.11) yields

$$\psi(\tau,\xi)=\int_{-B}^{B}S(f)e^{j2\pi f\xi}\sum_{n=-\infty}^{\infty}s(nT_{sam}-\tau-\xi)e^{j2\pi f(nT_{sam}-\tau-\xi)}df\ . \tag{A.12}$$

The inner summation in Eq. (A.12) is exactly $\rho(f)$ from Eq. (A.1) where γ is replaced with the sum of τ and ξ. Since $\rho(f)$ is independent of γ according to Lemma A.1, it readily follows that

$$\psi(\tau,\xi)=\int_{-B}^{B}\rho(f)S(f)e^{j2\pi f\xi}df=\psi(\xi)\,, \tag{A.13}$$

which completes the proof. □

Corollary A.3: Let $q_l(m)$ be samples at a rate $1/T_s=OVS/T$ of a band limited signal with bandwidth smaller than or equal to $1/T$, then Eq. (128) holds:

$$\left[Q_l(m,k)+Q_l(m+OVS/2,k)\right]=g_l(k)\,,\forall m,\,k\in\{0,OVS/2\}, \tag{A.14}$$

where $Q_l(m,k)$ is defined in Eq. (125).

Proof: The proof could be straightforward if we had set the function $Q_l(m,k)$ from Eq. (125) to be $\psi(\tau,\xi)$ from Theorem A.2 above. Generally speaking, Theorem A.2 does not apply directly to $Q_l(m,k)$ itself since $q_l(m)$ from Eq. (125) does not satisfy all the assumptions we have defined regarding $s(nT_{sam})$ in Theorem A.2. Specifically, we note that the samples $s(nT_{sam})$ should admit the Nyquist sampling theorem. However, the

pulse shape samples $q_l(m)$ in the term $Q_l(m,k)$ are of the form $q_l(n\cdot OVS)$, i.e., they are at the baud rate which is $1/T$. Since the bandwidth of this waveform is bounded by $1/T$ then its Nyquist rate is bounded by $2/T$ which implies that the sampling rate of $q_l(n\cdot OVS)$ alone does not meet the underlying assumption for Theorem A.2. Yet, we will show explicitly in the sequel that under some specific settings of *k*, Theorem A.2 is applicable to the sum $Q_l(m,k)+Q_l(m+OVS/2,k)$. This sum is comprised of samples of $q_l(m)$ which are spaced in time $T/2$ apart, or equivalently, samples of $q_l(m)$ at the Nyquist rate of this signal. Hence, we can set the samples $q_l(n\cdot OVS/2)$ which are sampled at twice the rate, to be $s(nT_{sam})$.

Another assumption made on the two samples of $s(nT_{sam})$ constituting the product $\psi(\tau,\xi)$ from Theorem A.2 is that there is a fixed time difference between them, ξ. Thus, the two factors of $q_l(n\cdot OVS)$ which constitute $Q_l(m,k)$ should have a constant index difference between them. This assumption is not satisfied in general, except for the certain choices $k=0$ or $k=OVS/2$. Specifically, under the choice $k=0$ we have from Eq. (125) that

$$\begin{aligned}&\left[Q_l(m,0)+Q_l(m+OVS/2,0)\right]\\&=\sum_{n=-\infty}^{\infty}q_l^2\left(n\cdot OVS+m \bmod OVS\right)+q_l^2\left(n\cdot OVS+(m+OVS/2) \bmod OVS\right)\\&=\sum_{n=-\infty}^{\infty}q_l^2\left(n\cdot OVS/2+m \bmod OVS\right),\end{aligned} \tag{A.15}$$

and similarly, the choice $k=OVS/2$ yields

$$
\begin{aligned}
&\left[Q_l(m, OVS/2) + Q_l(m + OVS/2, OVS/2)\right] \\
&= \sum_{n=-\infty}^{\infty} q_l\left((n-1)\cdot OVS + (m + OVS/2) \bmod OVS\right) \\
&\qquad \cdot q_l\left(n \cdot OVS + (m + OVS/2) \bmod OVS\right) \\
&\quad + \sum_{n=-\infty}^{\infty} q_l\left((n-1)\cdot OVS + m \bmod OVS\right) \cdot q_l\left(n \cdot OVS + m \bmod OVS\right) \\
&= \sum_{n=-\infty}^{\infty} q_l\left(n \cdot OVS/2 + m \bmod OVS\right) \cdot q_l\left((n-2)\cdot OVS/2 + m \bmod OVS\right).
\end{aligned}
\tag{A.16}
$$

Therefore, we can identify the sum $Q_l(m,k) + Q_l(m + OVS/2, k)$ with the function $\psi(\tau, \xi)$ from Eq. (A.14) if we set

$$
s(nT_{sam}) = q_l(n \cdot OVS/2)\,, \tag{A.17}
$$

$$
\xi = \begin{cases} 0, & k = 0 \\ 2T_{sam} = T, & k = OVS/2 \end{cases}, \tag{A.18}
$$

$$
\tau = \frac{T}{OVS} \cdot m \bmod OVS\,. \tag{A.19}
$$

The formulation above leads to the following representation of the left-hand side of Eq. (A.14)

$$
\left[Q_l(m,k) + Q_l(m + OVS/2, k)\right] = \psi(\tau, \xi)\,, \forall m,\, k \in \{0, OVS/2\}\,. \tag{A.20}
$$

Finally, we have from Theorem A.2 that

$$
\left[Q_l(m,k) + Q_l(m + OVS/2, k)\right] = \psi(\xi)\,, \forall m,\, k \in \{0, OVS/2\}\,. \tag{A.21}
$$

The expression on the right-hand side of Eq. (A.21) is independent of m according to Eq. (A.18) so the proof is now complete. □